THE UNIVERSITY OF OKLAHOMA

GRADUATE COLLEGE

THE MOLECULAR DIPOLE MODEL AND THE INTERNAL OPTIC MODES OF THE SULFATE ION IN DIFFERENT CRYSTALLINE SYSTEMS

A DISSERTATION

SUBMITTED TO THE GRADUATE FACULTY

in partial fulfillment of the requirements for the

degree of

DOCTOR OF PHILOSOPHY

BY

GUO-JEN WU

Norman, Oklahoma

1976

THE MOLECULAR DIPOLE MODEL AND THE INTERNAL OPTIC MODES OF THE SULFATE ION IN DIFFERENT CRYSTALLINE SYSTEMS

APPROVED BY

Roger Tkach

Norman Fogel

William N. Huff

DISSERTATION COMMITTEE

ACKNOWLEDGEMENTS

My deepest appreciation is expressed to Dr. Roger Frech for his direction and guidance during the course of these studies. Dr. Frech's attitude toward the students, especially, toward a foreign student like the author who has cultural barriers is greatly appreciated.

Prof. J. P. Devlin at the Oklahoma State University deserves my special gratitude for helping the author in obtaining the Raman spectra. Without his help this work is impossible.

Mr. Henry Nichols, my close friend and lab partner, deserves my gratitude also. The author will not forget in his life what has happened in the lab in the past four years.

Appreciation is also extended to Dr. Dick van der Helm for his kindness in providing the author a chance to do the x-ray structure determination. The author is happy to see a solution of the structure of auramine nitrate monohydrate crystal. Dr. van der Helm's kindness in letting the author use his typewriter in preparing this thesis is also greatly appreciated.

Many other members of the faculty of the Chemistry Department and friends deserve my thanks also. It is impossible to name all of them here and their friendship with the author is greatly appreciated.

The author would also like to thank the Chemistry Department for the teaching assistantship granted for the past five years and the OURI (Research Institute of the University of Oklahoma) for the fellowship during the author's last year of study here.

Finally to my parents, whose support never waned, goes my whole-hearted thanks.

TABLE OF CONTENTS

LIST OF TABLES

LIST OF FIGURES

LIST OF FIGURES

(Continued)

LIST OF FIGURES

(Continued)

CHAPTER I

Introduction

The point group of a free sulfate ion is T_d. It can be shown[1,2] that the sulfate ion has nine vibrational normal modes which are classified according to the irreducible representations of the point group T_d as $\Gamma_{vib} = A_1 + E + 2T_2$. By convention ν_1 is assigned to the mode belonging to the one dimensional representation A_1, ν_2 to the mode belonging to the two dimensional representation E, and ν_3 and ν_4 to the modes of the three dimensional representation T_2.

The description of normal coordinates is shown as[3] :

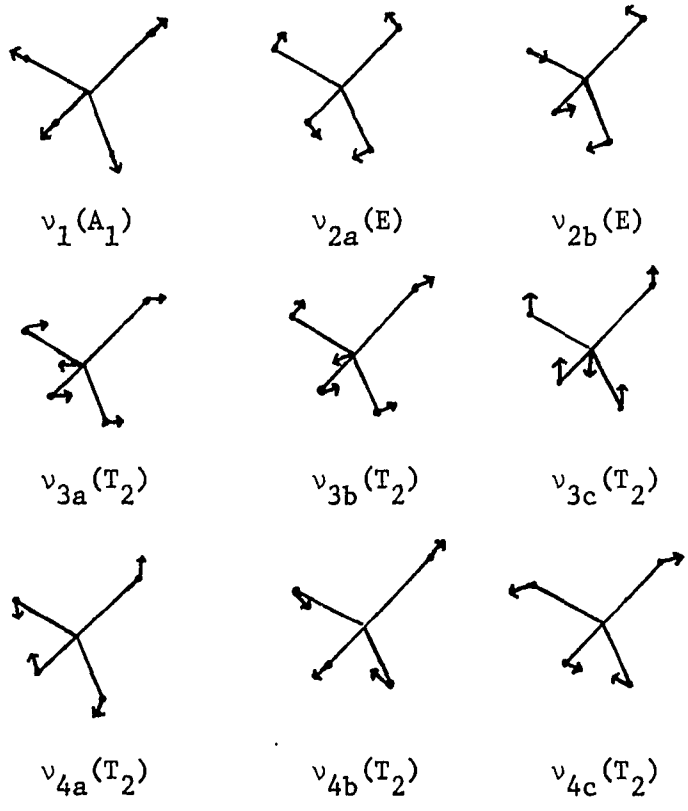

The frequencies of these modes are approximately ν_1 = 983 cm^{-1}, ν_2 = 450 cm^{-1}, ν_3 = 1105 cm^{-1}, and ν_4 = 610 cm^{-1}.[2]

The transformation properties of these modes are given by standard character tables as :

mode	symmetry	polarization
ν_1	A_1	xx + yy + zz
ν_2	E	(xx + yy - 2zz, xx - yy)
ν_3, ν_4	T_2	(x,y,z), (xy, yz, zx)

In a free sulfate ion all modes are Raman active, however, only $\nu_3$and ν_4 are infrared active.

A sulfate ion does not really exist in the free state but rather in a condensed phase, liquid or solid, with other cations. The various environments of a sulfate ion may lead to changes of vibrational frequencies through the reduction of the symmetry of the potential energy of the environment, coupling between a sulfate ion and other ions, new selection rules, and so on.

In the liquid state, the environment of a sulfate ion changes with time, so the effects observed in the laboratory are time-averaged because the time resolution of the measurements is much greater than the time scale of the changes involved. In the crystalline state the situation is quite different. The position of the atoms in a crystal are fixed relative to each other such that one can assign a point group to the site which a sulfur atom occupies. The symmetry of the potential energy environment of the whole sulfate ion can be approximated by

this point group (the so-called site group) for the convenience of the vibrational analysis. In a crystal the symmetry elements such as the translations, screw axes, rotation axes, glide planes, mirror planes, and inversion centers constitute the space group which characterized the symmetry properties of the crystal. More specifically, it is the unit cell group which is the factor group of the space group with respect to the invariant translation subgroup that characterizes the symmetry properties of the unit cell. The unit cell group is always isomorphic to one of the 32 point groups.

The effect of the site on the vibrational modes of a sulfate ion is determined by the electrostatic forces on the ion from the rest of the ions in their equilibrium positions. The effect is static since no dynamical couplings are involved. However in a crystal the vibrational motions of the sulfate ions are correlated through intermolecular forces. It is these dynamical intermolecular forces such as the vibrationally induced dipolar coupling that correlate the motions of sulfate ions on various sites within the symmetry species allowed by the unit cell group. This kind of consideration leads to the molecular dipole model of internal optic modes which enables one to calculate the static crystal field frequency (the frequency of an individual sulfate ion neglecting all site effects), dipole moment derivatives, and electronic polarizability components of anions at different sites and along different principal axes. This model is obviously a powerful tool to study the infrared and Raman spectra of molecular crystals.

Several sulfate crystals have been grown and the internal vibrations of the sulfate ions in these crystals were carefully studied with the dipole model. The static crystal frequencies, dipole moment derivatives, and electronic polarizabilities of these crystals were calculated. In an attempt to apply the dipolar theory to the K_2SO_4 crystal deeper insight into the vibrational coupling in phonon modes resulting from degenerate molecular modes whose degeneracies have been lifted due to site group effects was found. This is discussed in chapter VI. Based on the theory developed in chapter VI the dipole model was extended to the monoclinic system in chapter VIII in which the monoclinic $Li_2SO_4 \cdot H_2O$ crystal was studied.

References for Chapter I

1. E. Bright Wilson, Jr., J. C. Decius, and Paul C. Cross, Molecular Vibrations, McGraw-Hill, New York, 1955.

2. L. H. Hall, Group Theory and Symmetry in Chemistry, McGraw-Hill, New York, 1969.

3. G. Herzberg, Infrared and Raman Spectra, D. Van Nostrand Company, Inc., Princeton, N. J., 1959.

CHAPTER II

Review of the Theory of the Molecular Dipole Model

A. Preliminary

In a paper by M. Mandel and P. Mazur[1] in 1958 the total potential energy of a system of N unit cells which are composed of n polar and polarizable molecules in an external electric field was studied. Three contributions to the potential energy may be noted :

(a) the internal energy V_{def} due to the deformation of the particles by the local electric field $\underset{\sim}{F}$,

$$V_{def} = 1/2 \; \underset{\sim}{F}^{\dagger} \underset{\sim}{\alpha}_{o} \underset{\sim}{F} \tag{2-1}$$

(b) the electrostatic dipole-dipole energy V_{dip} between the molecules with total electric moment $\underset{\sim}{P}$,

$$V_{dip} = 1/2 \; \underset{\sim}{P}^{\dagger} \underset{\sim}{T} \underset{\sim}{P} \tag{2-2}$$

and (c) the interaction energy V_{int} of the molecules with the external electric field $\underset{\sim}{E}$,

$$V_{int} = -\underset{\sim}{P}^{\dagger} \underset{\sim}{E} \tag{2-3}$$

Here $\underset{\sim}{\alpha}_{o}$ is the 3nN x 3nN electronic polarizability matrix with nonzero diagonal elements and zero off-diagonal elements. $\underset{\sim}{T}$ is the 3nN x 3nN dipole field propoagation matrix with elements

$$\underset{\sim}{T}_{mm'} = \underset{\sim}{I} / \left| \underset{\sim}{x}(m) - \underset{\sim}{x}(m') \right|^{3}$$

$$- 3(\underset{\sim}{x}(m) - \underset{\sim}{x}(m'))\,(\underset{\sim}{x}(m) - \underset{\sim}{x}(m')) / \left| \underset{\sim}{x}(m) - \underset{\sim}{x}(m') \right|^{5} \tag{2-4}$$

where $\underset{\sim}{I}$ is the 3 x 3 identity matrix, $\underset{\sim}{x}(m)$ and $\underset{\sim}{x}(m')$ are the position

vectors between the sites m and m' with respect to an arbitrarily chosen origin, $\underset{\sim}{x}(m) - \underset{\sim}{x}(m')$ is the distance between m and m', and $(\underset{\sim}{x}(m) - \underset{\sim}{x}(m'))(\underset{\sim}{x}(m) - \underset{\sim}{x}(m'))$ is a dyad and can be written in matrix notation

$$\begin{bmatrix} xx & xy & xz \\ yx & yy & yz \\ zx & zy & zz \end{bmatrix}$$

The local electric field $\underset{\sim}{F}$ which is the field inside the crystal and the external electric field $\underset{\sim}{E}$ differ by the electric field due to the dipoles on the sites in a crystal. The relations between $\underset{\sim}{P}_\ell$, $\underset{\sim}{\alpha}_{o\ell\ell}$, $\underset{\sim}{F}_\ell$, $\underset{\sim}{E}_\ell$, and the intrinsic moment $\underset{\sim}{\mu}_\ell$ in a unit cell ℓ are

$$\underset{\sim}{P}_\ell = \underset{\sim}{\mu}_\ell + \underset{\sim}{\alpha}_{o\ell\ell}\underset{\sim}{F}_\ell \tag{2-5}$$

$$\underset{\sim}{F}_\ell = \underset{\sim}{E}_\ell - \sum_{\ell} \underset{\sim}{T}_{\ell\ell'}\underset{\sim}{P}_{\ell'} \tag{2-6}$$

The elements of the column matrices $\underset{\sim}{P}_\ell$, $\underset{\sim}{E}_\ell$, $\underset{\sim}{\mu}_\ell$, and $\underset{\sim}{F}_\ell$ are the total electric moment, external field, intrinsic moment, and local electric field at each site m in the unit cell. The property of translation symmetry in a crystal permits one to replace the index ℓ with o without loss of generality. Explicitly,

$$\underset{\sim}{P}_o = \begin{bmatrix} P_{1,x} \\ P_{1,y} \\ P_{1,z} \\ \vdots \\ P_{n,x} \\ P_{n,y} \\ P_{n,z} \end{bmatrix}, \quad \underset{\sim}{E}_o = \begin{bmatrix} E_{1,x} \\ E_{1,y} \\ E_{1,z} \\ \vdots \\ E_{n,x} \\ E_{n,y} \\ E_{n,z} \end{bmatrix}, \quad \underset{\sim}{\mu}_o = \begin{bmatrix} \mu_{1,x} \\ \mu_{1,y} \\ \mu_{1,z} \\ \vdots \\ \mu_{n,x} \\ \mu_{n,y} \\ \mu_{n,z} \end{bmatrix}, \quad \underset{\sim}{F}_o = \begin{bmatrix} F_{1,x} \\ F_{1,y} \\ F_{1,z} \\ \vdots \\ F_{n,x} \\ F_{n,y} \\ F_{n,z} \end{bmatrix}$$

and $\underset{\sim}{\alpha}_{oo} = \begin{pmatrix} \underset{\sim}{\alpha}_{o,1} & 0 \cdots & 0 \\ 0 & \underset{\sim}{\alpha}_{o,2} & \vdots \\ \vdots & \ddots & \vdots \\ 0 \cdots & & \underset{\sim}{\alpha}_{o,n} \end{pmatrix}$

Here $E_{1,\alpha} = E_{2,\alpha} = \cdots = E_{n,\alpha}$ for $\alpha = x,y,$ or z,

$$\underset{\sim}{\alpha}_{o,m} = \begin{pmatrix} \alpha_{o,m,x} & 0 & 0 \\ 0 & \alpha_{o,m,y} & 0 \\ 0 & 0 & \alpha_{o,m,z} \end{pmatrix} \quad , \text{ for } m = 1,2,\cdots, n$$

and the n individual sites in a particular unit cell t are designated by a running index. Equation (2-5) and (2-6) are now rewritten as :

$$\underset{\sim}{P}_o = \underset{\sim}{\mu}_o + \underset{\sim}{\alpha}_{oo} \underset{\sim}{F}_o \qquad (2\text{-}5)'$$

$$\underset{\sim}{F}_o = \underset{\sim}{E}_o - \sum_{\ell'} T_{o\ell'} \underset{\sim}{P}_o \qquad (2\text{-}6)'$$

The total potential energy $V_{total} = V_{def} + V_{dip} + V_{int}$ was shown[1] to be

$$1/2\ \underset{\sim}{\mu}^{\dagger} \underset{\sim}{T}(\underset{\sim}{I} + \underset{\sim}{\alpha}_o \underset{\sim}{T})^{-1} \underset{\sim}{\mu} - ((\underset{\sim}{I} + \underset{\sim}{\alpha}_o \underset{\sim}{T})^{-1} \underset{\sim}{\mu})^{\dagger} \underset{\sim}{E}$$

$$- 1/2\ \underset{\sim}{E}^{\dagger} \underset{\sim}{\alpha}_o (\underset{\sim}{I} + \underset{\sim}{\alpha}_o \underset{\sim}{T})^{-1} \underset{\sim}{E}$$

by eliminating $\underset{\sim}{P}$ and $\underset{\sim}{F}$ in (2-1), (2-2), and (2-3) with the relations (2-5) and (2-6). Here the first term is related to the frequency shift, the second to the infrared intensity, and the third to the Raman intensity.

Using the frequency shift term in the potential energy,

$$V_{shift} = 1/2\ \underset{\sim}{\mu}^{\dagger} \underset{\sim}{T}(\underset{\sim}{I} + \underset{\sim}{\alpha}_o \underset{\sim}{T})^{-1} \underset{\sim}{\mu} \qquad (2\text{-}7)$$

Decius[2] formally developed a molecular dipole model of internal optic modes in molecular crystals.

B. Formalism of the molecular dipole model of internal optic modes

Letting q_j be the molecular normal coordinate for some particular vibrational mode j in the unit cell ℓ and assuming that the intrinsic moment is along the α direction the intrinsic vibrationally induced dipole moment $\mu_{\ell,j,\alpha}$ can be expanded as

$$\mu_{\ell,\alpha}(0) + (\partial\mu_\alpha/\partial q_j)_\ell q_{j,\ell} + 1/2\ (\partial\mu_\alpha/\partial q_j)^2_\ell q^2_{j,\ell} + \cdots$$

The case where the intrinsic moment has components along both the α and β directions is discussed in chapter VI. If the permanent dipole moment $\mu_{\ell,\alpha}(0)$ and the electrical anharmonic terms

$$1/2\ (\partial\mu_\alpha/\partial q_j)^2 q^2_{j,\ell} + \cdots$$

are neglected, then

$$\mu_{\ell,j,\alpha} = (\partial\mu_\alpha/\partial q_j)_\ell q_{j,\ell} \tag{2-8}$$

Since $\mu_{\ell,j,\alpha}$ is independent of the unit cell index ℓ, one may re-write (2-8) as :

$$\mu_{\ell,j\ \alpha} = (\partial\mu_\alpha/\partial q_j) q_j \tag{2-9}$$

or in matrix notation

$$\underset{\sim}{\mu}_{\alpha,j} = (\partial\mu_\alpha/\partial\ q_j)\underset{\sim}{q}_j \tag{2-10}$$

Equation (2-7) now turns out to be

$$V_{shift,j} = 1/2\ \underset{\sim}{q}^\dagger_j \underset{\sim}{T}_{\alpha\alpha}(\underset{\sim}{I} + \underset{\sim}{\alpha}_{o,\alpha\alpha}\underset{\sim}{T}_{\alpha\alpha})^{-1}\underset{\sim}{q}_j(\partial\mu_\alpha/\partial q_j)^2 \tag{2-11}$$

Besides V_{shift}, there is an additional contribution to the total vibrational potential energy from the intramolecular vibrational potential energy $V_{o,j}$.

$$V_{o,j} = 1/2\ \underset{\sim}{q}_j^{\dagger}\ \omega_o^2\ \underset{\sim}{I}\ \underset{\sim}{q}_j \tag{2-12}$$

The static crystal frequency $\omega_{o,j}$ is determined by site group effects. The total vibrational potential energy of the jth mode is now

$$V_j = V_{o,j} + V_{shift,j} = 1/2\ \underset{\sim}{q}_j^{\dagger}(\omega_{o,j}^2 \underset{\sim}{I} + \underset{\sim}{T}_{\alpha\alpha}(\underset{\sim}{I} + \underset{\sim}{\alpha}_{o,\alpha\alpha}\underset{\sim}{T}_{\alpha\alpha})^{-1}$$

$$\text{x}\ \ (\partial\mu_\alpha/\partial q_j)^2)\underset{\sim}{q}_j \tag{2-13}$$

The localized coordinate $q_{j,\ell}$ can be transformed to a delocalized phonon coordinate $W(\underset{\sim}{k}_j)$ by the Wigner projection operator.

$$W(\underset{\sim}{k}_j) = 1/N^{1/2} \sum_{\ell=1}^{N} q_{j,\ell}\ \exp[-i\ \underset{\sim}{k}\cdot\underset{\sim}{x}(\ell)] \tag{2-14}$$

or in matrix notation

$$\underset{\sim}{W}_j = \underset{\sim}{X}\ \underset{\sim}{q}_j \tag{2-15}$$

where

$$\underset{\sim}{X}_{k,\ell} = 1/N^{1/2}\ \ \exp[\ i\ \underset{\sim}{k}\cdot\underset{\sim}{x}(\ell)]$$

and $\underset{\sim}{k}$ is the wave vector restricted to the first Brillouin zone. In terms of $\underset{\sim}{W}_j$, V_j can be written as :

$$1/2\ \underset{\sim}{W}_j^{\dagger}[\omega_{o,j}^2 \underset{\sim}{I}\ + \underset{\sim}{S}_{\alpha\alpha}(\underset{\sim}{k})(\underset{\sim}{I} + \underset{\sim}{\alpha}_{o,\alpha\alpha}\ \underset{\sim}{S}_{\alpha\alpha}(\underset{\sim}{k}))^{-1}(\partial\mu_\alpha/\partial q_j)^2]\underset{\sim}{W}_j \tag{2-16}$$

where

$$\underset{\sim}{S}_{\alpha\alpha}(\underset{\sim}{k}) = \underset{\sim}{X}\underset{\sim}{T}_{\alpha\alpha}\underset{\sim}{X}^{-1} \qquad (\ \underset{\sim}{k} = \underset{\sim}{k}'\ )$$

$\underset{\sim}{S}_{\alpha\alpha}$ is diagonal in $\underset{\sim}{k}$ space since

$$\underset{\sim}{S}_{\alpha\alpha}(\underset{\sim}{k}\underset{\sim}{k}') = \underset{\sim}{X}\underset{\sim}{T}_{\alpha\alpha}\underset{\sim}{X}^{-1}$$

$$= 1/N \sum_{\ell\ell'} \underset{\sim}{T}_{\alpha\alpha,\ell\ell'} \exp[-i\, \underset{\sim}{k}\cdot\underset{\sim}{x}(\ell)] \exp[i\, \underset{\sim}{k}'\cdot\underset{\sim}{x}(\ell')]$$

$$= \underset{\sim}{S}_{\alpha\alpha}(k)\, \delta_{kk'}$$

In the case of $k \simeq 0$ (the center of the Brillouin zone)

$$\underset{\sim}{S}_{\alpha\alpha}(0) = 1/N \sum_{\ell\ell'} \underset{\sim}{T}_{\alpha\alpha,\ell\ell'} = \sum_{\ell'} \underset{\sim}{T}_{\alpha\alpha,\ell\ell'} \qquad (2\text{-}17)$$

The treatment developed so far is appropriate for a simple crystal containing one molecule per unit cell. However, it is easy to generalize the formulae obtained to a crystal with n molecules per unit cell by simply enlarging the dimensions of the matrices and vectors. For instance, $\underset{\sim}{\mu}$ for a crystal with n molecules per unit cell is

$$\underset{\sim}{\mu} = \begin{bmatrix} \underset{\sim}{\mu}_1 \\ \underset{\sim}{\mu}_2 \\ \vdots \\ \underset{\sim}{\mu}_\ell \\ \vdots \\ \underset{\sim}{\mu}_N \end{bmatrix}, \text{ where } \underset{\sim}{\mu}_\ell = \begin{bmatrix} \underset{\sim}{\mu}_{\ell,1} \\ \underset{\sim}{\mu}_{\ell,2} \\ \vdots \\ \underset{\sim}{\mu}_{\ell,n} \end{bmatrix}, \text{ and } \underset{\sim}{\mu}_\ell = \begin{bmatrix} \mu_{\ell,i,x} \\ \mu_{\ell,i,y} \\ \mu_{\ell,i,z} \end{bmatrix}$$

(N dimensional) (n dimensional) (3 dimensional)

In crystals with more than one molecule per unit cell, the vibrationally induced dipoles in the unit cell form combinations (correlate under the factor group) which are characterized by the irreducible representations of the factor group. Let γ refer to a particular irreducible representation of the factor group and m to all identical molecular units in a unit cell. A new unit cell symmetrized coordinate[3] is :

$$Q(\underset{\sim}{k}_{j\gamma}) = \sum_m B(\underset{\sim}{k}\underset{\sim}{k}_{\gamma m})\ W(\underset{\sim}{k}_{mj}) \qquad (2\text{-}18)$$

The transformation matrix B is block diagonal in $\underset{\sim}{k}$. In terms of this new cooedinate the potential energy V_j in (2-13) turns out to be

$$1/2\ Q(\underset{\sim}{k}_{j\gamma})\ [\omega_o^2 + S_{\alpha\alpha}(\underset{\sim}{k}_{\gamma})\ (I + \alpha_{o,\alpha\alpha}S_{\alpha\alpha}(\underset{\sim}{k}_{\gamma}))^{-1}(\partial\mu_\alpha/\partial q_j)^2]\ Q(\underset{\sim}{k}_{j\gamma}) \quad (2\text{-}19)$$

Comparing (2-19) with

$$V_j = 1/2\ Q(\underset{\sim}{k}_{j\gamma})\ \omega^2(\underset{\sim}{k}_{j\gamma})\ Q(\underset{\sim}{k}_{j\gamma}) \quad (2\text{-}20)$$

one has immediately that

$$\omega^2(\underset{\sim}{k}_{j\gamma}) = \omega_o^2(j) + S_{\alpha\alpha}(\underset{\sim}{k}_{\gamma})\ (I + \alpha_{o,\alpha\alpha}S_{\alpha\alpha}\ (\underset{\sim}{k}_{\gamma}))^{-1}(\partial\mu_\alpha/\partial q_j)^2 \quad (2\text{-}21)$$

Here $\omega(\underset{\sim}{k}_{j\gamma})$ is the vibrational frequency of the phonon mode including the effect of dipolar coupling, and

$$S_{\alpha\alpha}(\underset{\sim}{k}_{\gamma})\ (I + \alpha_{o,\alpha\alpha}S_{\alpha\alpha}(\underset{\sim}{k}_{\gamma}))^{-1}(\partial\mu_\alpha/\partial q_j)^2$$

is the dipolar coupling shift term. The difference between $\omega_o(j)$ and $\omega(\underset{\sim}{k}_{j\gamma})$ is called the site group-factor group correlation splitting.

For modes near $\underset{\sim}{k} = 0$

$$\omega^2(\gamma_j) = \omega_o^2(j) + S_{\alpha\alpha}\ (\gamma)\ (I + \alpha_{o,\alpha\alpha}S_{\alpha\alpha}(\gamma))^{-1}(\partial\mu_\alpha/\partial q_j)^2 \quad (2\text{-}22)$$

C. Calculation of S

The dipolar interaction matrix S may be calculated from its definition,

$$\underset{\sim}{S}_{\alpha\alpha}\ (\underset{\sim}{k}) = 1/N\ \Sigma_{\ell\ell'}\ \underset{\sim}{T}_{\alpha\alpha}\ \ell\ell'\ \exp[i\ \underset{\sim}{k}\cdot(\underset{\sim}{x}(\ell) - \underset{\sim}{x}(\ell'))] \quad (2\text{-}23)$$

Howerer, it converges very slowly. In a paper by Nijboer and deWette[4]

a method for calculating the slowly convergent series is discussed. Suppose $f(x)$ is a smooth function and $S = \sum_{n=1}^{\infty} f(n)$ converges slowly. The method consists in introducing an auxiliary function $F(x)$ for which $F(0)$ is finite and which approaches zero quickly as $x \to \infty$. We may write

$$S = \sum_{n=1}^{\infty} f(n)F(n) + \sum_{n=1}^{\infty} f(n)[1 - F(n)] \qquad (2\text{-}24)$$

The first series in (2-24) will have good convergence whereas the second series will have the same rate of convergence as the original expression. Since the Fourier transform of a smooth function is a function which approaches zero rapidly for increasing argument, we may expect that the "flatter" the function $f(x)[1 - F(x)]$ is, the better the convergence of the Fourier transform (FT) of $\Sigma f(n)[1 - F(n)]$ will be. With the relation

$$\Sigma\, f(n)[1 - F(n)] = \Sigma\, \mathrm{FT}[f(n)]\, \mathrm{FT}[1 - F(n)] \qquad (2\text{-}25)$$

(2-24) can now be calculated with rapid convergence.

Ewald[5] had used this method to derive a quickly converging series for calculating S in 1921. His formula for the ith component of S, in a more convenient notation[6,7] than the earier paper, is

$$S_i = \sum_{\text{direct lattice}} [(1/t^3 - 3t_i^2/t^5)G(\varepsilon t) + 2\varepsilon/\pi^{1/2} \times (1/t^2 - 3t_i^2/t^4) \exp[-(\varepsilon t)^2] - 4\varepsilon^3/\pi^{1/2}\, t_i^2/t^2 \times \exp[-(\varepsilon t)^2]]$$

$$+ 4\pi/v \sum_{\substack{\text{reciprocal}\\ \text{lattice}}} [(k_i/k)^2 \exp(-k^2/4\varepsilon^2)] - 4\varepsilon^3/3\pi^{1/2} \quad (2\text{-}26)$$

In this equation v is the volume of the unit cell and k_i is the ith component of a reciprocal lattice vector $\underset{\sim}{k}$ whose absolute value is indicated by k. The quantities t_i and t have an analogous meaning in the direct space lattice. Also, $G(\varepsilon t)$ is equal to $1 - \mathrm{erf}(\varepsilon t)$ where $\mathrm{erf}(\varepsilon t)$ denotes the error function and $\varepsilon (= \pi^{1/2} v^{-1/3})$ is a parameter chosen to simultaneously ensure rapid convergence of the direct lattice sum and the reciprocal lattice sum.

The trace of S was shown by Mueller[8] to be $-4\pi/v$. The invariance of the trace and its value for a dipolar summation over any lattice or sublattice provide a useful check on the numerical methods used to obtain S.

Once the dipolar interaction matrix $\underset{\sim}{S}_{\alpha\alpha}(\underset{\sim}{k})$ is constructed with elements $S_{\alpha\alpha}(\underset{\sim}{k}^{mm'})$ which are the dipole sums between a site m and all sites in the crystal translationally equivalent to site m' one needs to transform it into a form containing $S_{\alpha\alpha}(\underset{\sim}{k}_\gamma)$, the dipole sums of particular irreducible representations γ of the factor group, since it is $S_{\alpha\alpha}(\underset{\sim}{k}_\gamma)$ that appears in (2-21). The transformation is discussed in chapter III.

C. Vibrational Dynamics of the Solid State

a. General description[9,10]

A crystal with n atoms per unit cell and $N = N_1 \times N_2 \times N_3$ units cells has 3nN vibrational degrees of freedom. There will be three branches of acoustic modes ($\omega \to 0$ as $\underset{\sim}{k} \to 0$) and 3n - 3 branches of optic modes ($\omega \not\to 0$ as $\underset{\sim}{k} \to 0$). Each of the 3n branches has N normal modes labeled by the wave vector $\underset{\sim}{k}$. The 3n - 3 branches of optic modes can be divided into two groups, one composed of external modes which are primarily due to intermolecular vibrations of the crystal lattice with frequencies usually less than 300 cm^{-1}; the other composed of internal modes which are primarily

due to intramolecular vibrations of molecular species in the crystal with frequencies greater than 300 cm^{-1}. In many cases the internal modes and external modes may be treated as decoupled. The wave vector $\underset{\sim}{k}$ can be restricted to the first Brillouin zone by writing

$$\underset{\sim}{k} = \ell_1/N_1\ \hat{b}_1 + \ell_2/N_2\ \hat{b}_2 + \ell_3/N_3\ \hat{b}_3$$

where $\ell_1 = 0,1,\cdots,N_1-1$; $\ell_2 = 0,1,\cdots,N_2-1$; $\ell_3 = 0,1,\cdots,N_3-1$. The vectors $\hat{b}_1$, $\hat{b}_2$, $\hat{b}_3$ are the bases of the reciprocal lattice in reciprocal space.

This physical picture can be easily understood with the aid of dispersion diagram which gives $\nu(\underset{\sim}{k})$ for the various branches as a function of $\underset{\sim}{k}$ for some particular direction in the first Brillouin zone.

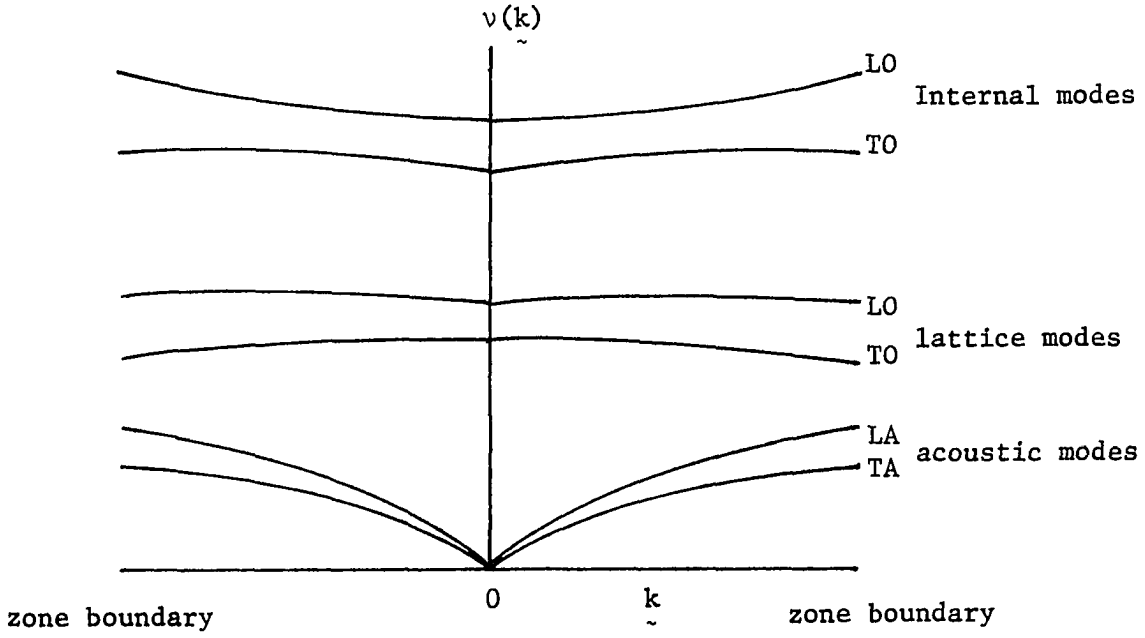

Here L designates the longitudinal motion in which the direction of the vibration of the particles is in the same direction as $\underset{\sim}{k}$, while T denotes the transverse motion in which the direction of the vibration of the particles is perpendicular to $\underset{\sim}{k}$.

b. Selection rules[9]

When a photon with frequency ν_{pt} and wave vector $\underset{\sim}{k}_{pt}$ interacts with vibrational mode of the crystal (phonon with frequency ν_{pn} and wave vector $\underset{\sim}{k}_{pn}$) the following conditions must be satisfied :

$$h\nu_{pt} = h\nu_{pn} \qquad \text{(energy conservation)} \tag{2-28}$$

$$\hbar\underset{\sim}{k}_{pt} = \hbar\underset{\sim}{k}_{pn} \qquad \text{(wave vector conservation)} \tag{2-29}$$

Since $\underset{\sim}{k}_{pt} \simeq 0$ and a light wave is a transverse electromagnetic field only transverse phonons with $\underset{\sim}{k} \simeq 0$ may be excited by direct absorption of the photon.

Additional selection rules arise from the symmetry properties of the phonons which govern whether phonons are infrared active or Raman active. This problem is adaquetely discussed in the standard texts on group theory.[11,12]

c. Calculation of the dispersion curve with the molecular dipole model

The formula derived in section B for the frequency of some normal mode

$$\omega^2(\underset{\sim}{k}_j) = \omega_o^2(j) + S_{\alpha\alpha}(\underset{\sim}{k}_\gamma)[I + \alpha_{o,\alpha\alpha}S_{\alpha\alpha}(\underset{\sim}{k}_\gamma)]^{-1}(\partial\mu_\alpha/\partial q_j)^2 \tag{2-21}$$

applies to transverse modes only. For longitudinal modes, we have to add $4\pi/v$ to S. This is discussed in the paper by Frech and Decius.[13]

The factor group of the crystal at points in the Brillouin zone other than the center in general will be different than the factor group at the Brillouin zone center. Therefore, if one wants

to use (2-21) to calculate the dispersion curve for a particular branch it is necessary to consider the appropriate γ for different k. Howerer, for crystals like NaN_3 and $KBrO_3$ with one molecule per unit cell $S_{\alpha\alpha}[I + \alpha_{o,\alpha\alpha}S_{\alpha\alpha}]^{-1}$ is independent of γ and (2-21) can easily be used to calculate the dispersion curves and frequency distribution functions.[14,15]

References for Chapter II

1. M. Mandel and P. Mazur, Physica 24, 116 (1958).

2. J. C. Decius, J, Chem. Phys. 49, 1387 (1968).

3. R. Frech, J. Chem. Phys. 58, 5067 (1973).

4. B. R. A. Nijboer and F. W. DeWette, Physica 23, 309 (1957).

5. P. P. Ewald, Ann. Phys. (Leipz) 64, 253 (1921).

6. C. Kittel, Introduction to Solid State Physics, Wiley, New York, 1953, 2nd ed., Appendix I.

7. R. Frech, J. Chem. Phys. 58, 2177 (1973).

8. H. Mueller, Phys. Rev. 47, 947 (1935).

9. C. Kittel, Introduction to Solid State Physics, Wiley, New York, 1971, 4th ed.

10. M. Born and K. Huang, Dynamical Theory of Crystal Lattices, Oxford University Press, London, 1954.

11. E. Bright Wilson, Jr., J. C. Decius, and Paul C. Cross, Molecular Vibrations, McGraw-Hill, New York, 1955.

12. G. F. Koster, Solid State Phys. 5, 173 (1957).

13. R. Frech and J. C. Decius, J. Chem. Phys. 51, 1536 (1969).

14. R. Frech, J. Chem. Phys. 60, 2354 (1974).

15. A. Maradudin, E. Montroll, and G. Weiss, Theory of Lattice Dynamics in the Harmonic Approximation, Academic Press, New York, 1963.

CHAPTER III

Crystal Structures, Site Symmetries, and Unit Cell Groups

This chapter contains the appropriate structural data and symmetry properties of each crystal studied. Included are : (1) the structure of the unit cell with the site symmetry of the sulfate ion, (2) the correlation diagram for the vibrational modes of the sulfate ion under the point group approximation, site group approximation, and unit cell group analysis together with the irreducible representations and the transformation properties, and (3) the symmetry operations of the unit cell group which are shown in a standard character table and in a diagram denoting their locations in the unit cell.

It is necessary to use the projection operator to obtain the properly symmetrized linear combination of the sites in the unit cell in order to calculate the $\underset{\sim}{S}$ matrix. This problem is equivalent to transforming the matrix $\underset{\sim}{S}'$ with $(s_1, s_2, \cdots, s_n)$ as a basis where $s_1, s_2, \cdots, s_n$ are the sites (or more correctly, the x, y, or z coordinate at each site) in the unit cell, into a new matrix $\underset{\sim}{S}$ with the basis $(R_1, R_2, \cdots, R_m)$ where $R_1, R_2, \cdots$, and R_m are linear combinations of $s_1, s_2, \cdots, s_n$. The proper linear combinations for each irreducible representation of the unit cell group are presented for each crystal.

$LiKSO_4$

Crystals of lithium potassium sulfate[1] are hexagonal with a bimolecular cell with edges $a_o = 5.1457$ Å, and $c_o = 8.6298$ Å (26^oC) The space group is C_6^6 $(P6_3)$ and atoms are put in the positions :

K(2a) : 0,0,u ; 0,0,u + 1/2 with u = 0

S(2b) : 1/3,2/3,u ; 2/3,1/3,u + 1/2 with u = 0.17

O(1)(2b) : with u = 0

O(2)(6c) : x,y,z ; $\bar{y}$,x - y,z ; y - x,$\bar{x}$,z ; $\bar{x}$,$\bar{y}$,z + 1/2 ;
y,y - x,z + 1/2 ; x - y,x,z + 1/2 with x = 0.33,
y = 0.94, z = 0.25

The lithium atoms are presumed to occupy another set of (2b) with a value of u greater than 1/2. For simplicity in calculating $\underset{\sim}{S}$ matrix a lithium atom is assumed to be at an equal distance from the two sulfate ions (1/3,2/3,0.17) and (1/3,2/3,1.17), i.e. u = 0.67.

The site group of the sulfate ion is C_3, the unit cell group is C_6^6, and the correlation table[2] is

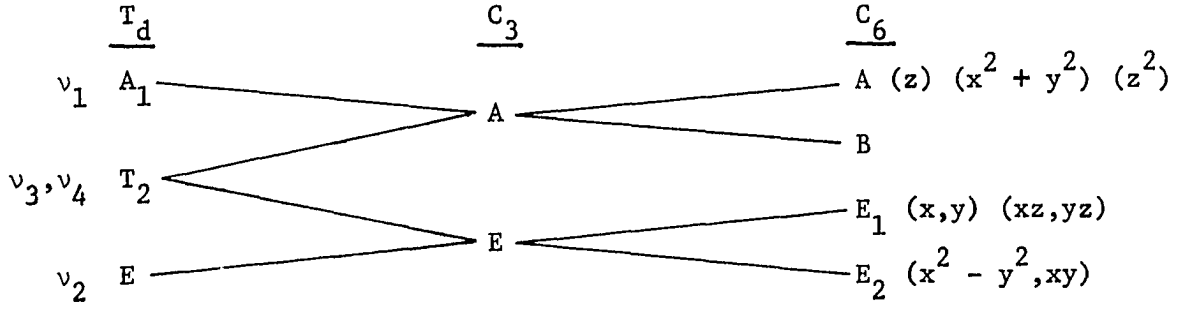

The symmetry operations of the unit cell group in a standard character table[2] and their locations denoted as (operator) in the unit cell[3] are shown in Figure (3-1).

The various atoms in the unit cell are denoted by Li(1), Li(2), K(1), K(2), S(1), and S(2) are located at the sites (1/3,2/3,0.67), (2/3,1/3,0.17), (0,0,0), (0,0,1/2), (1/3,2/3,0.17), and (2/3,1/3,0.67), respectively. The normalized linear combinations of sites which belong to the irreducible representations A, B, E_1, and E_2 of the unit cell group C_6^6 are :

Figure (3-1)

(1) Character table of C_6

C_6	E	C_6	C_3	C_2	C_3^2	C_6^5		
A	1	1	1	1	1	1	z	$x^2 + y^2$, z^2
B	1	-1	1	-1	1	-1		
E_1	2	1	-1	-2	-1	1	(x,y)	(xz,yz)
E_2	2	-1	-1	2	-1	-1		$(x^2 - y^2, xy)$

(2) Locations of symmetry operations in the unit cell group C_6^6

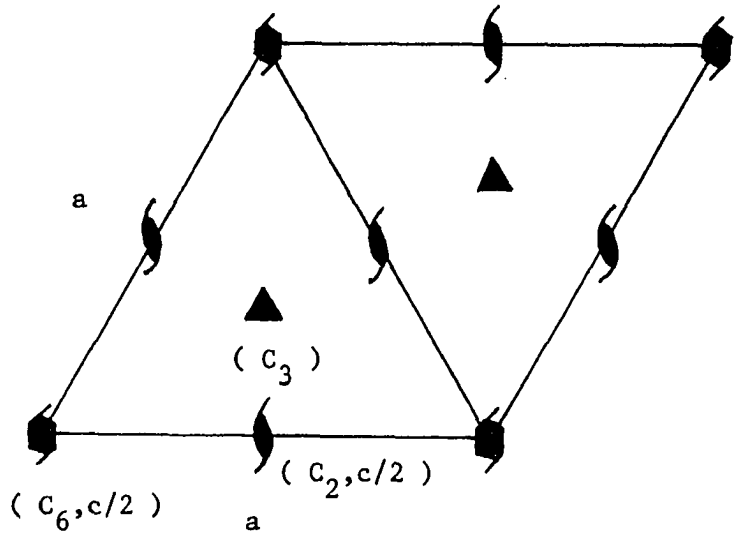

$$A, E_1 : 1/2^{1/2}\,[Li(1) + Li(2)],\ 1/2^{1/2}\,[K(1) + K(2)],$$
$$1/2^{1/2}\,[S(1) + S(2)]$$
$$B, E_2 : 1/2^{1/2}\,[Li(1) - Li(2)],\ 1/2^{1/2}\,[K(1) - K(2)],$$
$$1/2^{1/2}\,[S(1) - S(2)]$$

$KNaSO_4$

Potassium sodium sulfate[1] has a hexagonal unit with edges $a_o = 5.643$ Å, $c_o = 7.269$ Å and two molecules per unit cell. The space group is D_{3d}^3 ($P\bar{3}m1$). Atoms have been put in the following special positions :

Na(1)(1a) : 0,0,0

Na(2)(1b) : 0,0,1/2

K(2d) : $\pm(1/3,2/3,u)$ $u = 0.618$

S(2d) : with $u = 0.220$

O(1)(2d) : with $u = 0.000$

O(2)(6i) : $\pm(u,\bar{u},v\ ;\ u,2u,v\ ;\ 2\bar{u},\bar{u},v)$ with $u = 0.200$, $v = 0.294$

It is also reported[1] that Na(2) can be replaced by K^+ with the formation of K_3NaSO_4 which has the same space group and the same site symmetries for Na^+, K^+, S, O(1), and O(2) as in $KNaSO_4$. There are only small changes in the unit cell edges ($a_o = 5.66$ Å, $c_o = 7.33$ Å) and the locations of sites ($u = 0.625$ for K^+ and $u = 0.23$ for S) which are not expected to significantly affect the internal optic modes.

The site group of the sulfate ion is C_{3v}, the unit cell group is D_{3d}^3, and the correlation table[2] is

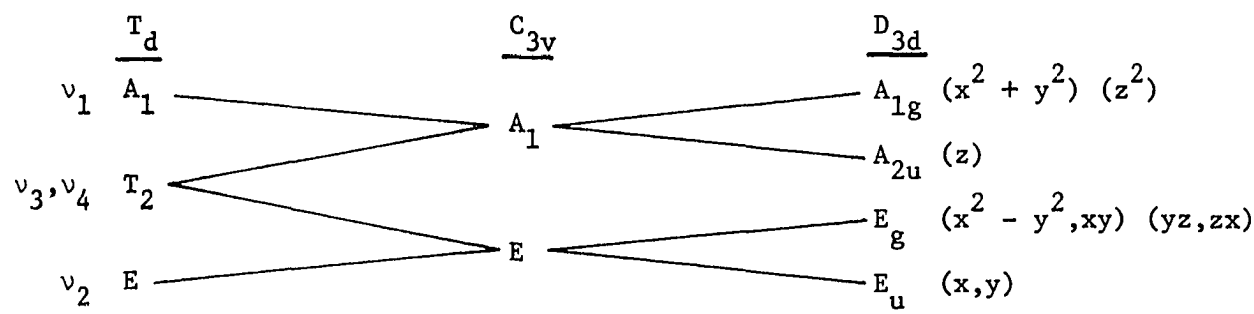

The symmetry operations of the unit cell group in a standard character table[2] and their locations denoted as (operator) in the unit cell[3] are shown in Figure (3-2).

If the atoms denoted by K(1), K(2), Na(1), Na(2),S(1), and S(2) are located on the respective sites (2/3,1/3,0.382), (1/3,2/3,0.618), (0,0,0), (0,0,1/2), (1/3,2/3,0.220), and (2/3,1/3,0.780) then the normalized linear combinations of sites for the irreducible representations A_{1g}, A_{2u}, E_g, and E_u of the unit cell group D_{3d}^3 are :

A_{1g}, E_g : $1/2^{1/2}$ [K(1) - K(2)], $1/2^{1/2}$ [S(1) - S(2)]

A_{2u}, E_u : Na(1), Na(2), $1/2^{1/2}$ [K(1) + K(2)],

$1/2^{1/2}$ [S(1) + S(2)]

Na_2SO_4

Crystals of sodium sulfate[1] are orthorhombic with eight molecules per unit cell with edge lengths: a_o = 9.821 Å, b_o = 12.304 Å, c_o = 5.863 Å (25°C). (The crystallographic axes have been relabeled to conform to the convention for orthorhombic system c<a<b.) The space group is D_{2h}^{24} (F_{ddd}) and atoms are put in the positions :

Na(16g) : ±(u,1/8,1/8 ; 1/4 - u,1/8,1/8) ; F.C. u = 0.436

S(8a) : ±(1/8,1/8,1/8) ; F.C.

O(32h) : ±(x,y,z ; x,1/4 - y,1/4 - z ; 1/4 - x,y,1/4 - z ;

1/4 - x,1/4 - y,z) ; F.C. with x = -0.022,

y = 0.056, z = 0.214

Here F.C.(face-centered) means that the stated coordinates are to be repeated about the remaining three lattice points 0,1/2,1/2 ; 1/2,0,1/2 ; 1/2,1/2,0.

Figure (3-2)

(1) Character table of D_{3d}

D_{3d}	E	$2C_3$	$3C_2$	i	$2S_6$	$3\sigma_d$		
A_{1g}	1	1	1	1	1	1		$x^2 + y^2$, z^2
A_{2u}	1	1	-1	-1	-1	1	z	
E_g	2	-1	0	2	-1	0		$(x^2 - y^2, xy)(yz, zx$
E_u	2	-1	0	-2	1	0	(x,y)	

(2) Locations of symmetry operations in the unit cell group D_{3d}^3

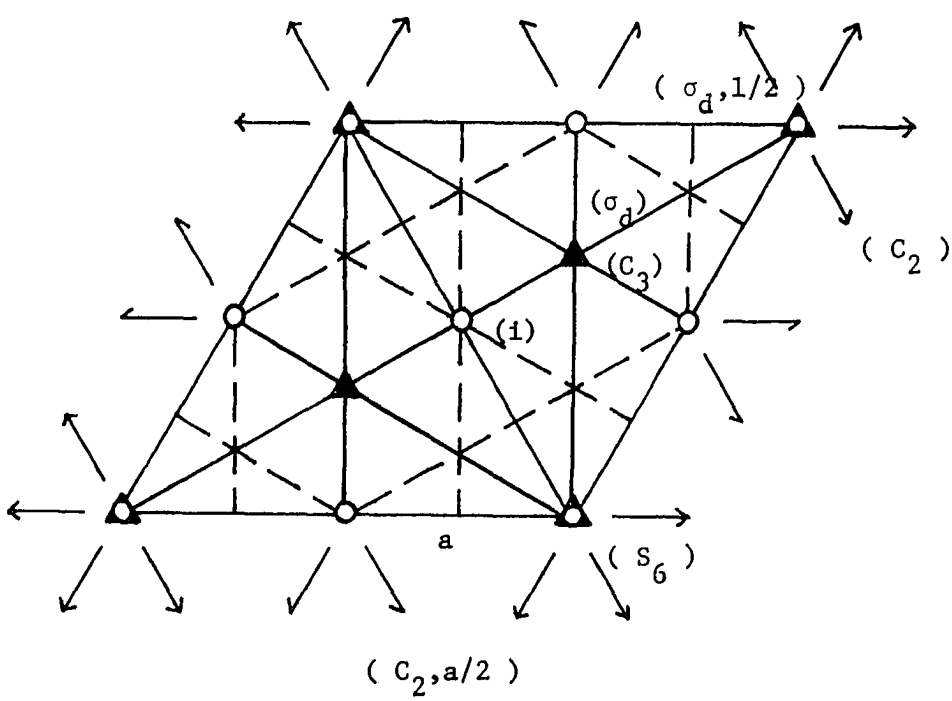

The site group of the sulfate ion is D_2, the unit cell group is D_{2h}^{24}, and the correlation table[2] is

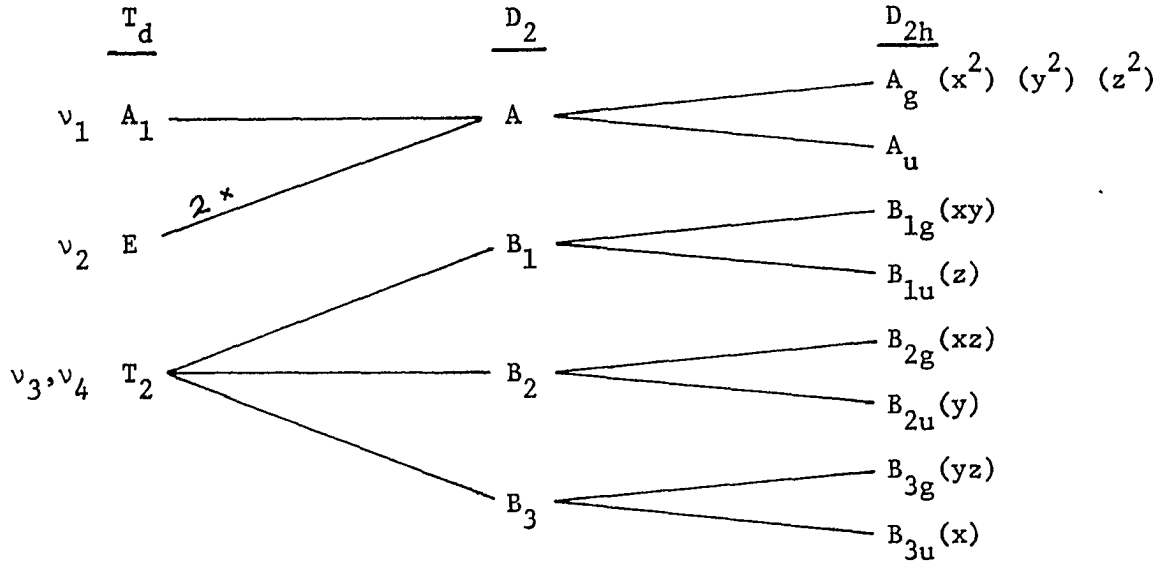

The symmetry operations of the unit cell group in a standard character table[2] and their locations denoted as (operator) in the unit cell[3] are shown in Figure (3-3).

The coordinates of the various atoms are :

Na(1) : 0.436,1/8,1/8	;	Na(2) : 0.936,5/8,1/8
Na(3) : 0.936,1/8,5/8	;	Na(4) : 0.436,5/8,5/8
Na(5) : -0.436,-1/8,-1/8	;	Na(6) : 0.064,3/8,-1/8
Na(7) : 0.064,-1/8,3/8	;	Na(8) : -0.436,3/8,3/8
Na(9) : -0.186,1/8,1/8	;	Na(10) : 0.314,5/8,1/8
Na(11) : 0.314,1/8,5/8	;	Na(12) : -0.186,5/8,5/8
Na(13) : 0.186,-1/8,-1/8	;	Na(14) : 0.686,3/8,-1/8
Na(15) : 0.686,-1/8,3/8	;	Na(16) : 0.186,3/8,3/8
S(1) : 1/8,1/8,1/8	;	S(2) : 5/8,5/8,1/8
S(3) : 5/8,1/8,5/8	;	S(4) : 1/8,5/8,5/8
S(5) : -1/8,-1/8,-1/8	;	S(6) : 3/8,3/8,-1/8
S(7) : 3/8,-1/8,3/8	;	S(8) : -1/8,3/8,3/8

Figure (3-3)

(1) Character table of D_{2h}

D_{2h}	E	$C_2(z)$	$C_2(y)$	$C_2(x)$	i	$\sigma(xy)$	$\sigma(xz)$	$\sigma(yz)$		
A_g	1	1	1	1	1	1	1	1		x^2, y^2, z^2
B_{1g}	1	1	-1	-1	1	1	-1	-1		xy
B_{2g}	1	-1	1	-1	1	-1	1	-1		xz
B_{3g}	1	-1	-1	1	1	-1	-1	1		yz
A_u	1	1	1	1	-1	-1	-1	-1		
B_{1u}	1	1	-1	-1	-1	-1	1	1	z	
B_{2u}	1	-1	1	-1	-1	1	-1	1	y	
B_{3u}	1	-1	-1	1	-1	1	1	-1	x	

(2) Locations of symmetry operations in the unit cell group D_{2h}^{24}

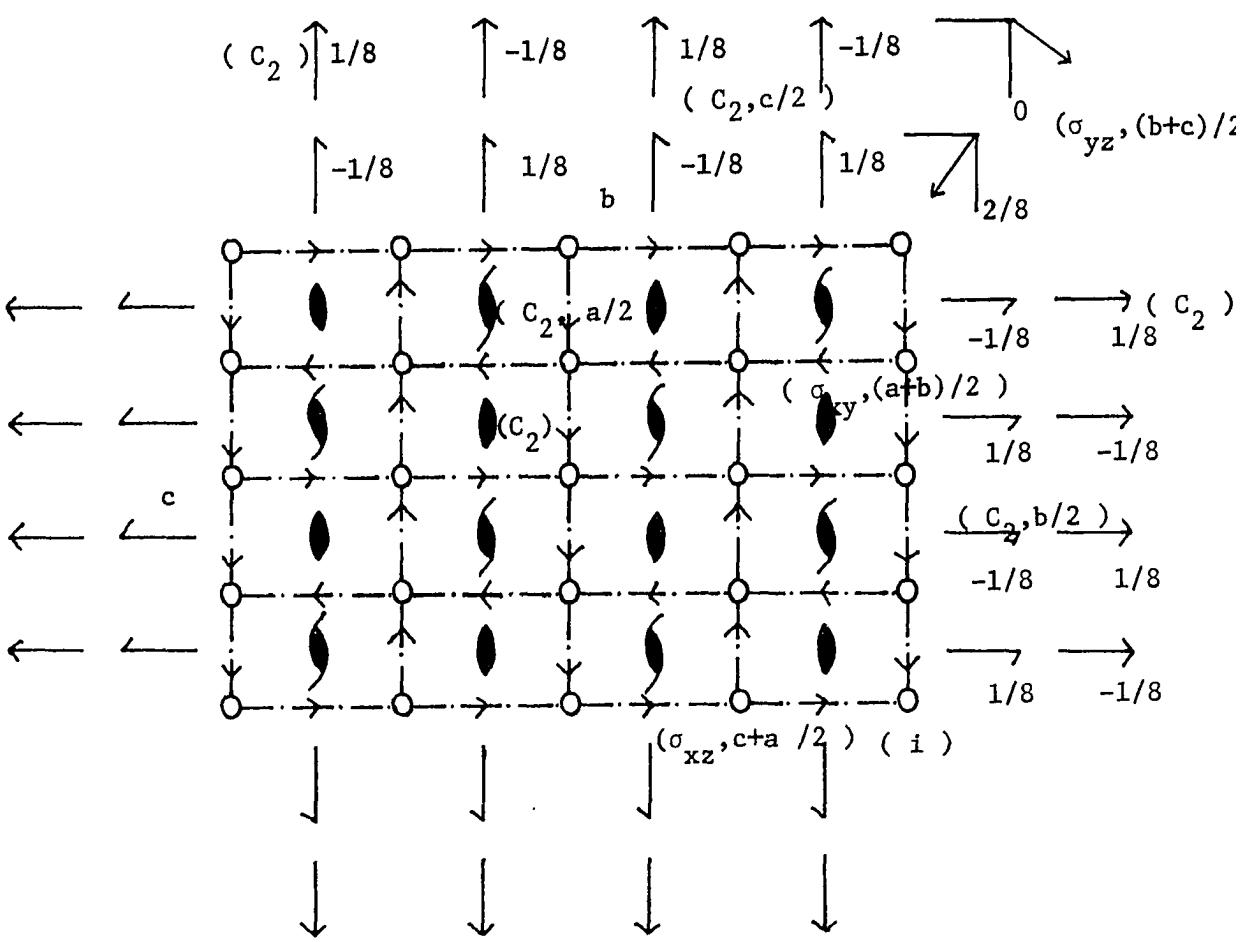

The normalized linear combinations of sites for the irreducible repredentations B_{1g}, B_{1u}, B_{2g}, B_{2u}, B_{3g}, and B_{3u} of the unit cell group D_{2h}^{24} are :

$$B_{1g}, B_{2g}, B_{3g} : 1/8^{1/2} \left[\sum_{i=1}^{4} Na(i) - \sum_{i=5}^{8} Na(i) \right],$$

$$1/8^{1/2} \left[\sum_{i=9}^{12} Na(i) - \sum_{i=13}^{16} Na(i) \right],$$

$$1/8^{1/2} \left[\sum_{i=1}^{4} S(i) - \sum_{i=5}^{8} S(i) \right]$$

$$B_{1u}, B_{2u}, B_{3u} : 1/8^{1/2} \left[\sum_{i=1}^{8} Na(i) \right],$$

$$1/8^{1/2} \left[\sum_{i=9}^{16} Na(i) \right],$$

$$1/8^{1/2} \left[\sum_{i=1}^{8} S(i) \right]$$

K_2SO_4

Crystals of potassium sulfate[1] are orthorhombic with a tetramolecular cell of edge lengths : $a_o = 7.483$ Å, $b_o = 10.072$ Å, $c_o = 5.772$ Å (at 25^oC). (The crystallographic axes have been relabeled to conform to the convention for orthorhombic system c<a<b.) The space group is D_{2h}^{16} (P_{nma}) and atoms are put in the positions :

K(1)(4c) : $\pm$(u,v,1/4 ; u + 1/2,1/2 - v,1/4)
with u = 0.6768, v = 0.4182

K(2)(4c) : with u = -0.0115, v = -0.2954

S(4c) : with u = 0.2358, v = 0.4155

O(1)(4c) : with u = 0.0315, v = 0.4032

O(2)(4c) : with u = 0.2970, v = 0.5579

O(3)(8d) : $\pm$(x,y,z ; x + 1/2,1/2 - y,1/2 - z ; x,y,1/2 - z ; 1/2 - x,y + 1/2,$\bar{z}$) with x = 0.2997, y = 0.3484, z = 0.0410

The site group of the sulfate ion is C_s ($\sigma_h = \sigma_{xy}$), the unit cell group is D_{2h}^{16}, and the correlation table[2] is

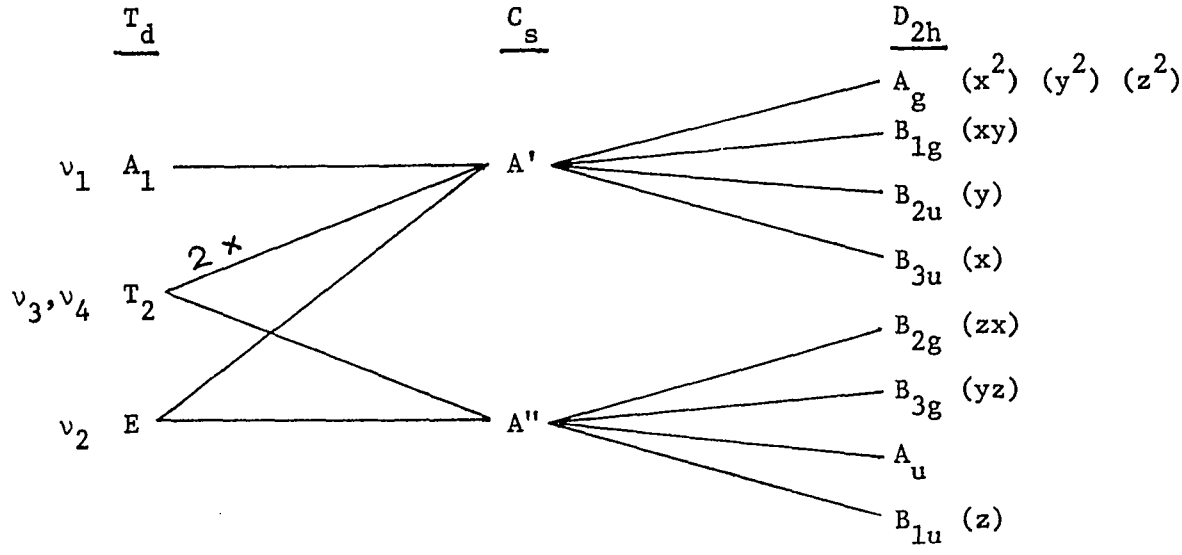

The character table of the point group isomorphic to the unit cell group is identical to that of Na_2SO_4 as shown in Figure (3-3).

The locations of the symmetry operations denoted as (operator) in the unit cell[3] are shown in Figure (3-4).

The properly symmetrized linear combinations are the subject of chapter VI because of their signigicance.

$K_2Mg_2(SO_4)_3$

Crystals of potassium magnesium sulfate[1] are cubic with a tetramolecular cell of edge length $a_o = 9.920$ A. The space group is T^4 ($P_{2_1}3$) and atoms are put in the positions :

K(1)(4a) : u,u,u ; u + 1/2,1/2 - u,$\bar{u}$; $\bar{u}$,u + 1/2,1/2 - u ;

1/2 - u,$\bar{u}$,u + 1/2 with u = 0.068

K(2)(4a) : with u = 0.297

Mg(1)(4a) : with u = 0.584

Mg(2)(4a) : with u = 0.850

Figure (3-4) Locations of symmetry operations in the unit cell group D_{2h}^{16}

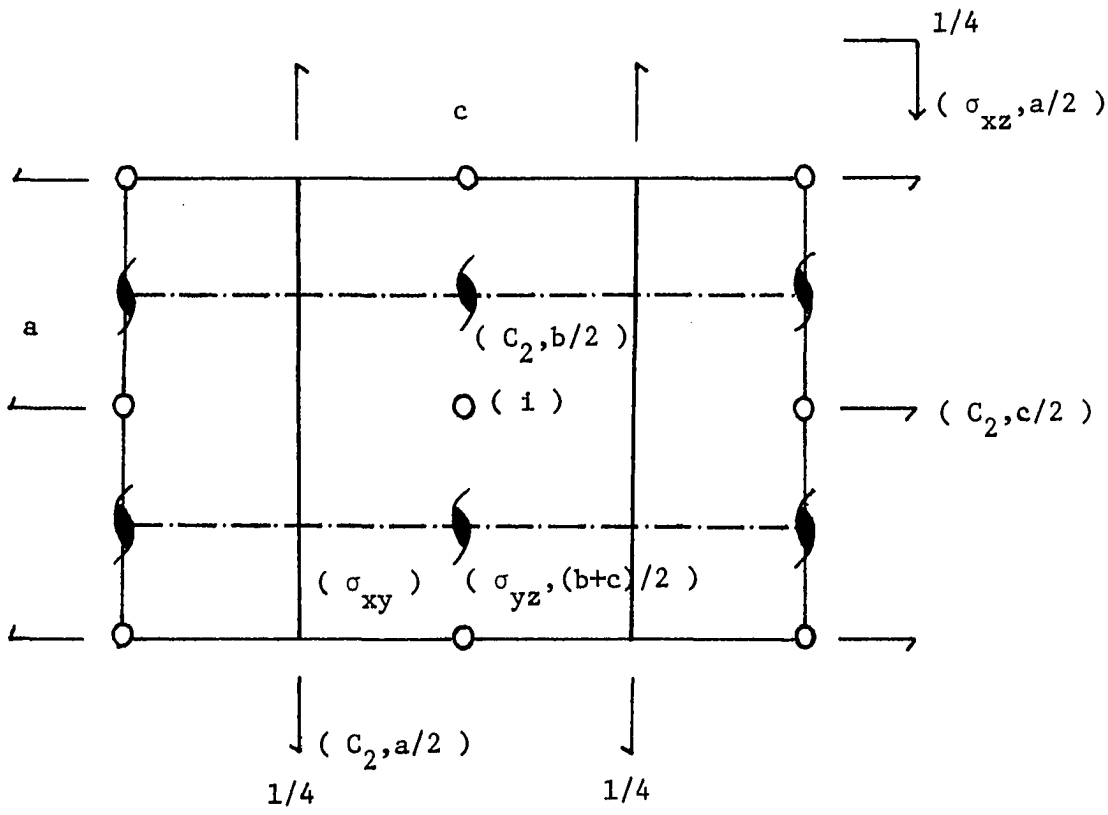

S(12b) : x,y,z ; x + 1/2,1/2 - y,$\bar{z}$; $\bar{x}$,y + 1/2,1/2 - z ;

1/2 - x,$\bar{y}$,z + 1/2 ; z,x,y ; z + 1/2,1/2 - x,$\bar{y}$;

$\bar{z}$,x + 1/2,1/2 - y ; 1/2 - z,$\bar{x}$,y + 1/2 ; y,z,x ;

y + 1/2,1/2 - z,$\bar{x}$; $\bar{y}$,z + 1/2,1/2 - x ; 1/2 - y,$\bar{z}$,x + 1/2

with x = 0.625, y = 0.467, z = 0.268

O(1)(12b) : with x = 0.651, y = 0.498, z = 0.412

O(2)(12b) : with x = 0.754, y = 0.488, z = 0.196

O(3)(12b) : with x = 0.573, y = 0.327, z = 0.258

O(4)(12b) : with x = 0.521, y = 0.557, z = 0.213

The site group of the sulfate ion is C_1, the unit cell group is T^4, and the correlation table[2] is

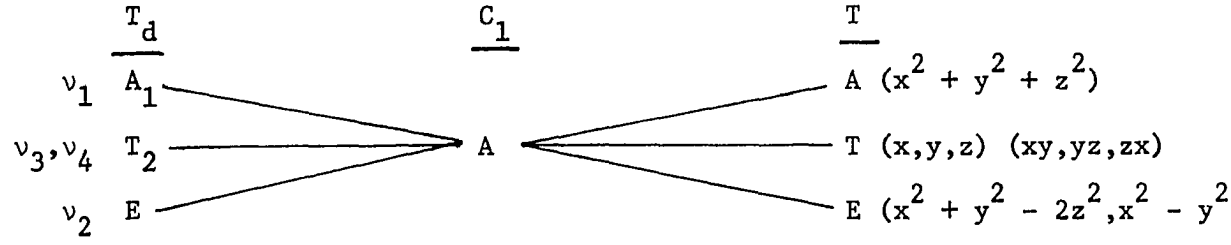

The symmetry operators in the unit cell group are :

$(x,y,z) \xrightarrow{(C_2)} (x + 1/2,1/2 - y,\bar{z})$, etc.

$(x,y,z) \xrightarrow{(C_3),(C_3^2)} (z,x,y)$, (y,z,x), etc.

and the standard character table[2] for these symmetry operations is :

T	E	$4C_3$	$4C_3^2$	$3C_2$		
A	1	1	1	1		$(x^2 + y^2 + z^2)$
E	2	-1	-1	2		$(x^2 + y^2 - 2z^2, x^2 - y^2)$
T	3	0	0	-1	(x,y,z)	(xy,yz,zx)

The normalized linear combinations of sites in the unit cell for irreducible representation T are simply

$$1/2 \sum_{i=1}^{4} K_i(1), \quad 1/2 \sum_{i=1}^{4} K_i(2), \quad 1/2 \sum_{i=1}^{4} Mg_i(1),$$
$$1/2 \sum_{i=1}^{4} Mg_i(2), \quad 1/2 \sum_{i=1}^{12} S(i)$$

Remark :

It is obvious from the above analysis that for infrared active modes of the unit cell group the linear combinations of sites are of the form site(1) + site(2) + ··· while for other modes (including Raman active modes) they are site(1) - site(2) + ··· - ···. This can be physically understood in that there must be a net dipole moment in the unit cell for the mode to be infrared active while for other modes (including Raman active modes) the net dipole moment is zero. The case of K_2SO_4 needs more attention and is discussed in chapter VI.

References for Chapter III

1. R. W. Wyckoff, Crystal Structures, Interscience Publishers, Inc., New York, 1948.

2. E. Bright Wilson, Jr., J. C. Decius, and Paul C. Cross, Molecular Vibrations, McGraw-Hill, New York, 1955.

3. International Tables for X-ray Crystallography, K. Lonsdale et. al., Eds., The Kynoch Press, Birmingham, England, 1952, Vol. 1.

CHAPTER IV

Polarizabilities of Sulfate Ions in Different Crystalline Environments

A. Theory

In chapter II one has

$$\underset{\sim}{P}_o = \underset{\sim}{\mu}_o + \underset{\sim}{\underset{\sim}{\alpha}}_{oo} \underset{\sim}{F}_o \qquad (2\text{-}5)'$$

and

$$\underset{\sim}{F}_o = \underset{\sim}{E}_o - \sum_{\ell} \underset{\sim}{T}_{o\ell} \underset{\sim}{P}_o \qquad (2\text{-}6)'$$

Substituting (2-6)' into (2-5)' one obtains

$$\underset{\sim}{P}_o = \underset{\sim}{\mu}_o + \underset{\sim}{\underset{\sim}{\alpha}}_{oo} [\underset{\sim}{E}_o - \sum_{\ell} \underset{\sim}{T}_{o\ell} \underset{\sim}{P}_o] \qquad (4\text{-}1)$$

Since $\sum_{\ell} \underset{\sim}{T}_{o\ell} = \underset{\sim}{S}$ (4-1) can be written as

$$\underset{\sim}{P}_o = \underset{\sim}{\mu}_o + \underset{\sim}{\underset{\sim}{\alpha}}_{oo} \underset{\sim}{E}_o - \underset{\sim}{\underset{\sim}{\alpha}}_{oo} \underset{\sim}{S} \underset{\sim}{P}_o \qquad (4\text{-}2)$$

or

$$[\underset{\sim}{I} + \underset{\sim}{\underset{\sim}{\alpha}}_{oo} \underset{\sim}{S}] \underset{\sim}{P}_o = \underset{\sim}{\mu}_o + \underset{\sim}{\underset{\sim}{\alpha}}_{oo} \underset{\sim}{E}_o \qquad (4\text{-}3)$$

where I is the identity matrix. Multiplying both sides by $[\underset{\sim}{I} + \underset{\sim}{\underset{\sim}{\alpha}}_{oo} \underset{\sim}{S}]^{-1}$ one has

$$\underset{\sim}{P}_o = [\underset{\sim}{I} + \underset{\sim}{\underset{\sim}{\alpha}}_{oo} \underset{\sim}{S}]^{-1} (\underset{\sim}{\mu}_o + \underset{\sim}{\underset{\sim}{\alpha}}_{oo} \underset{\sim}{E}_o) \qquad (4\text{-}4)$$

When the frequency of the external electric field

is much greater than that of the vibrations of the molecules in a crystal (e.g. visible light) $\underset{\sim}{\mu}_o$ will be zero and (4-4) reduces to

$$\underset{\sim}{P}_o = [\underset{\sim}{I} + \underset{\sim}{\alpha}_o \underset{\sim}{S}]^{-1} \underset{\sim}{\alpha}_o \underset{\sim}{E}_o \qquad (4\text{-}5)$$

From electrostatic theory it is known that the dielectric constant ε_α is related to the electric polarization P_α through

$$\varepsilon_\alpha = 4\pi P_\alpha / E_\alpha + 1 \qquad (4\text{-}6)$$

The dielectric constant is further related to the refractive index n_α by

$$\varepsilon_\alpha = n_\alpha^2 \qquad (4\text{-}7)$$

where α refers to a cartesian component. In general ε and n are three dimensional tensors of rank two and (4-6) and (4-7) are true only when principal dielectric axes are chosen such that ε and n are diagonalized. The principal dielectric axes for the cubic and orthorhombic systems coincide with the crystal axes. For uniaxial systems such as hexagonal, rhombohedral, and tetragonal crystals one of the principal axes is along the optic axis and the remaining two axes can be chosen in any direction in the plane perpendicular to the optical axis as long as they are orthogonal to each other.

The electric polarization P_α is

$$P\alpha = (P_{1,\alpha} + P_{2,\alpha} + \cdots + P_{n,\alpha})/v \qquad (4\text{-}8)$$

where v is the volume of the unit cell and n is the number of particles in a unit cell. The α component of the polarization in equation (4-5) is

$$\underset{\sim}{P}_{o\alpha} = [\underset{\sim}{I} + \underset{\sim}{\alpha}_{o} \underset{\alpha\alpha}{\underset{\sim}{S}}_{\alpha\alpha}]^{-1} \underset{\sim}{\alpha}_{o} \underset{\alpha\alpha}{\underset{\sim}{E}}_{o\alpha} \qquad (4\text{-}9)$$

$$\text{where } \underset{\sim}{P}_{o\alpha} = \begin{bmatrix} P_{1\alpha} \\ P_{2\alpha} \\ \vdots \\ P_{n\alpha} \end{bmatrix}, \text{ and } \underset{\sim}{E}_{\alpha} = \begin{bmatrix} E_{1\alpha} \\ E_{2\alpha} \\ \vdots \\ E_{n\alpha} \end{bmatrix} \qquad (4\text{-}10)$$

With (4-10) (4-8) can be written in matrix notation as

$$P_{\alpha} = \underset{\sim}{U}^{\dagger} \underset{\sim}{P}_{o\alpha}/v \qquad (4\text{-}11)$$

where U is the column matrix with all elements equal to 1. Eliminating ε_{α}, P_{α}, $P_{o\alpha}$, and E_{α} from (4-6),(4-7),(4-9), and (4-11) and re-writing $\underset{\sim}{\alpha}_{o} \underset{\alpha\alpha}{}$ as $\underset{\sim}{\alpha}_{o\alpha\alpha}$ to avoid confusion one has

$$n_{\alpha}^{2}-1 = 4\pi/v \; \underset{\sim}{U}^{\dagger} [\underset{\sim}{I} + \underset{\sim}{\alpha}_{o\alpha\alpha} \underset{\alpha\alpha}{\underset{\sim}{S}}_{\alpha\alpha}]^{-1} \underset{\sim}{\alpha}_{o\alpha\alpha} \underset{\sim}{U} \qquad (4\text{-}12)$$

B. Calculation of the Polarizability Components

In the calculation of the electronic polarizability of the anions, the polarizabilities of cations have to be assumed. The values used in calculation are from the work by Tessman, Kahn, and Shockley[1] and Pierenne and Karthenser[2]. Two variables α_M and α_m are set in an algorithm such that $\alpha_M > \alpha_m$ and the electronic polarizability of the sulfate ion is approached by the mean value of α_M and α_m. Since the electronic polarizability of the anion is usually less than 10 Å^3 in initialization α_M and α_m are set as 10 and 0, respectively.

The algorithm is :

Step 1 (initialization) Set $\alpha_M \leftarrow 10$, $\alpha_m \leftarrow 0$

Step 2 Calculate $F = 4\pi/v\ \underset{\sim}{U}^{\dagger}(\underset{\sim}{I} + \underset{\sim}{\alpha}_{\sim}^{o}{}_{\alpha\alpha}\underset{\sim}{S}_{\alpha\alpha})^{-1}\underset{\sim}{\alpha}_{\sim}^{o}{}_{\alpha\alpha}\underset{\sim}{U}$ with $\alpha_{anion} = (\alpha_M + \alpha_m)/2$.

If $F < n_\alpha^2 - 1$ and $\left| F - (n_\alpha^2 - 1) \right| > 0.00009$, go to step 3.

If $F > n_\alpha^2 - 1$ and $\left| F - (n_\alpha^2 - 1) \right| > 0.00009$, go to step 4.

Otherwise, set $\alpha_{so_4} \leftarrow \alpha_{anion}$, then stop.

Step 3 Set $\alpha_m \leftarrow \alpha_{anion}$, then go to step 2.

Step 4 Set $\alpha_M \leftarrow \alpha_{anion}$, then go to step 2.

C. Results

(1) $LiKSO_4$ site symmetry of sulfate ion : C_3

Refractive index[3]	Cation polarizability($\AA^3$)[2]	Sulfate polarizability($\AA^3$)
$n_{x,y} = 1.4721$	$\alpha_{Li^+} = 0.029$	$\alpha_{x,y} = 5.43$
	$\alpha_{K^+} = 1.03$	
$n_z = 1.4715$	$\alpha_{Li^+} = 0.029$	$\alpha_z = 5.79$
	$\alpha_{K^+} = 1.03$	

(2) $KNaSO_4$ site symmetry of sulfate ion : C_{3v}

Refractive index[3]	Cation polarizability($\AA^3$)[2]	Sulfate polarizability($\AA^3$)
$n_{x,y} = 1.4885$	$\alpha_{K^+} = 1.03$	$\alpha_{x,y} = 5.75$
	$\alpha_{Na^+} = 0.41$	
$n_z = 1.494$	$\alpha_{K^+} = 1.03$	$\alpha_z = 4.92$
	$\alpha_{Na^+} = 0.41$	

(3) K_2SO_4 site symmetry of sulfate ion : C_s ($\sigma_h = \sigma_{xy}$)

Refractive index[3,4]	Cation polarizability($\AA^3$)[2]	Sulfate polarizability($\AA^3$)
$n_x = 1.4973$	$\alpha_{K^+} = 1.03$	$\alpha_x = 5.20$
$n_y = 1.4935$	$\alpha_{K^+} = 1.03$	$\alpha_y = 5.25$
$n_z = 1.4947$	$\alpha_{K^+} = 1.03$	$\alpha_z = 5.20$

(4) Na_2SO_4 site symmetry of sulfate ion : D_2

Refractive index[3,4]	Cation polarizability($\AA^3$)[2]	Sulfate polarizability($\AA^3$)
$n_x = 1.464$	$\alpha_{Na^+} = 0.41$	$\alpha_x = 4.66$
$n_y = 1.474$	$\alpha_{Na^+} = 0.41$	$\alpha_y = 4.74$
$n_z = 1.485$	$\alpha_{Na^+} = 0.41$	$\alpha_z = 5.60$

(5) $K_2Mg_2(SO_4)_3$ site symmetry of sulfate ion : C_1

Refractive index[3]	Cation polarizability($\AA^3$)[2]	Sulfate polarizability($\AA^3$)
$n = 1.5329$	$\alpha_{K^+} = 1.03$ (with $\alpha_{Mg^{++}}$ neglected which is about 0.094 by Pauling)	$\alpha_{x,y,z} = 5.34$

D. Discussion

In the $KNaSO_4$ crystal α_z is less than $\alpha_{x,y}$, where the z direction is along an S–O bond. The same orientation of the sulfate ion occurs in $LiKSO_4$, however, the difference between α_z and $\alpha_{x,y}$ is not as large as in $KNaSO_4$. In the Na_2SO_4 crystal the site symmetry of the sulfate ion is D_2 and the x, y, and z axes of the sulfate ion are equivalent. However α_z turns out to be quite different from α_x and α_y. In the K_2SO_4 crystal the values of α_x, α_y, and α_z are similar despite the fact that the x direction is along an S–O bond. In $K_2Mg_2(SO_4)_3$ the electronic polarizability calculated is an average value along different directions since the system is cubic.

These observations can be more thoroughly understood by referring to Figures (4-1) and (4-2), and noting that in the $LiKSO_4$ crystal the nearest two cations to the sulfur atom at (1/3, 2/3, 0.17) are the lithium ion at (1/3, 2/3, 0.67) and the potassium ion at (0,0,0) with distances of 4.315 Å and 4.768 Å from the sulfur atom, respectively, while in the $KNaSO_4$ crystal the nearest two cations to the sulfur atom at (1/3, 2/3, 0.220) are the

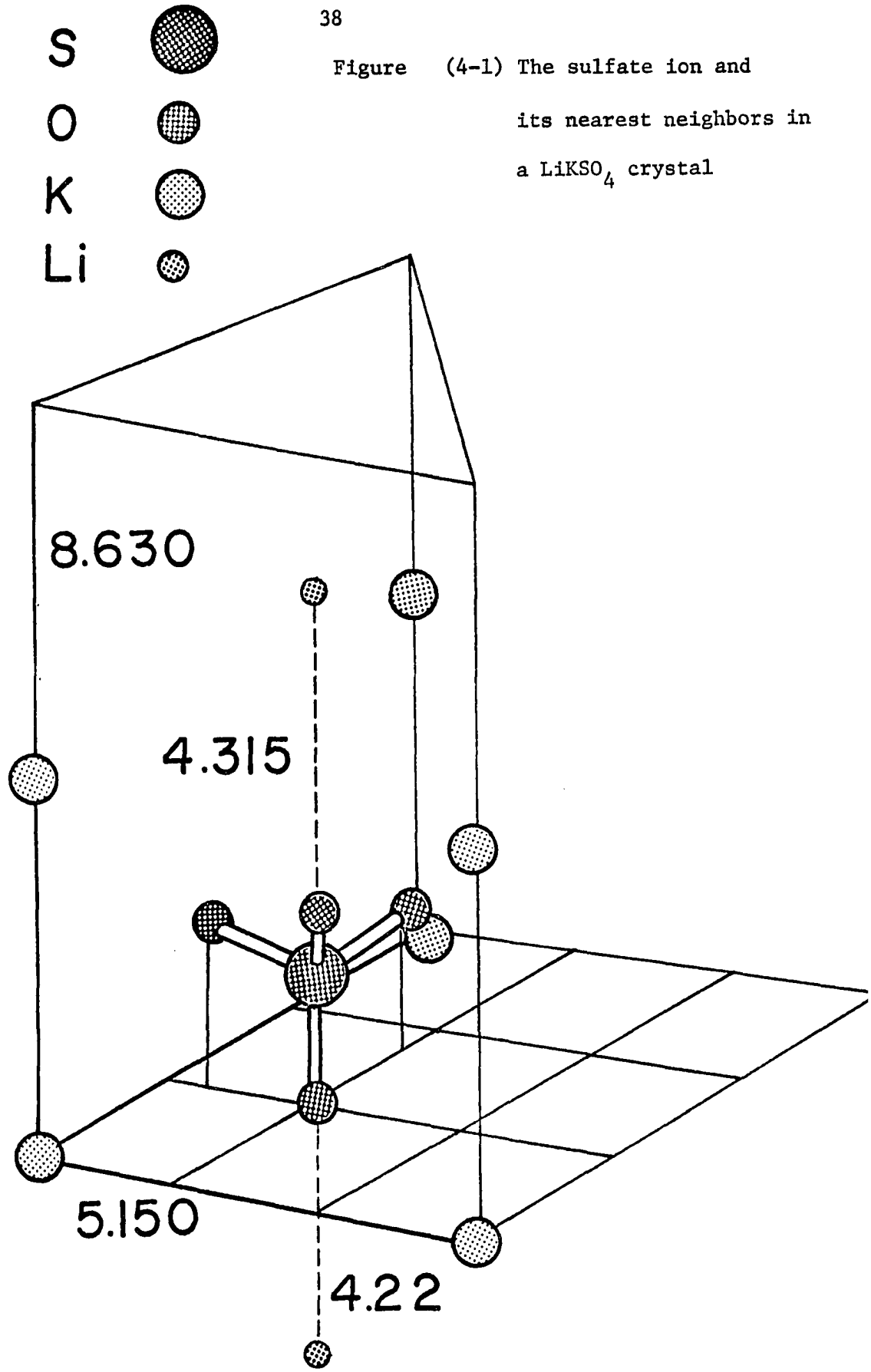

Figure (4-1) The sulfate ion and its nearest neighbors in a $LiKSO_4$ crystal

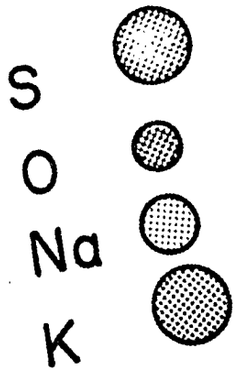

Figure (4-2) The sulfate ion and its nearest neighbors in a $KNaSO_4$ crystal

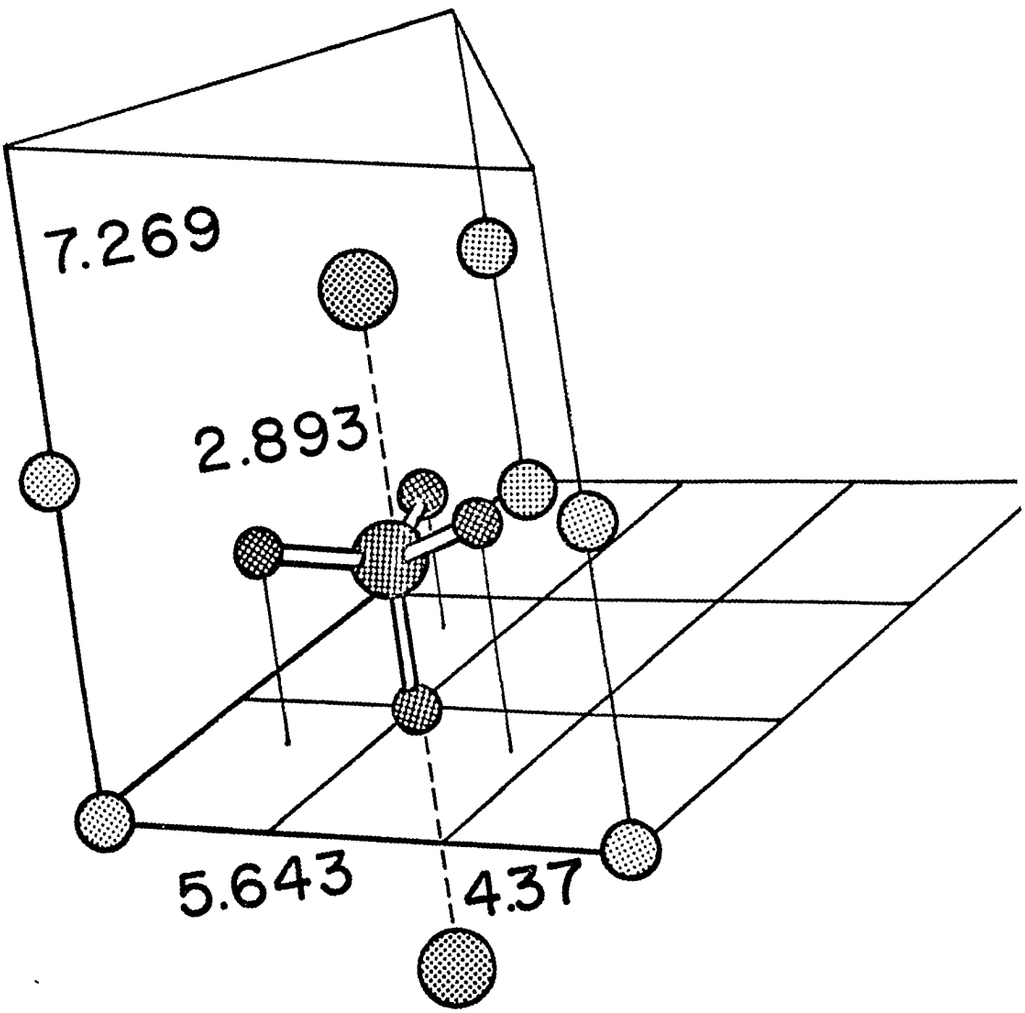

potassium ion at (1/3, 2/3, 0.618) and the sodium ion at (0,0,0) with distances of 2.893 Å and 3.630 Å from the sulfur atom, respectively. In the $LiKSO_4$ crystal the large value of $\alpha_z(SO_4^{=})$ relative to that in the $KNaSO_4$ crystal is due to the presence of the Li^+ ion in a direction collinear with an S-O bond in the z direction. The polarizing ability of the Li^+ ion is much greater than either the Na^+ ion or the K^+ ion, hence the increase of $\alpha_z(SO_4^{=})$ in the $LiKSO_4$ crystal.

In the K_2SO_4 crystal the nearest potassium ions to the sulfur atom at (0.2358, 0.4155, 1/4) in the x, y, and z directions (approximately) are at (0.6768, 0.4182, 1/4), (0.1768, 0.0818, 1/4), and (0.3232, 0.5818, -1/4) with the distances of 3.300 Å, 3.390 Å, and 3.400 Å, respectively. (See Figure (4-3)). These distances are quite similar and it is not unexpected that the polarizability components along x, y, and z directions are also quite similar.

In the Na_2SO_4 crystal the nearest sodium ions to the sulfur atom at (1/8, 1/8, 1/8) are at (0.436, 1/8, 1/8), (0.064, 3/8, -1/8), and (-0.016, 1/8, 5/8) with the distances of 3.054Å, 3.460Å, and 4.208 Å. (See Figure (4-4)) As stated before the x, y, and z directions of the sulfate ion are equivalent. Here it is more difficult to interpret the differences in the polarizability components in terms of the nearest neighbor cation environment since none of the cation-sulfur directions are collinear with the S-O bonds of the sulfate ion.

However, from these considerations it may be concluded that different crystalline environments around a sulfate ion play an important role in determining the electronic polarizability components of the sulfate ion.

Figure (4-3) The sulfate ion and its nearest neighbors in a K_2SO_4 crystal

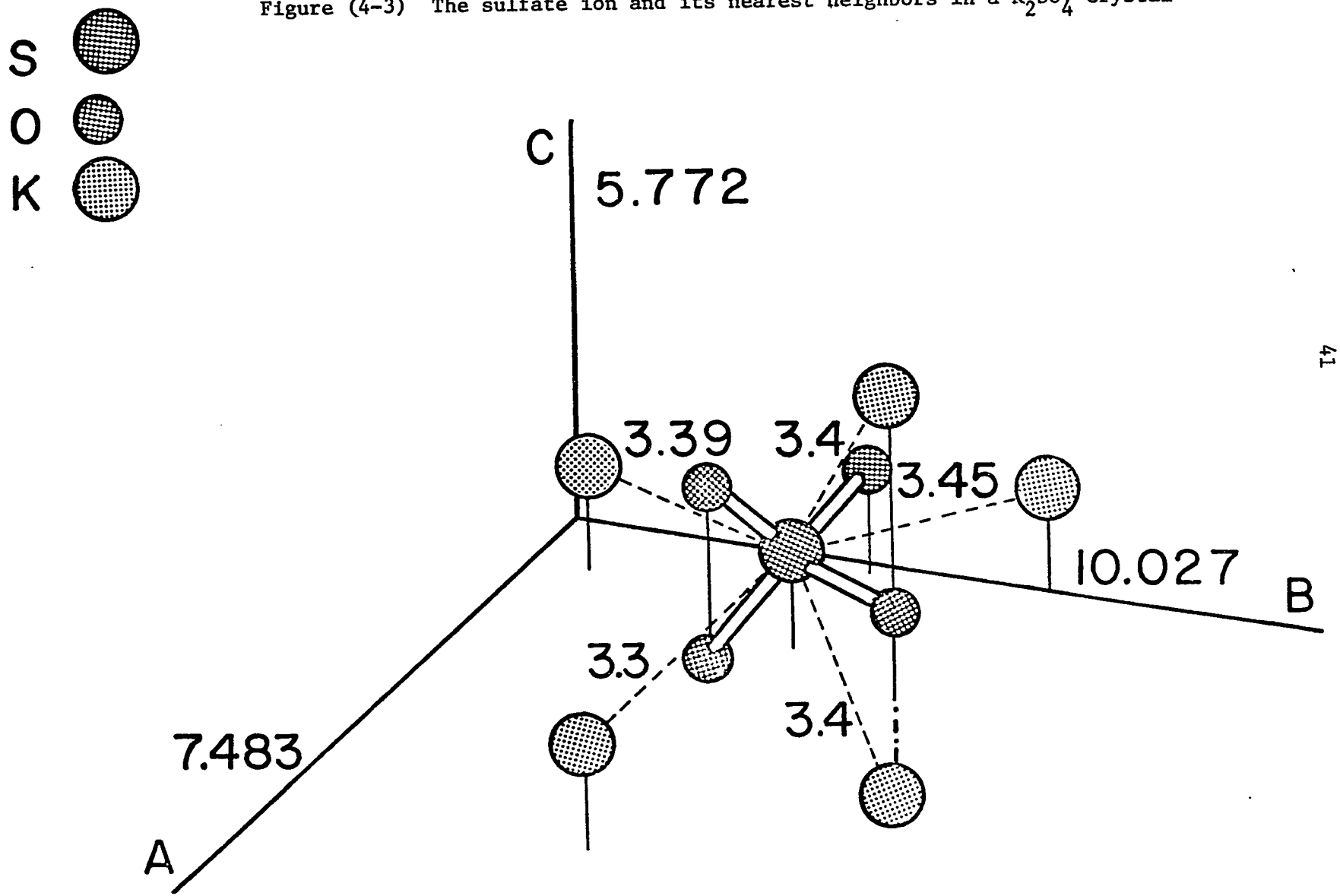

Figure (4-4) The sulfate ion and its nearest neighbors in a Na_2SO_4 crystal

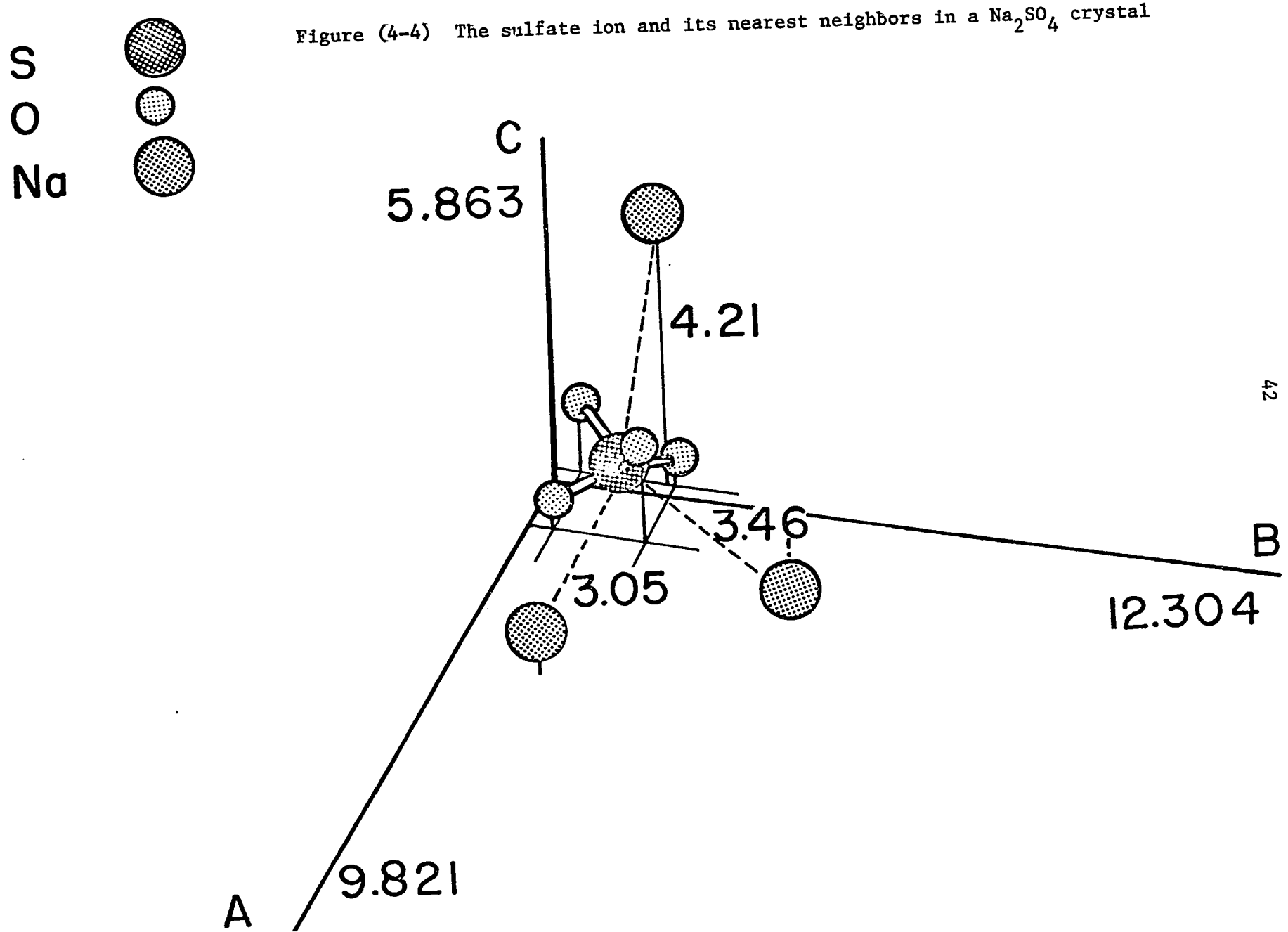

The sulfate ion electronic polarizability values calculated by Tessman, Kahn, and Shockley[1] for several crystalline environments are 5.19 $\mathring{A}^3$ in $LiKSO_4$, 5.09 $\mathring{A}^3$ in Na_2SO_4, and 4.80 $\mathring{A}^3$ in K_2SO_4 which are quite similar to those calculated in this work. In the work by TKS the calculations are based on the assumptions that the crystals considered are purely ionic and that the electronic polarizability of a crystal is simply the sum of the electronic polarizabilities of the individual ions neglecting anisotropic effects. TKS further assumed that the local field at a site was given by the Lorentz-Lorenz internal field, an assumption which is strictly true only for cubic systems at sites of T_d point symmetry or higher. The local (or effective) field E_{eff} acting on any ion of a crystal was assumed to be

$$E_{eff} = F + LP$$

where F is the applied field, P is the electronic polarization or electronic dipole moment per unit volume, and L is the Lorentz factor. F and P were assumed to be in the same direction, and L was assumed to be the same for all ions in all crystals with a value of $4\pi/3$.

References for Chapter IV

1. J. Tessman, A. Kahn, and W. Shockley, Phys. Rev. 92, 890 (1953).

2. J. Pirenne and E. Karthenser, Physica 30, 2005 (1964).

3. International Critical Tables of Numerical Data; Physics, Chemistry, and Technology, McGraw-Hill, New York, 1926.

4. A. Winchell and H. Winchell, The Microscopic Characteristics of Artificial Inorganic Solid Substances, Academic Press, New York, 1964.

CHAPTER V

Spectra, Static Crystal Field Frequencies, Dipole Moment Derivatives, and Correlations

A. Experimental Preparation of Crystals

Sulfate crystals are usually easy to grow from aqueous solutions at room temperature. Large single crystals of $LiKSO_4$, $KNaSO_4$, and $K_2Mg_2(SO_4)_3$ were grown from aqueous solutions of equimolar mixtures of the component single salts. Bigger single crystals of $LiKSO_4$ and $KNaSO_4$ can be grown at 50°C. Orthorhombic Na_2SO_4 crystals were grown at 37°C. All reagents used were analytical grade. Crystals of $LiKSO_4$ and $KNaSO_4$ are uniaxial crystals and were examined with a polarizing microscope to check the alignment of the optic axis. This method was also used to check that the crystals of $K_2Mg_2(SO_4)_3$ used were cubic. The crystal axes of Na_2SO_4 and $K_2Mg_2(SO_4)_3$ were determined by x-ray diffraction methods through the courtesy of Mr. Steve Ealick and Dr. K. K. Wu, respectively.

B. Infrared and Raman Measurements

Near normal incidence infrared reflection spectra were obtained at an average angle of incidence of 17° using the mirror arrangement as shown in Figure (5-1a) The spectra were recorded on a Beckman IR-12 spectrophotometer. Raman spectra were obtained through the courtesy of Prof. J. P. Devlin at Oklahoma State University using a system constructed around the Jarrell-Ash 25-100 dual monochromator. The geometrical arrangement of the Raman scattering experiments is described in Figure (5-1b). Frequencies of longitudinal and transverse modes of infrared active modes were estimated from the inflection points of near normal incidence

Figure (5-1-a) Mirror Arrangement in Reflectivity Experiments

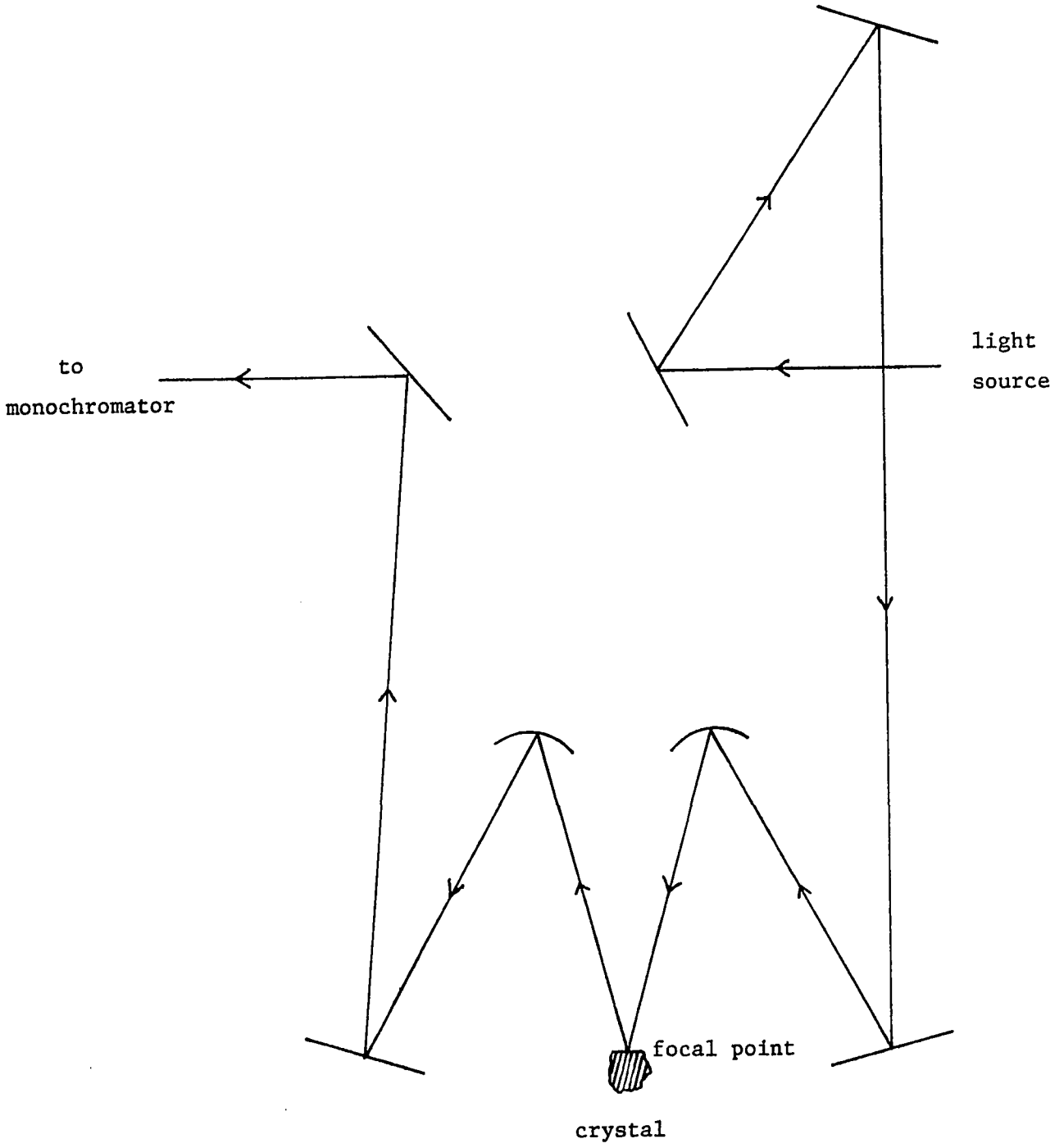

Figure (5-1-b) The Geometrical Arrangement of the Raman Scattering Experiments : In the uniaxial systems z axis is chosen parallel to the optic axis and x and y axes are orthogonal to each other and lie in the plane perpendicular to the z axis. In the orthorhombic systems x, y, and z axes are chosen such that they are parallel to the crystal axes a, b, and c respectively. In the cubic systems x, y, and z axes are parallel to the crystal axes.

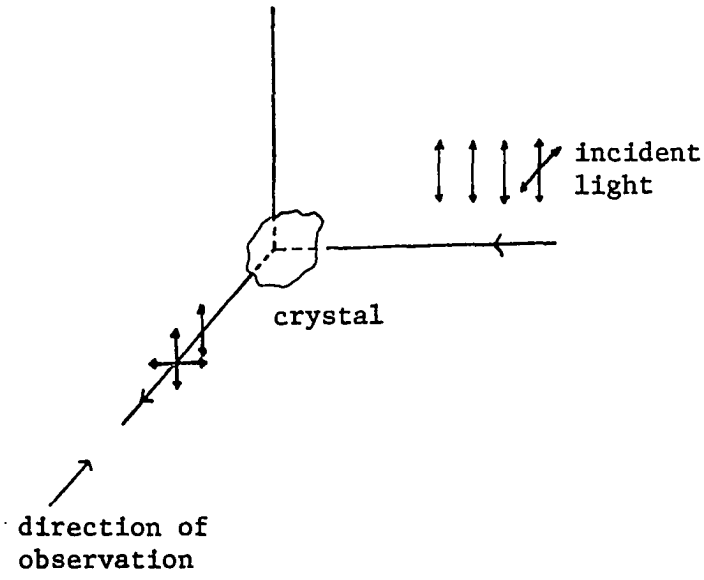

$\alpha(\beta\gamma)\delta$

α : direction of the incident light

β : polarization of the incident light

γ : polarization of the outgoing light

δ : direction of the outgoing light

$\alpha,\beta,\gamma,\delta$ are the Cartesian coordinates x, y, or z.

reflection spectra. The modes are simultaneously infrared and Raman active in crystals which are not centro-symmetric. Therefore the frequencies of the modes can be measured in a Raman scattering experiment as well as near normal incidence infrared reflection. The frequencies obtained from Raman measurements. are more accurate than those from near normal incidence infrared reflection measurements. In crystals which are centrosymmetric the modes are not simultaneously infrared and Raman active (rule of mutual exclusion). Therefore Raman scattering and near normal incidence infrared reflection methods are complementary.

C. $LiKSO_4$

a. Near normal incidence infrared reflection spectra are shown in Figures (5-2)-(5-4).

b. Vibrational frequencies as measured by near normal incidence infrared reflection or the Raman method are shown in Table (5-1).

c. The $S(\gamma)[I + \alpha_o S(\gamma)]^{-1}$ factors for different irreducible representations of the unit cell group C_6^6 are :

γ	Polarization (α)	$S(\gamma)[I + \alpha_o S(\gamma)]^{-1}(cm^{-5}sec^2)$
A	z (transverse)	-1.54875
	(longitudinal)	1.48068
E_1	x,y (transverse)	-1.72741
	(longitudinal)	1.55031
B	z	1.41779
E_2	x,y	-1.40915

d. The static crystal field frequencies, dipole moment derivatives, and calculated normal mode frequencies compared with the measured frequencies which are Raman active are shown below :

	γ	$\omega_o(cm^{-1})$	$(\partial\mu/\partial q)_{x,y}$	$(\partial\mu/\partial q)_z$ $(cm^{3/2}sec^{-1})$	ω_{calc}	ω_{exp}
ν_1	A	1017	--	--	--	--
ν_2	E_2	473	78	--	464	463
ν_3	B	1162	--	252	1200	--
	E_2	1162	242	--	1125	1115
ν_4	B	630	--	71	636	--
	E_2	643	84	--	635	631

e. The correlation diagram of the internal optic modes is shown in Figure (5-5).

Figure (5-2) Near normal incidence infrared reflection spectra of $LiKSO_4$ crystal

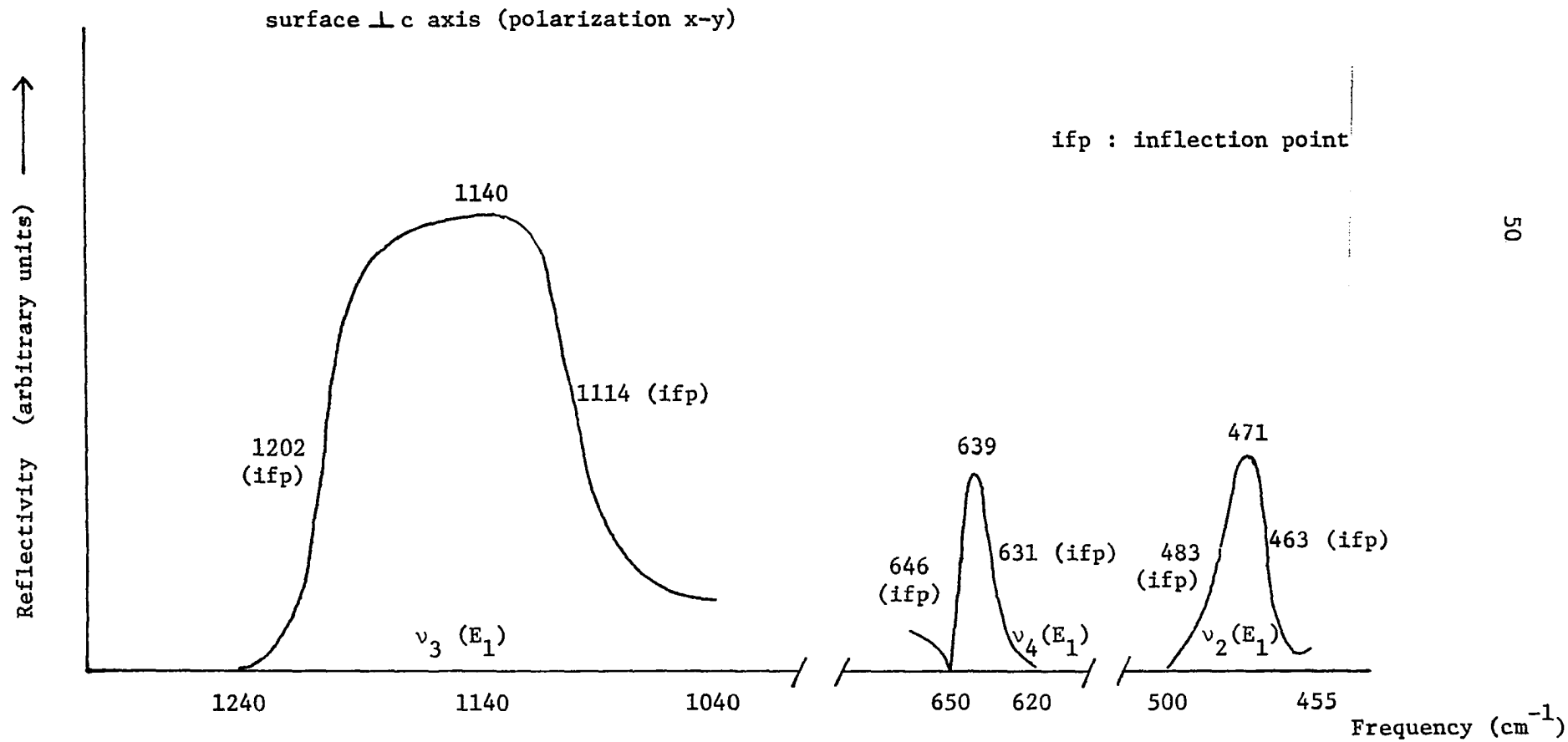

Figure (5-3) Near normal incidence infrared reflection spectra of $LiKSO_4$ crystal

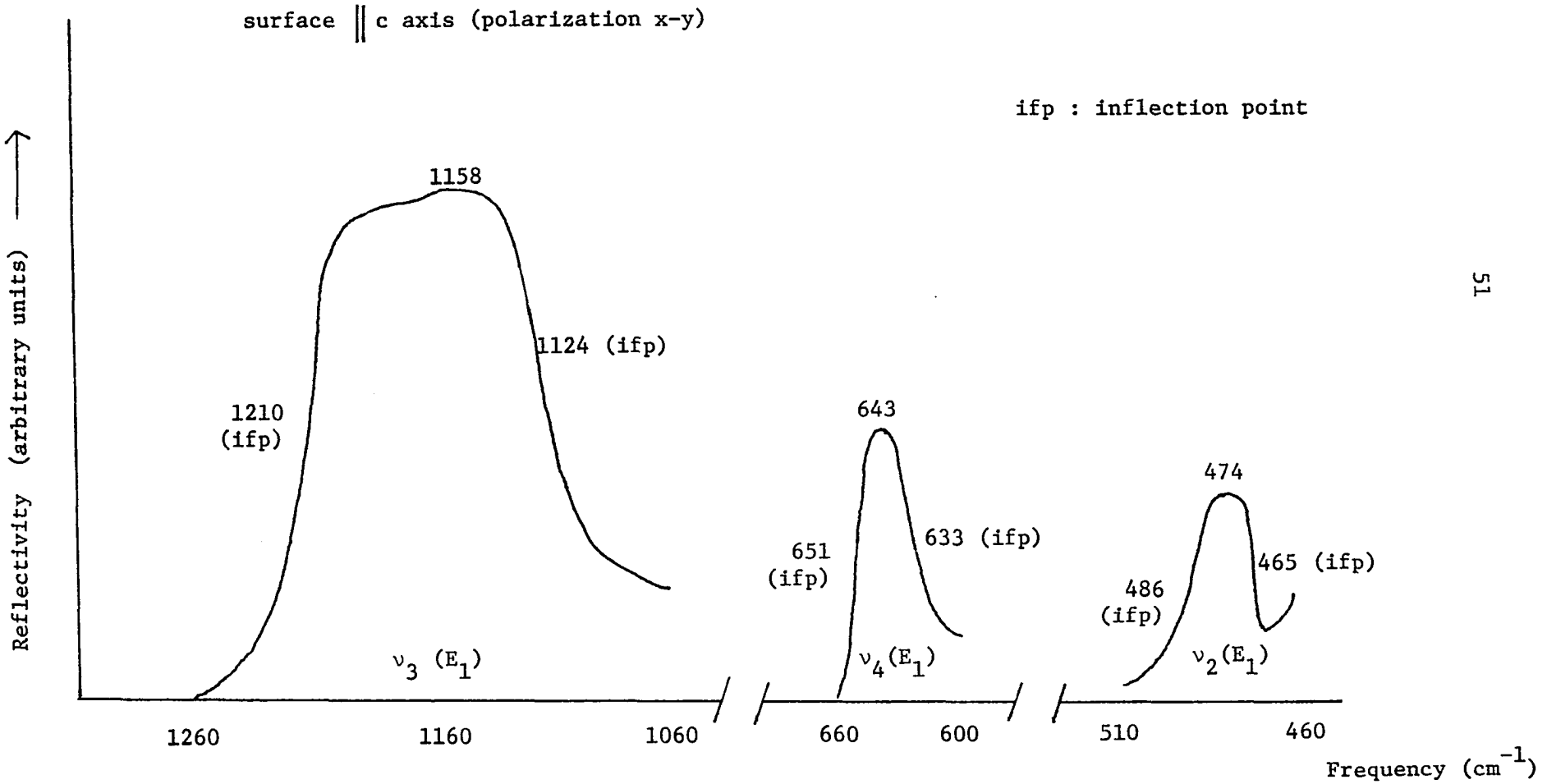

Figure (5-4) Near normal incidence infrared reflection spectra of $LiKSO_4$ crystal

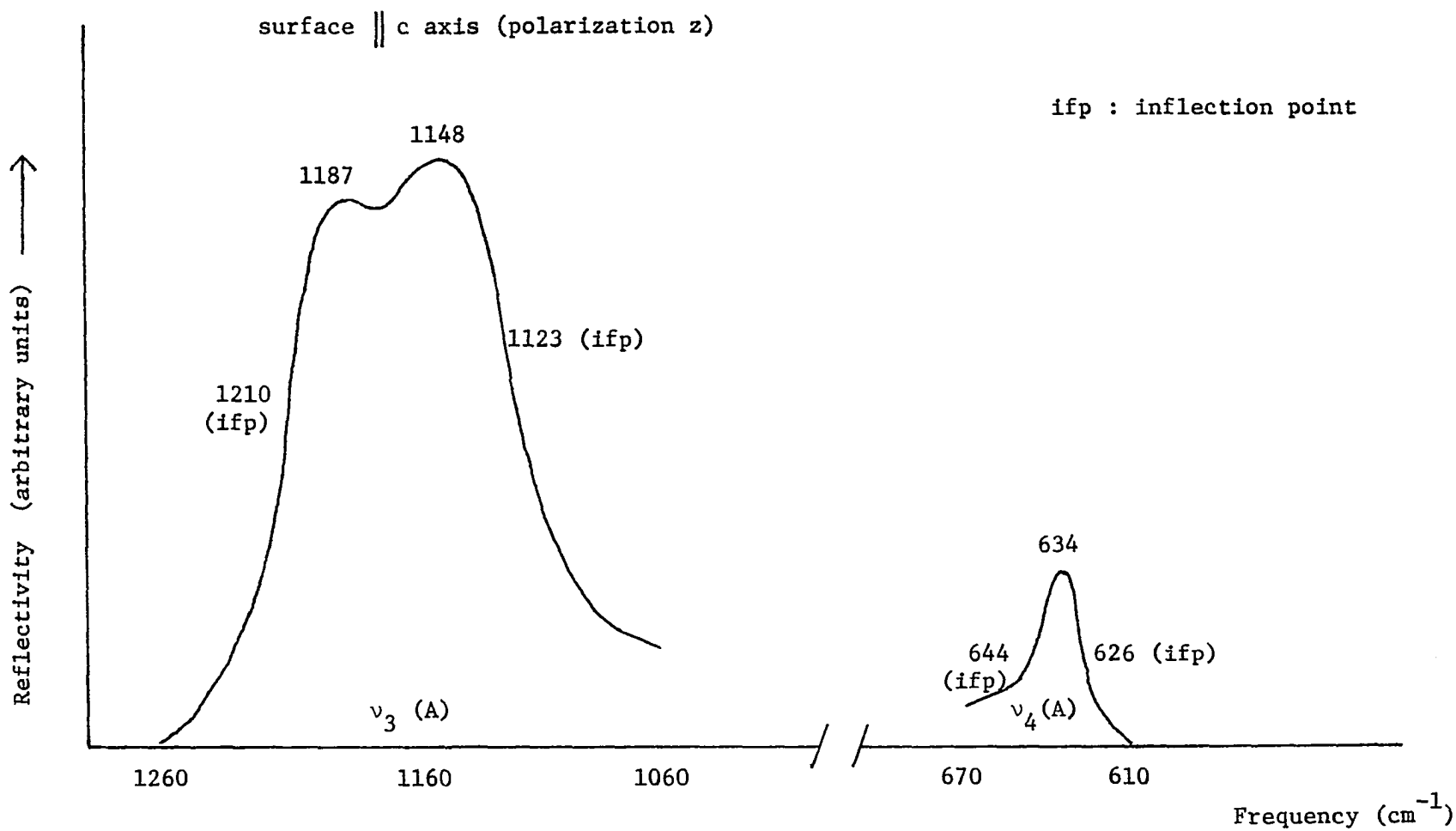

Table (5-1) Vibrational frequencies of $LiKSO_4$ crystal as measured by near normal incidence infrared reflection or the Raman method. (frequencies in cm^{-1})

	γ	ω_L	ω_T	ω	method
ν_1	A	1017	--	--	R z(xx)z
		--	1017	--	R y(xx)y
ν_2	E_1	486	465	--	IR surface ∥ c axis
		483	462	--	IR surface ⊥ c axis
		--	462	--	R z(yz)x
	E_2	--	--	463	R x(yx)z, x(yy)z
ν_3	A	1210	1123	--	IR surface ∥ c axis
		1198	1117	--	R z(yy)x
		1198	1117	--	R x(yy)z
		1202	--	--	R z(xx)z
		--	1119	--	R y(xx)z
	E_1	1210	1124	--	IR surface ∥ c axis
		1202	1114	--	IR surface ⊥ c axis
		1196	1112	--	R z(yz)x, x(zx)z
					R x(yz)y
		1200	1117	--	R y(zx)z
	E_2	--	--	1115	R z(xy)x
		--	--	1116	R x(yx)z
ν_4	A	644	626	--	IR surface ∥ c axis
		636	624	--	R z(xx)$\bar{z}$
		635	625	--	R z(yy)x
	E_1	651	633	--	IR surface ∥ c axis
		646	631	--	IR surface ⊥ c axis
		--	634	--	R z(yz)x
	E_2	--	--	631	R x(yy)z
		--	--	631	R x(yx)z

Figure (5-5) Correlation diagram of the internal optic modes of $LiKSO_4$ crystal (frequencies in cm^{-1})

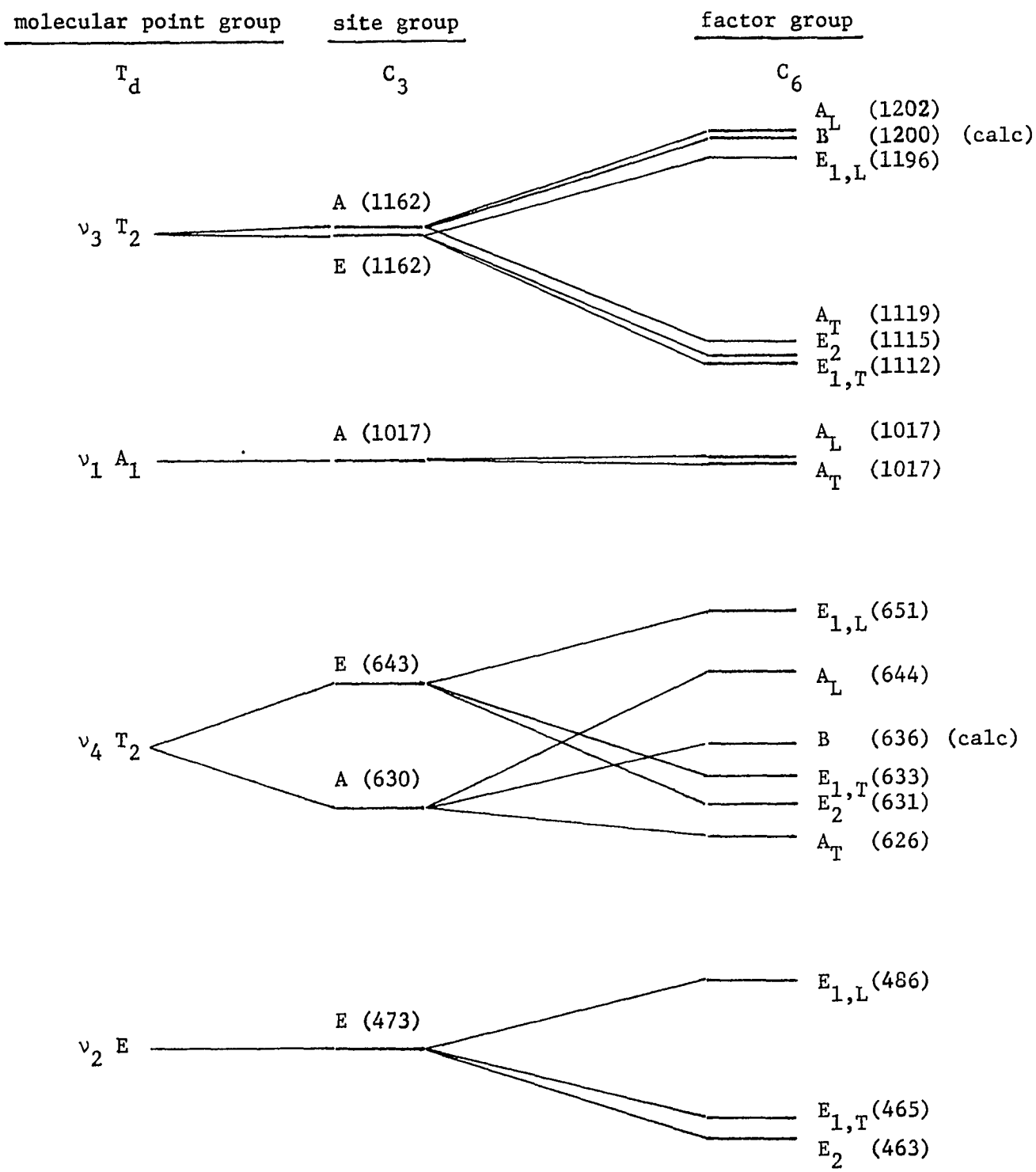

D. $KNaSO_4$

a. Near normal incidence infrared reflection spectra are shown in Figures (5-6)-(5-8).

b. Vibrational frequencies as measured by near normal incidence infrared reflection or the Raman method are shown in Table (5-2).

c. The $S(\gamma)[I + \alpha_o S(\gamma)]^{-1}$ factors for different irreducible representations of the unit cell group D_{3d}^3 are :

γ	Polarization (α)	$S(\gamma)[I + \alpha_o S(\gamma)]^{-1}(cm^{-5}sec^2)$
A_{2u}	z (transverse)	-2.23185
	(longitudinal)	1.50476
E_u	x,y (transverse)	-1.48937
	(longitudinal)	1.44831
A_{1g}	z	2.11736
E_g	x,y	-0.39438

d. The static crystal field frequencies, dipole moment derivatives, and calculated normal mode frequencies compared with the measured frequencies which are Raman active are shown below :

	γ	$\omega_o(cm^{-1})$	$(\partial\mu/\partial q)_{x,y}$	$(\partial\mu/\partial q)_z (cm^{3/2}sec^{-1})$	ω_{calc}	ω_{exp}
ν_1	A_{1g}	993	--	71	998	996
ν_3	A_{1g}	1217	--	199	1251	1206
	E_g	1131	242	--	1121	1087
ν_4	A_{1g}	625	--	73	634	634
	E_g	624	80	--	622	625

e. The correlation diagram of the internal optic modes is shown in Figure (5-9).

Figure (5-6) Near normal incidence infrared reflection spectra of $KNaSO_4$ crystal

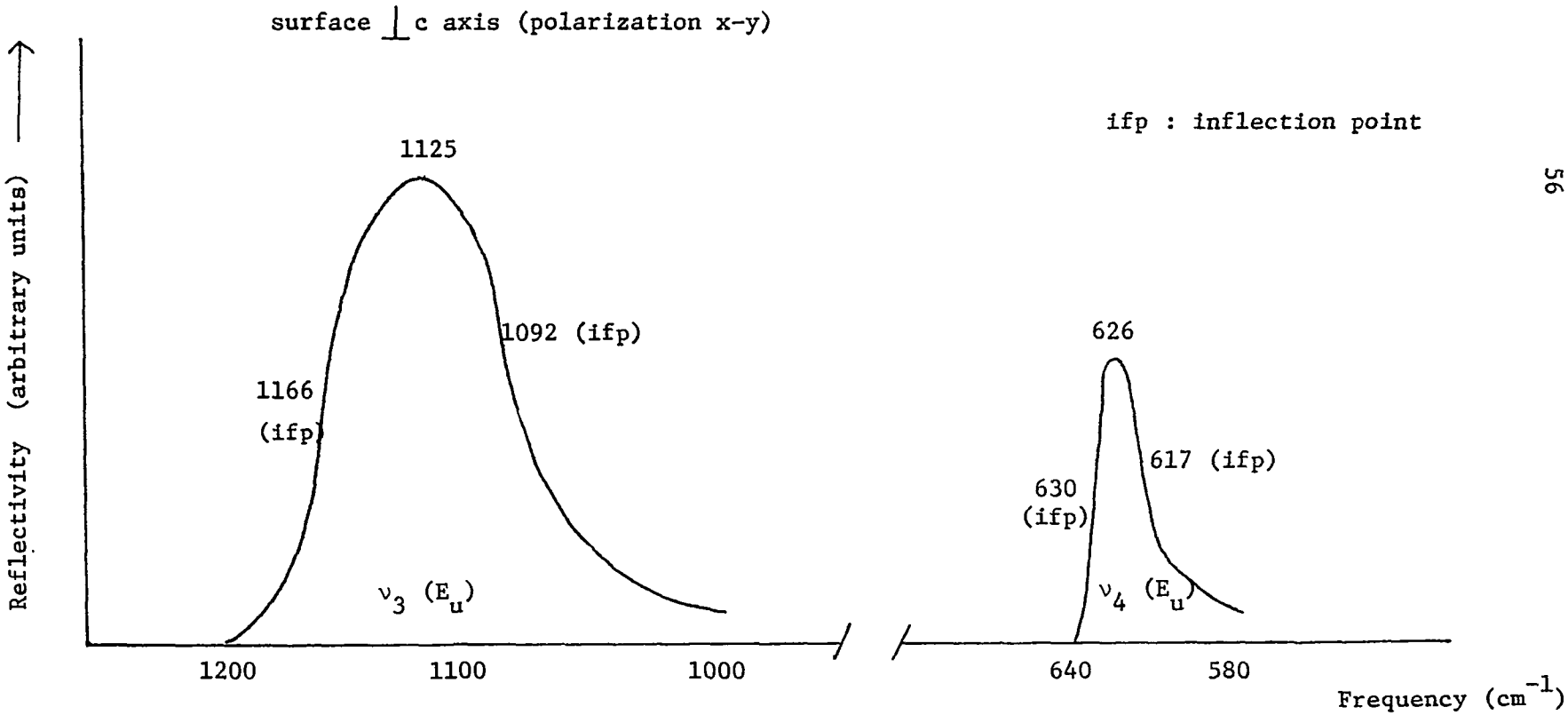

Figure (5-7) Near normal incidence infrared reflection spectra of $KNaSO_4$ crystal

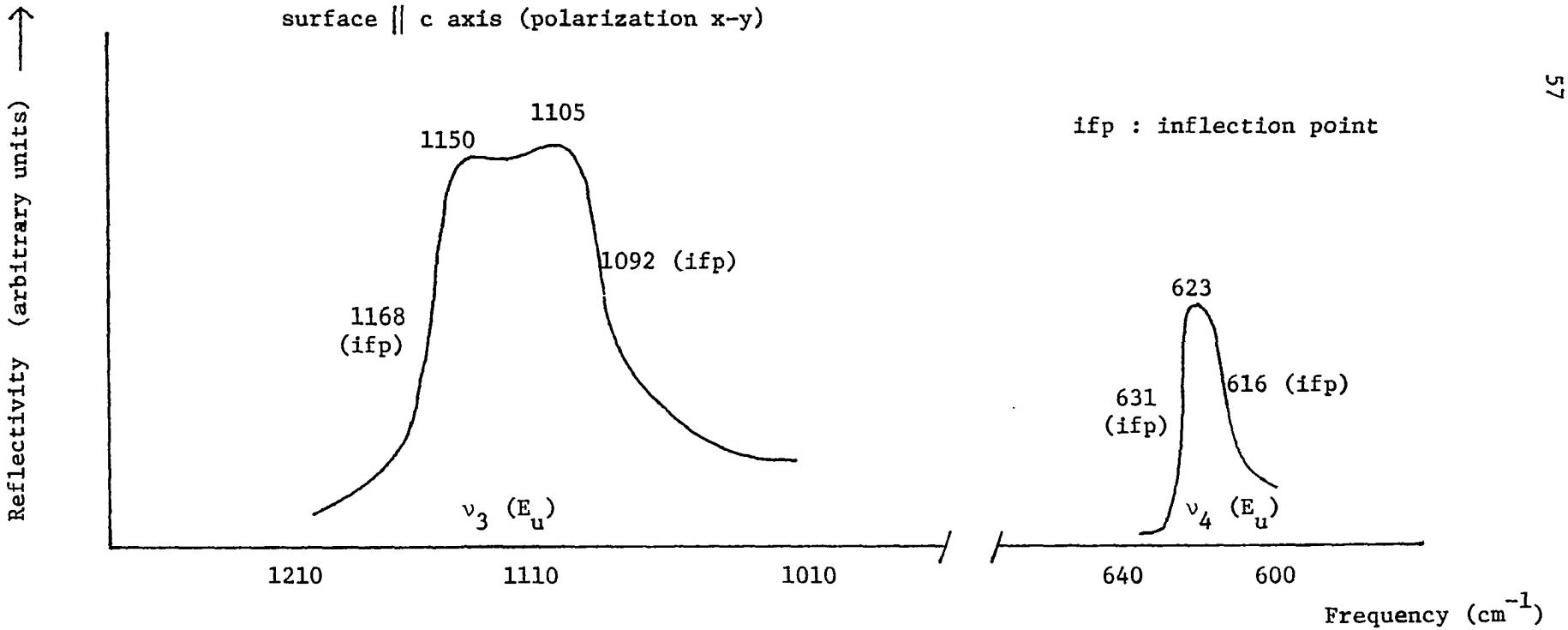

Figure (5-8) Near normal incidence infrared reflection spectra of $KNaSO_4$ crystal

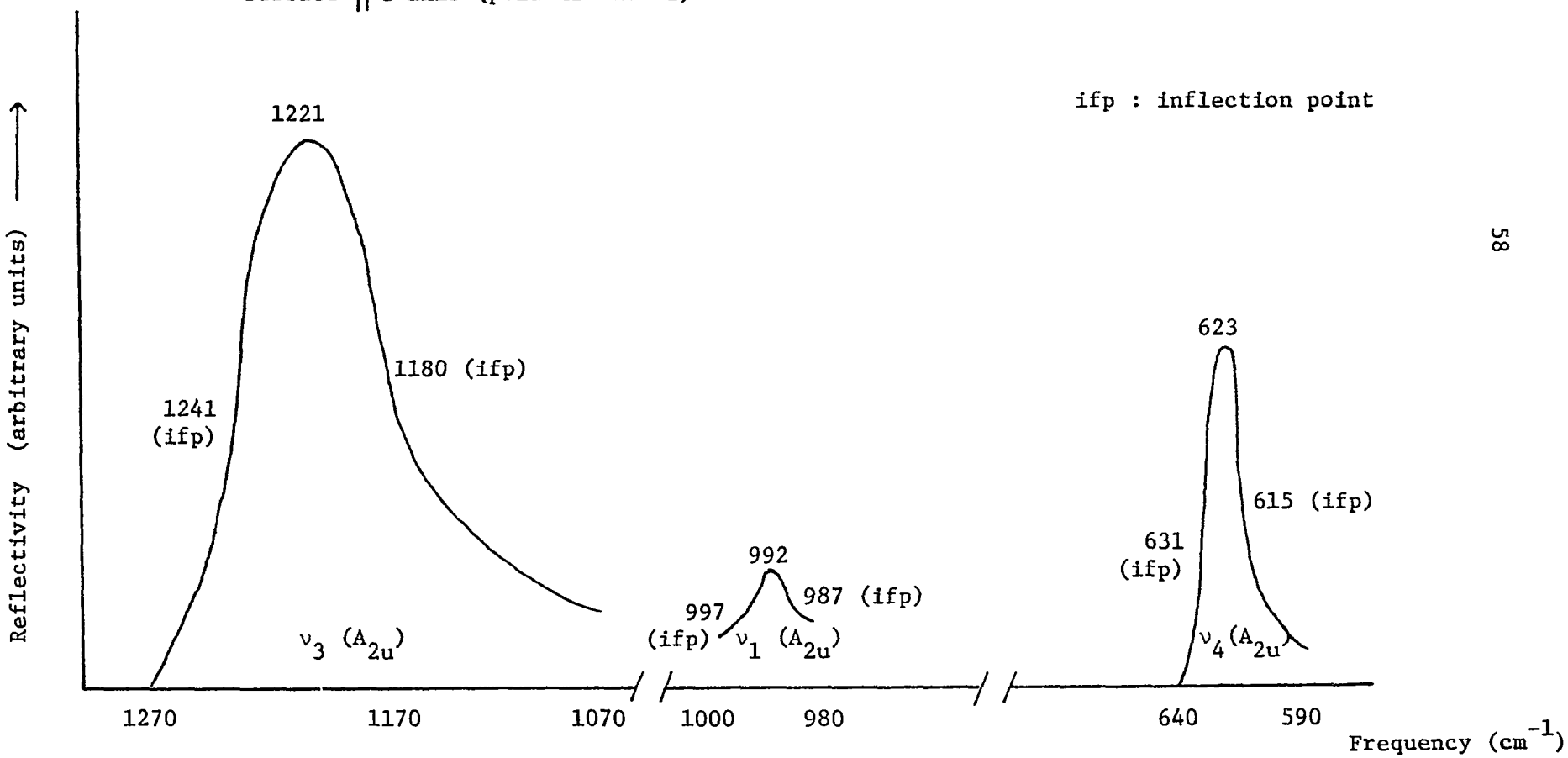

Table (5-2) Vibrational frequencies of $KNaSO_4$ crystal as measured by near normal incidence infrared reflection or the Raman method. (frequencies in cm^{-1})

	γ	ω_L	ω_T	ω	method
ν_1	A_{2u}	997	987	--	IR surface ‖ c axis
	A_{1g}	--	--	996	R z(xy)x
		--	--	996	R z(yy)x
ν_2	E_g	--	--	451	R z(xy)x
		--	--	453	R z(yy)x
ν_3	A_{2u}	1241	1180	--	IR surface ‖ c axis
	A_{1g}	--	--	1206	R z(xx)y
	E_u	1168	1092	--	IR surface ‖ c axis
	E_g	--	--	1087	R z(xy)x
		--	--	1087	R z(yy)x
ν_4	A_{2u}	631	615	--	IR surface ‖ c axis
	A_{1g}	--	--	634	R z(xy)x
		--	--	633	R z(yy)x
	E_u	631	616	--	IR surface ‖ c axis
	E_g	--	--	626	R z(xy)x
		--	--	624	R z(yy)x

Figure (5-9) Correlation diagram of the internal optic modes of $KNaSO_4$ crystal (frequencies in cm^{-1})

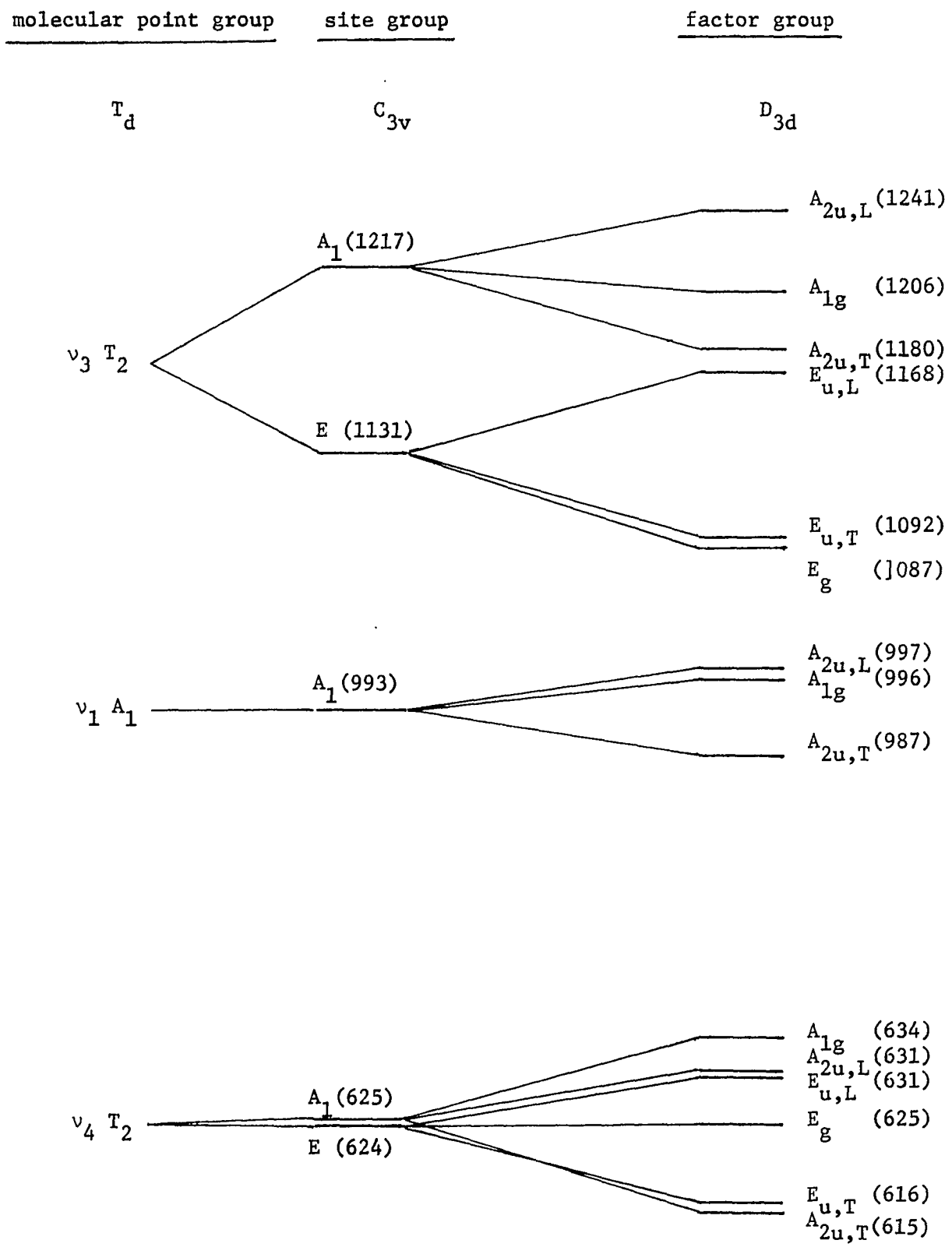

E. Na_2SO_4

a. Near normal incidence infrared reflection spectra are shown in Figures (5-10)-(5-15).

b. Vibrational frequencies as measured by near normal incidence infrared reflection or the Raman method are shown in Table (5-3).

c. The $S(\gamma)[I + \alpha_o S(\gamma)]^{-1}$ factors for different irreducible representations of the unit cell group D_{2h}^{24} are :

γ	Polarization (α)	$S(\gamma)[I + \alpha_o S(\gamma)]^{-1}(cm^{-5}sec^2)$
B_{1g}	z	-1.21467
B_{1u}	z (transverse)	-1.33925
	(longitudinal)	1.78845
B_{2g}	y	0.43310
B_{2u}	y (transverse)	-2.87480
	(longitudinal)	1.39536
B_{3g}	x	-0.71508
B_{3u}	x (transverse)	-2.32869
	(longitudinal)	1.67149

d. The static crystal field frequencies, dipole moment derivatives, and calculated normal mode frequencies compared with the measured frequencies which are Raman active are shown below :

Table (5-3) Vibrational frequencies of Na_2SO_4 crystal as measured by near normal incidence infrared reflection or the Raman method. (frequencies in cm^{-1})

	γ	ω_L	ω_T	ω	method
ν_1	A_g	--	--	996	R y(zz)x
ν_2	A_g	--	--	453	R y(zz)x
		--	--	465	R y(zz)x
ν_3	B_{1g}	--	--	1103	R y(xy)x
	B_{1u}	1207	1126	--	IR surface $\perp$ b axis
	B_{2g}	--	--	1158	R y(xz)x
	B_{2u}	1188	1103	--	IR surface $\perp$ a axis
	B_{3g}	--	--	1134	R y(zy)x
	B_{3u}	1204	1116	--	IR surface $\perp$ c axis
ν_4	B_{1g}	--	--	623	R y(xy)x
	B_{1u}	628	612	--	IR surface $\perp$ b axis
	B_{2g}	--	--	635	R y(xz)x
	B_{2u}	630	609	--	IR surface $\perp$ a axis
	B_{3g}	--	--	650	R y(zy)x
	B_{3u}	651	634	--	IR surface $\perp$ c axis

	γ	$\omega_o(cm^{-1})$	$(\partial\mu/\partial q)_x$	$(\partial\mu/\partial q)_y$	$(\partial\mu/\partial q)_z$ $(cm^{3/2}sec^{-1})$	ω_{calc}	ω_{exp}
ν_1	A_g	996	--	--	--	--	--
ν_2	A_g	453	--	--	--	--	--
	A_g	465	--	--	--	--	--
ν_3	B_{1g}	1161	--	--	246	1129	1103
	B_{2g}	1161	--	214	--	1169	1158
	B_{3g}	1168	226	--	--	1152	1134
ν_4	B_{1g}	619	--	--	75	614	623
	B_{2g}	623	--	78	--	625	635
	B_{3g}	644	74	--	--	641	650

e. The correlation diagram of the internal optic modes is shown in Figure (5-16) and (5-17).

Figure (5-10) Near normal incidence infrared reflection spectra of Na_2SO_4 crystal

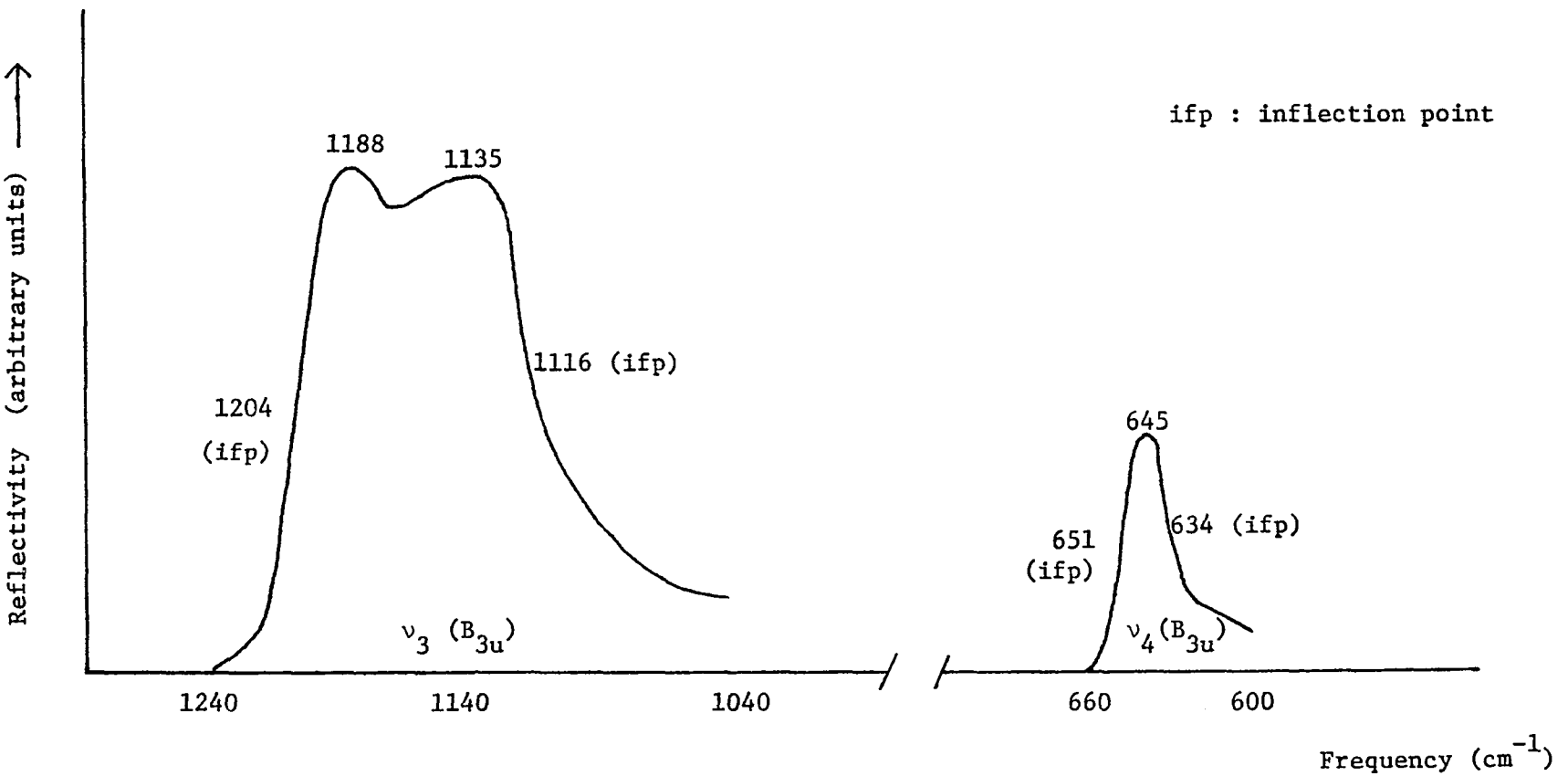

Figure (5-11) Near normal incidence infrared reflection spectra of Na_2SO_4 crystal

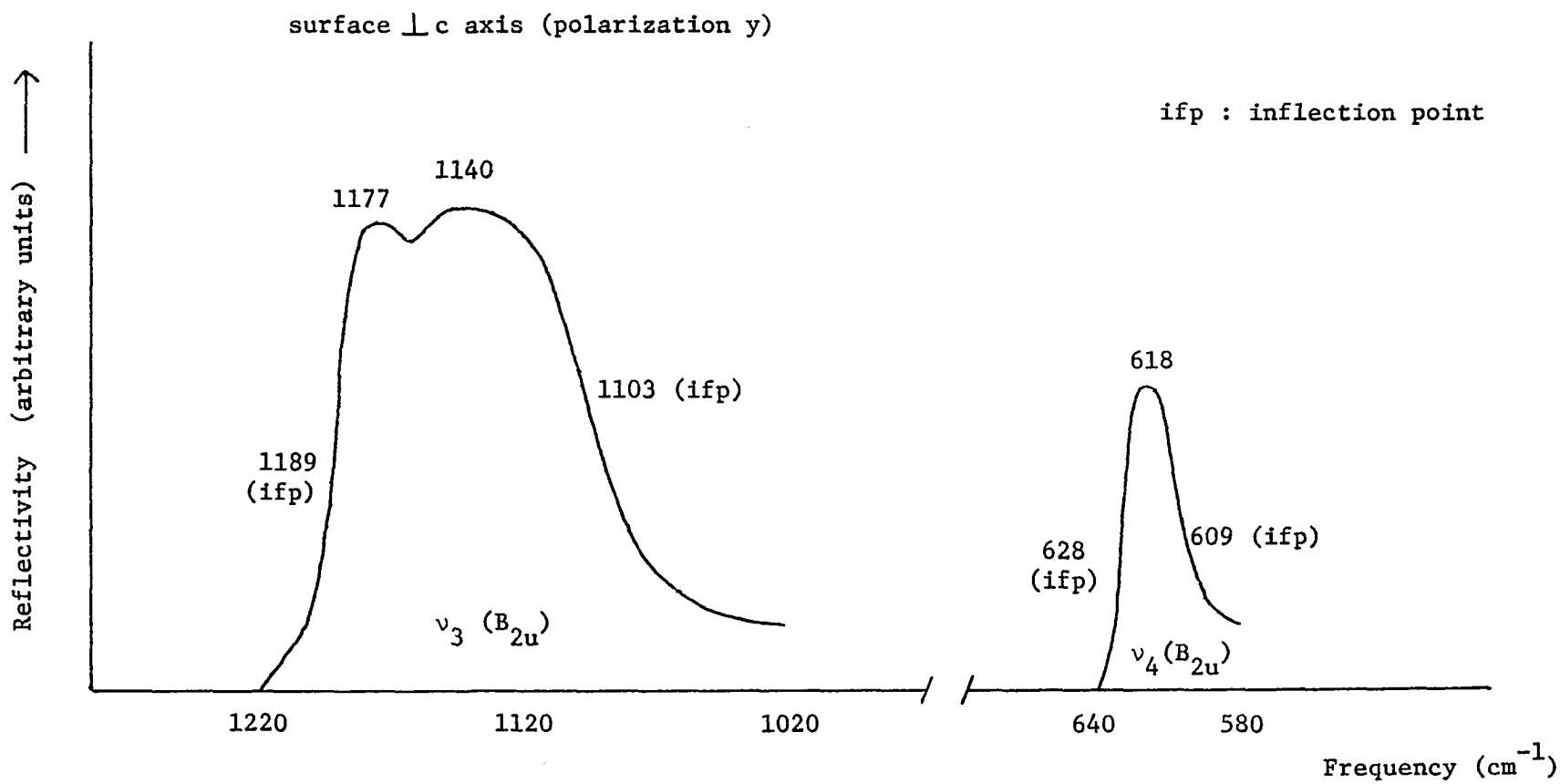

Figure (5-12) Near normal incidence infrared reflection spectra of Na_2SO_4 crystal

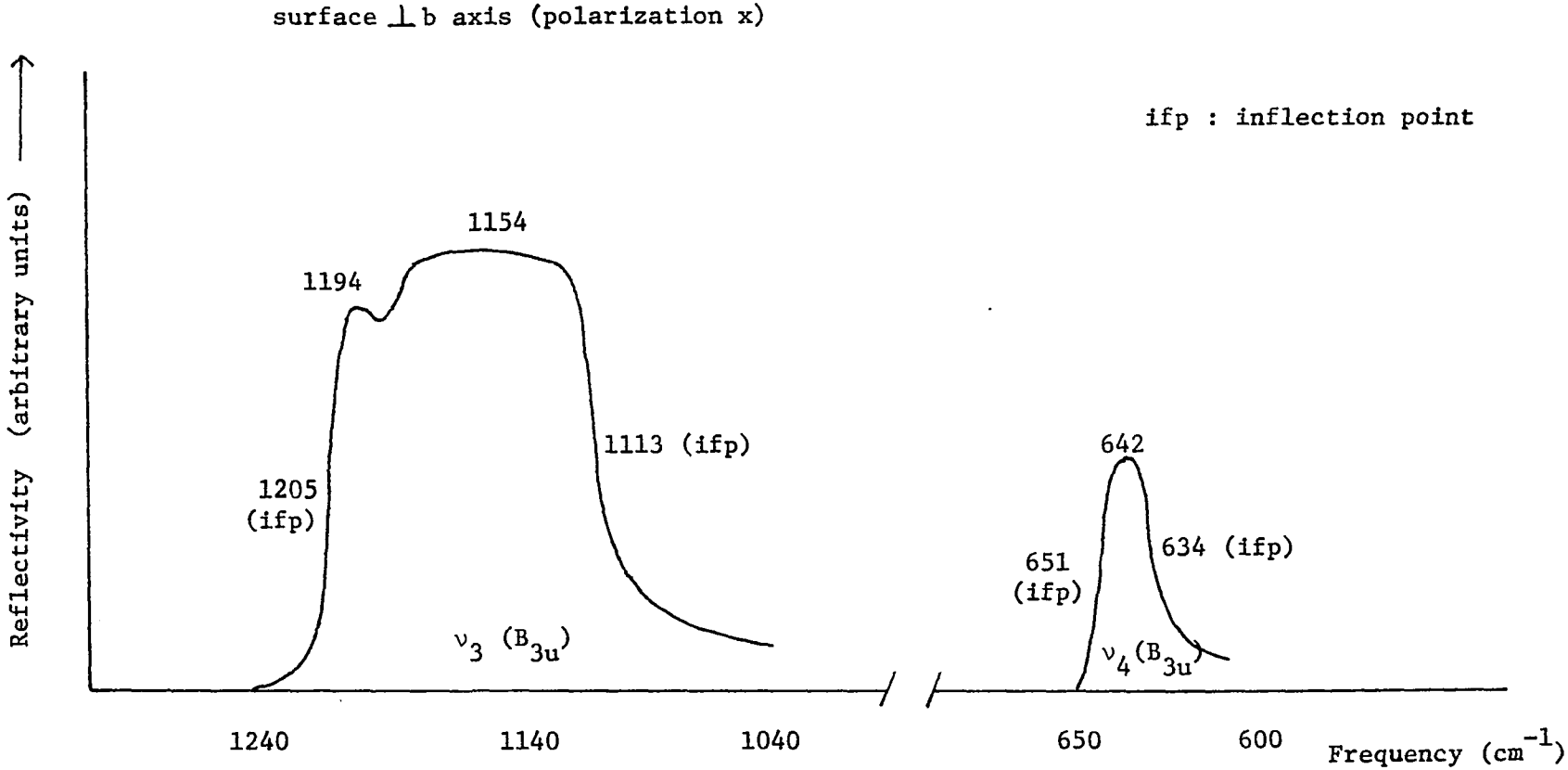

Figure (5-13) Near normal incidence infrared reflection spectra of Na_2SO_4 crystal

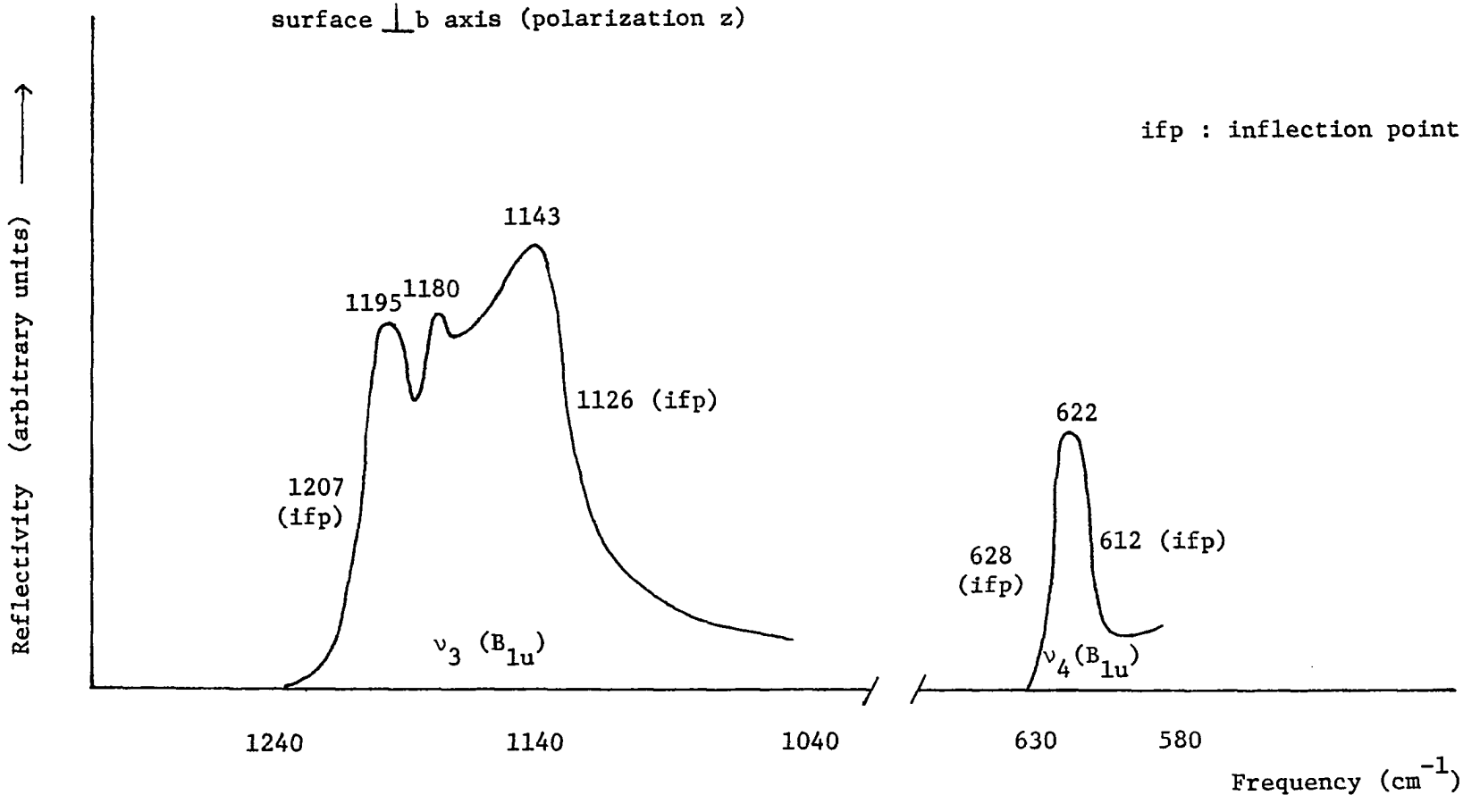

Figure (5-14) Near normal incidence infrared reflection spectra of Na_2SO_4 crystal

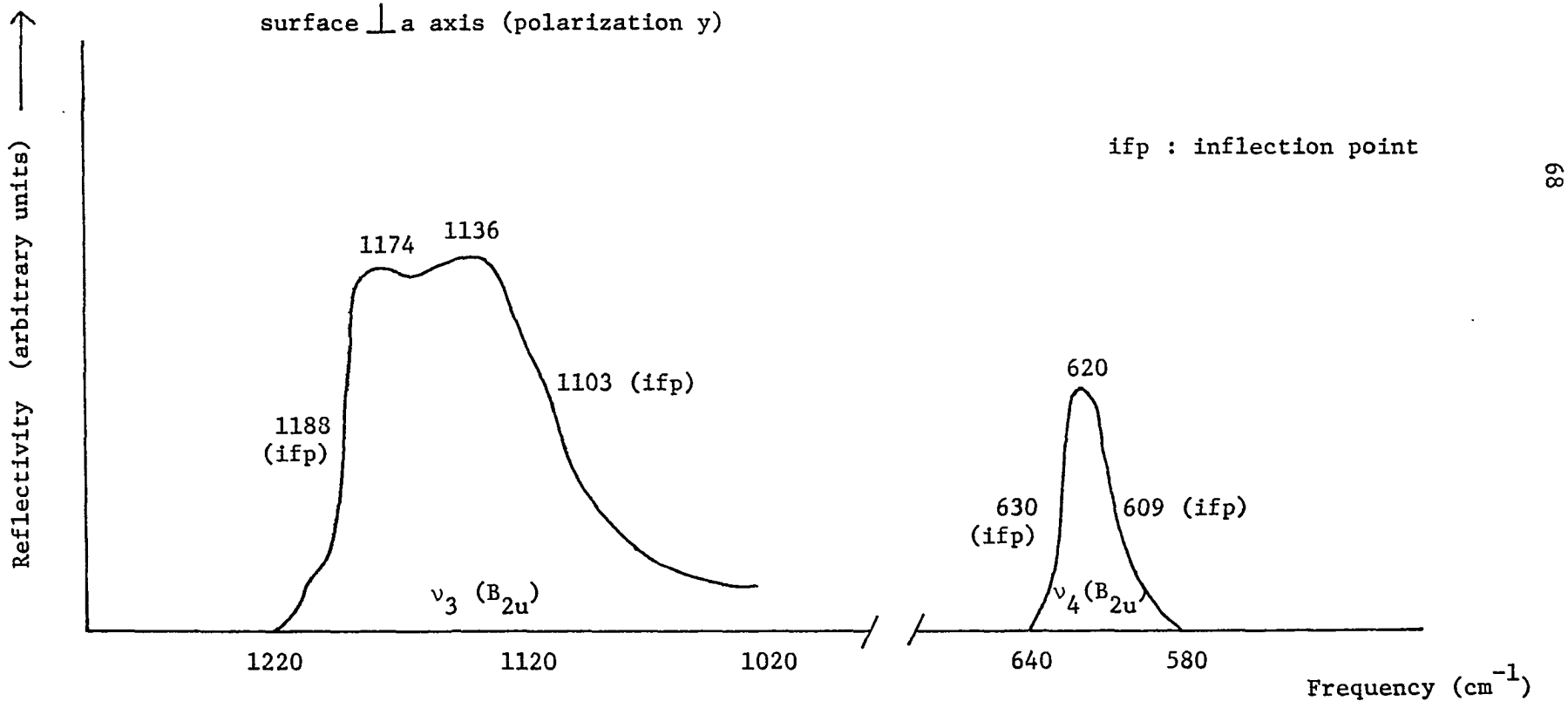

Figure (5-15) Near normal incidence infrared reflection spectra of Na_2SO_4 crystal

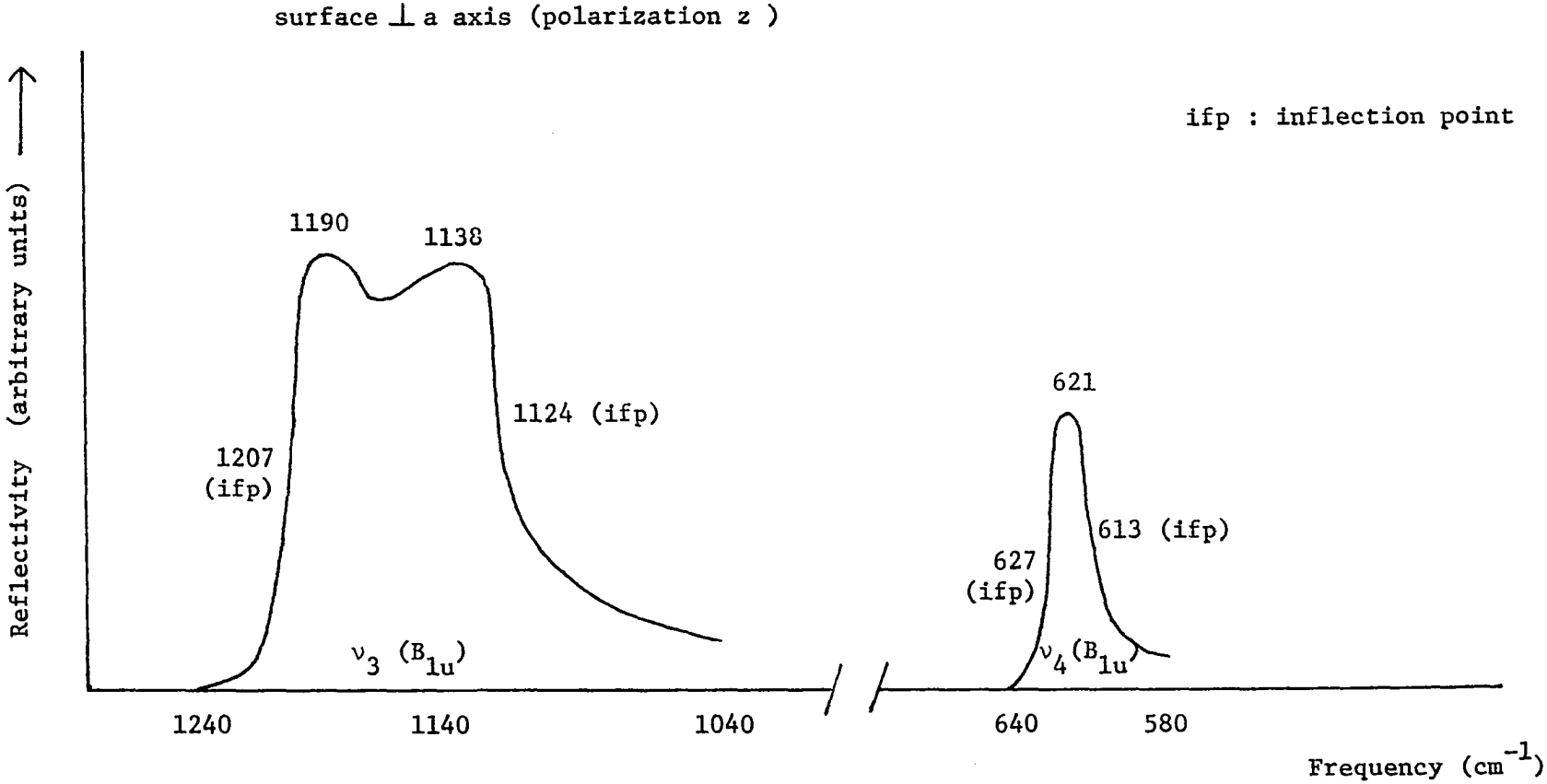

Figure (5-16) Correlation diagram of the internal optic modes of Na_2SO_4 crystal (frequencies in cm^{-1})

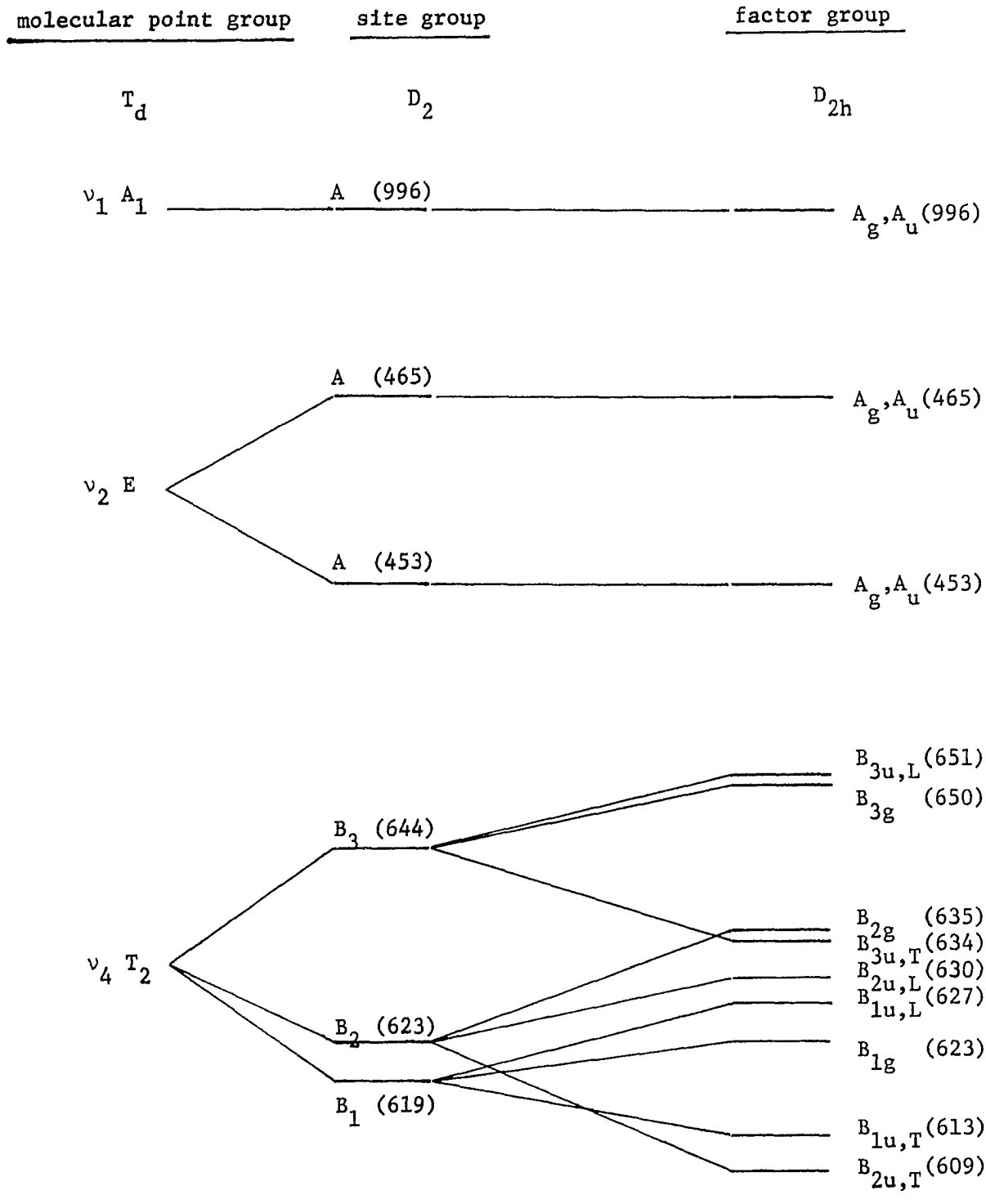

Figure (5-17) Correlation diagram of the internal optic modes of Na_2SO_4 crystal (frequencies in cm^{-1})

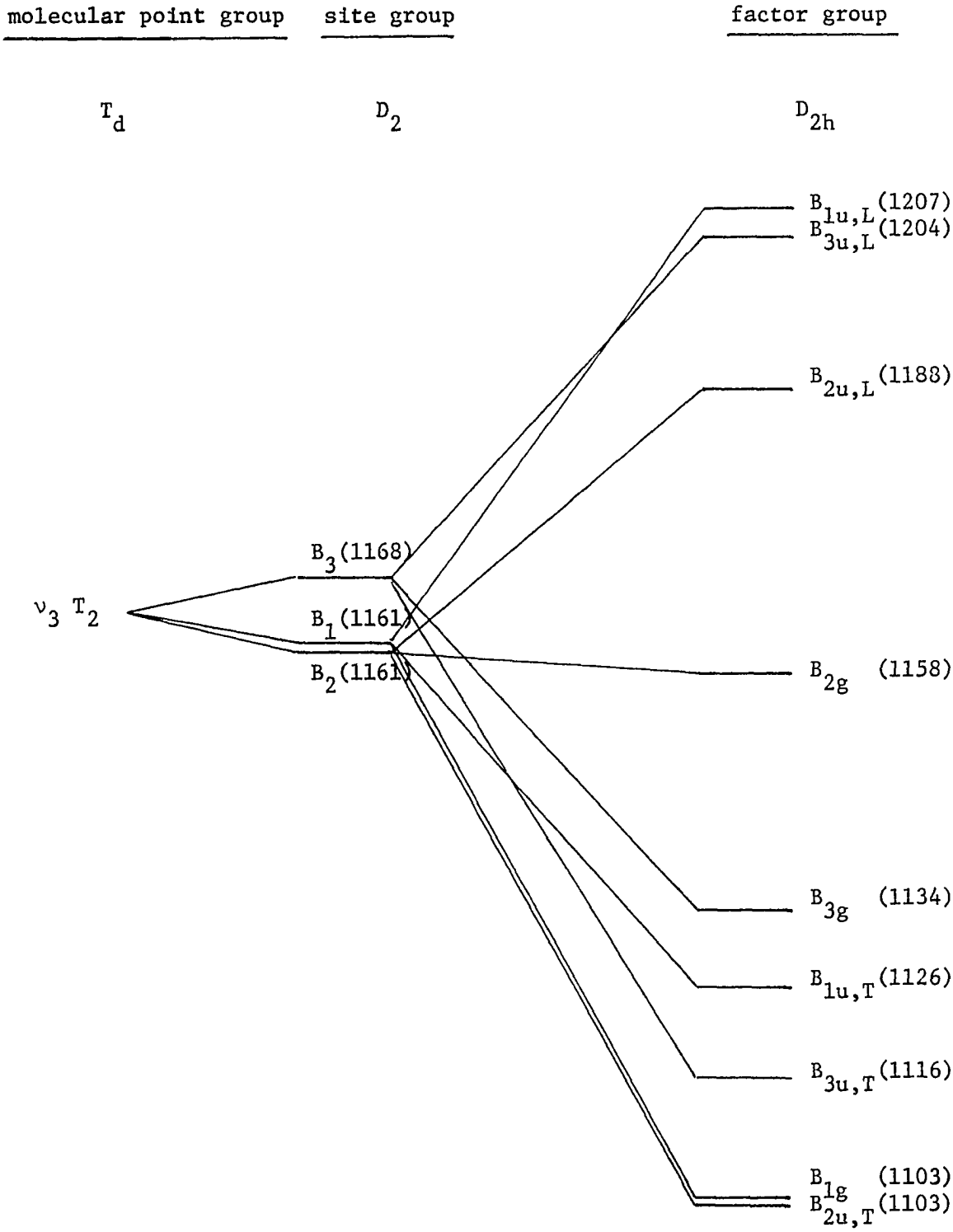

F. $K_2Mg_2(SO_4)_3$

a. Near normal incidence infrared reflection spectra are shown in Figure (5-18). The splittings of the triply degenerate ν_3 and ν_4 are easily observed.

b. Vibrational frequencies as measured by near normal incidence infrared reflection or the Raman method are shown in Table (5-4). The cartesian axes along the three orthogonal crystal axes are designated as x, y, z while another set of axes obtained by a 45^o rotation around the z axis are given by x', y', z. It has been shown by Hartwig, Rousseau, and Porto[1] that in a z(xx)y experiment vibrational modes of symmetries A and E will be excited while in the z(y'x')y' experiment only the modes of E symmetry will be excited. Simple consideration also shows that both transverse and longitudinal modes will be excited in the z(xz)y experiment and only transverse modes will be excited in the z(yz)y experiment. Hence, in principle, the transverse and longitudinal modes of symmetry T and the modes of symmetries A and E can be resolved and identified. Raman spectra show that not all modes predicted by the site group-factor group correlation are seen and sometimes modes of symmetries A and E are not easily resolved from those of symmetry T. The polarizability derivatives and hence the scattering intensities of the missing modes are believed to be so small that they are not seen. The results are summarized as follows for the various spectral regions :

ν_1 : The Raman spectra are shown in Figure (5-19). One peak with frequency 985 cm^{-1} is seen in all four different scattering experiments. This may be understood by assuming that the dipole moment derivative is so small that the correlation field splitting

Figure (5-18) Near normal incidence infrared reflection spectra of $K_2Mg_2(SO_4)_3$

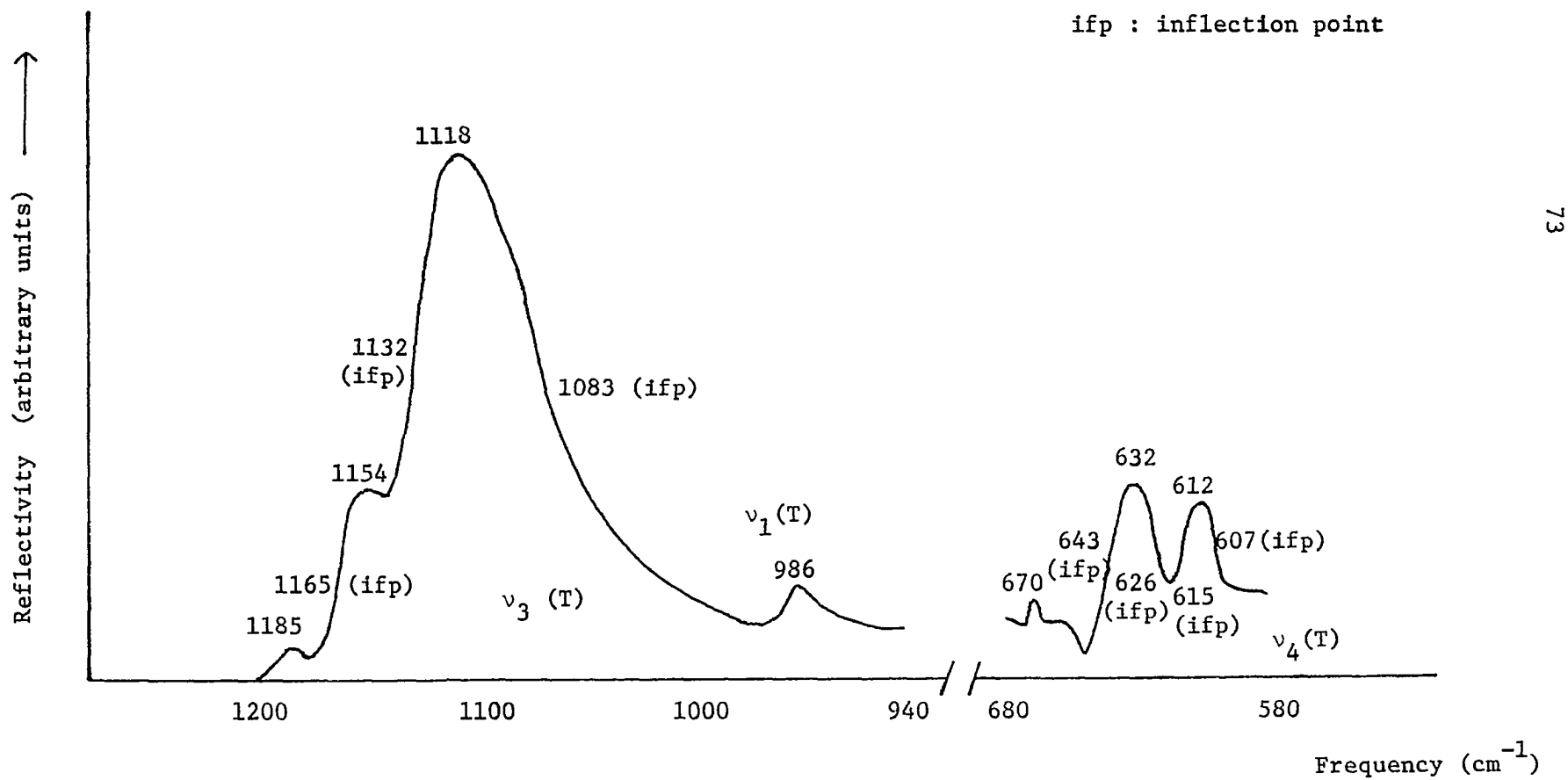

Table (5-4) Vibrational frequencies of $K_2Mg_2(SO_4)_3$ crystal as measured by near normal incidence infrared reflection or the Raman method. (frequencies in cm^{-1})

	γ	ω_L	ω_T	ω	method
ν_1	T				R z(yz)y
	A	One peak with frequency 985 cm^{-1}			R z(xz)y
	E	appears in all scatterings.			R z(xx)y
					R z(x'y')y'
	T	∿986			IR
ν_2	T	462			R z(xz)y
			447		R z(yz)y
	A			459	R z(xx)y
	E			446	R z(y'x')y'
ν_3	T	1111			R z(xz)y
			1080		R z(yz)y
	T	1156			R z(xz)y
			1125		R z(yz)y
	T	∿1185			IR
ν_4	T	615			IR
			606		z(xz)y
			607		IR
	T	643			IR
			632		R z(yz)y
	T	∿670			IR
	A			619	R z(xx)y
	E			609	R z(x'y')y'
	E			631	R z(x'y')y'

Figure (5-19) Single crystal Raman spectra of $K_2Mg_2(SO_4)_3$ in the ν_1 spectral region (frequencies in cm^{-1})

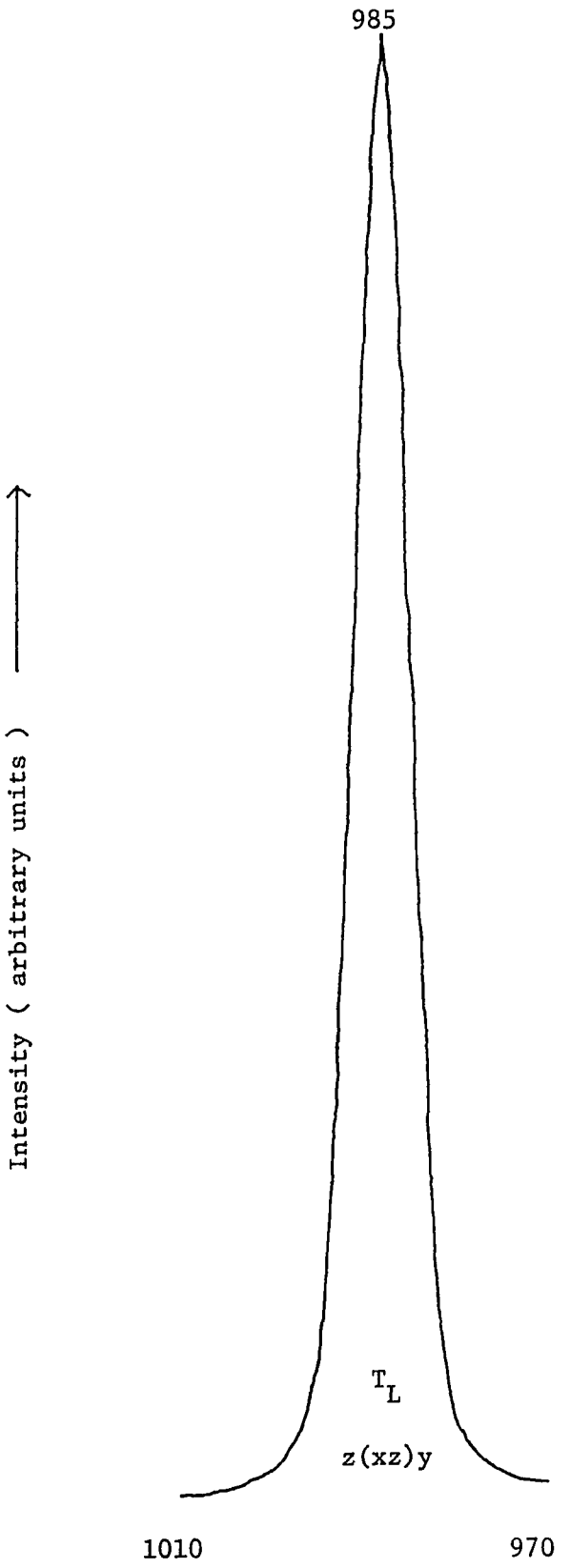

between the T, E, and A modes is not resolved.

ν_2 : The Raman spectra are shown in Figures (5-20) and (5-21). Only one mode of T symmetry, one mode of A symmetry, and one mode of E symmetry are seen rather than the two modes of each symmetry species as predicted by the site group-factor group correlation. The mode with frequency 458 cm^{-1} in the z(x'y')y' experiment is is believed to be a"leaking"A mode.

ν_3 : The Raman spectra are shown in Figure (5-22). Two T modes are seen instead of three as predicted by the site group-factor group correlation. The mode with frequency 1075 cm^{-1} in the z(xz)y experiment may not be a pure transverse mode since the frequency is 5 cm^{-1} less than that observed in other experiments. None of the A or E modes can be unambiguously identified from the polarization measurements.

ν_4 : The Raman spectra are shown in Figures (5-23) and (5-24). Only the transverse modes of two T modes and one A and two E modes are seen. The mode with frequency 620 cm^{-1} in the z(xz)y experiment is believed to be a"leaking"A mode.

c. The $S(\gamma)[I + \alpha_o S(\gamma)]^{-1}$ factors for the transverse and longitudinal modes of irreducible representation T of the unit cell group T^4 are calculated to be -2.08074 and 1.80822 $cm^{-5}sec^2$, respectively.

d. The static crystal field frequencies and dipole moment derivatives are shown below :

Figure (5-20) Single crystal Raman spectra of $K_2Mg_2(SO_4)_3$ in the ν_2 spectral region (frequencies in cm^{-1})

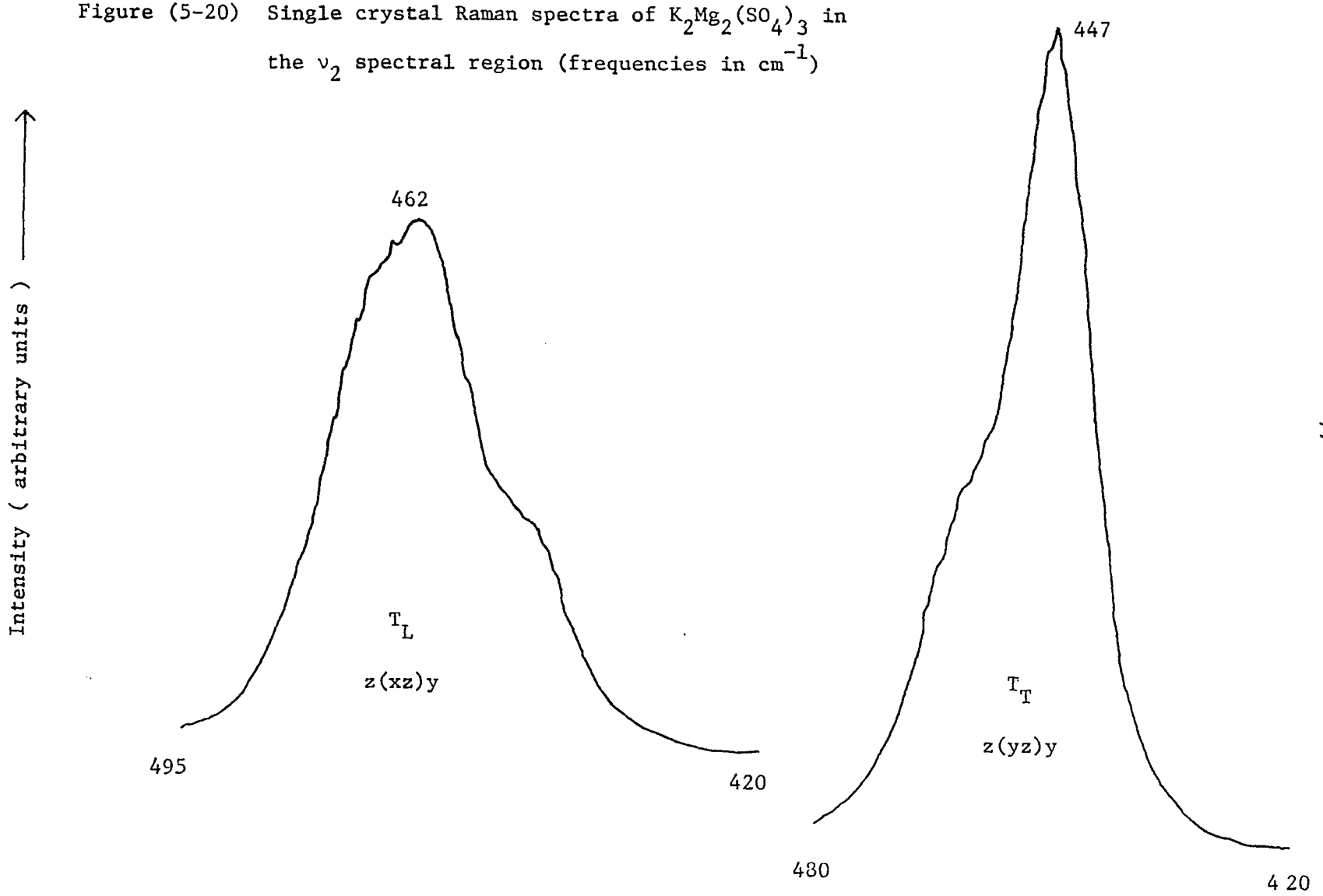

Figure (5-21) Single crystal Raman spectra of $K_2Mg_2(SO_4)_3$ in the ν_2 spectral region (frequencies in cm^{-1})

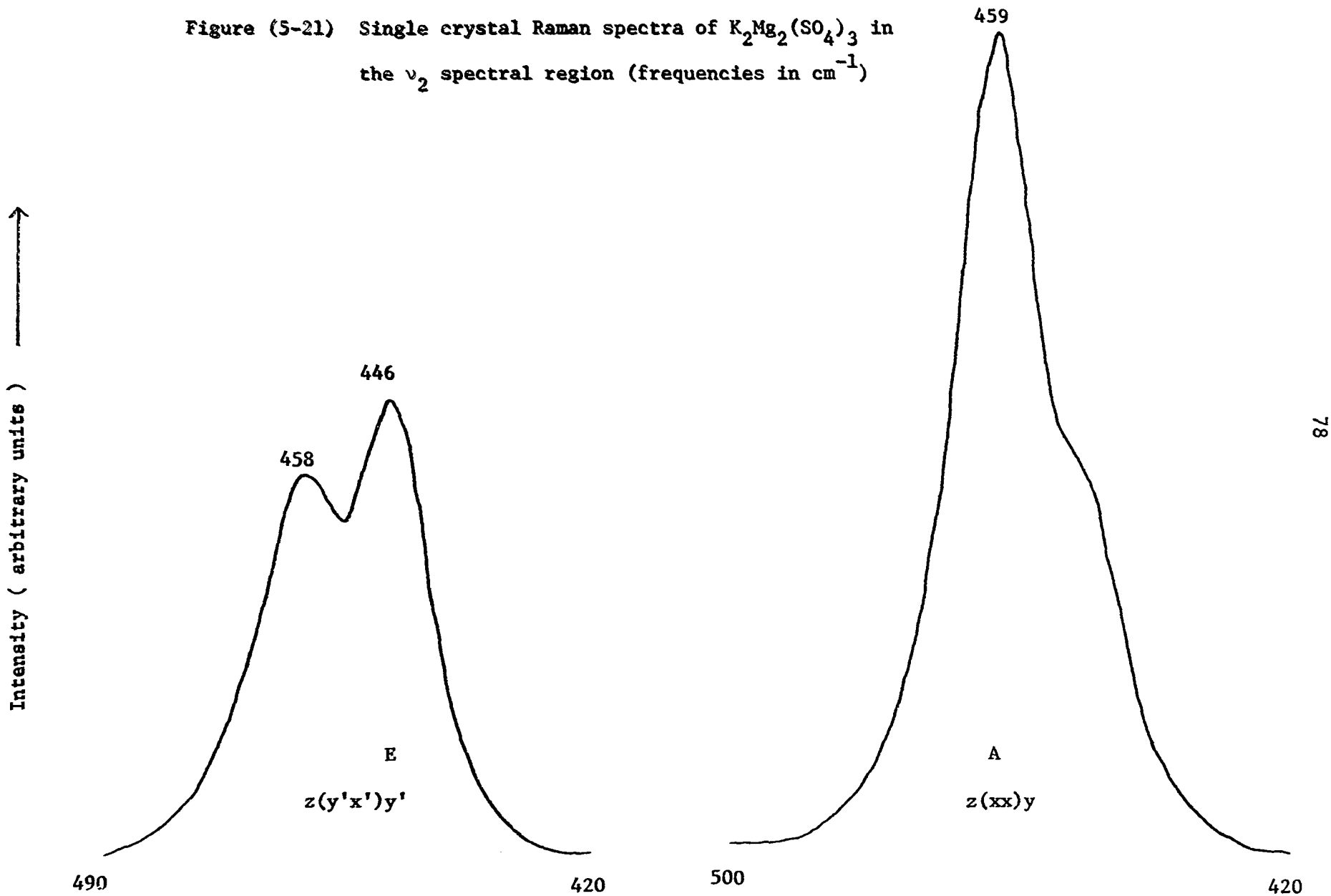

Figure (5-22) Single crystal Raman spectra of $K_2Mg_2(SO_4)_3$ in the ν_3 spectral region (frequencies in cm^{-1})

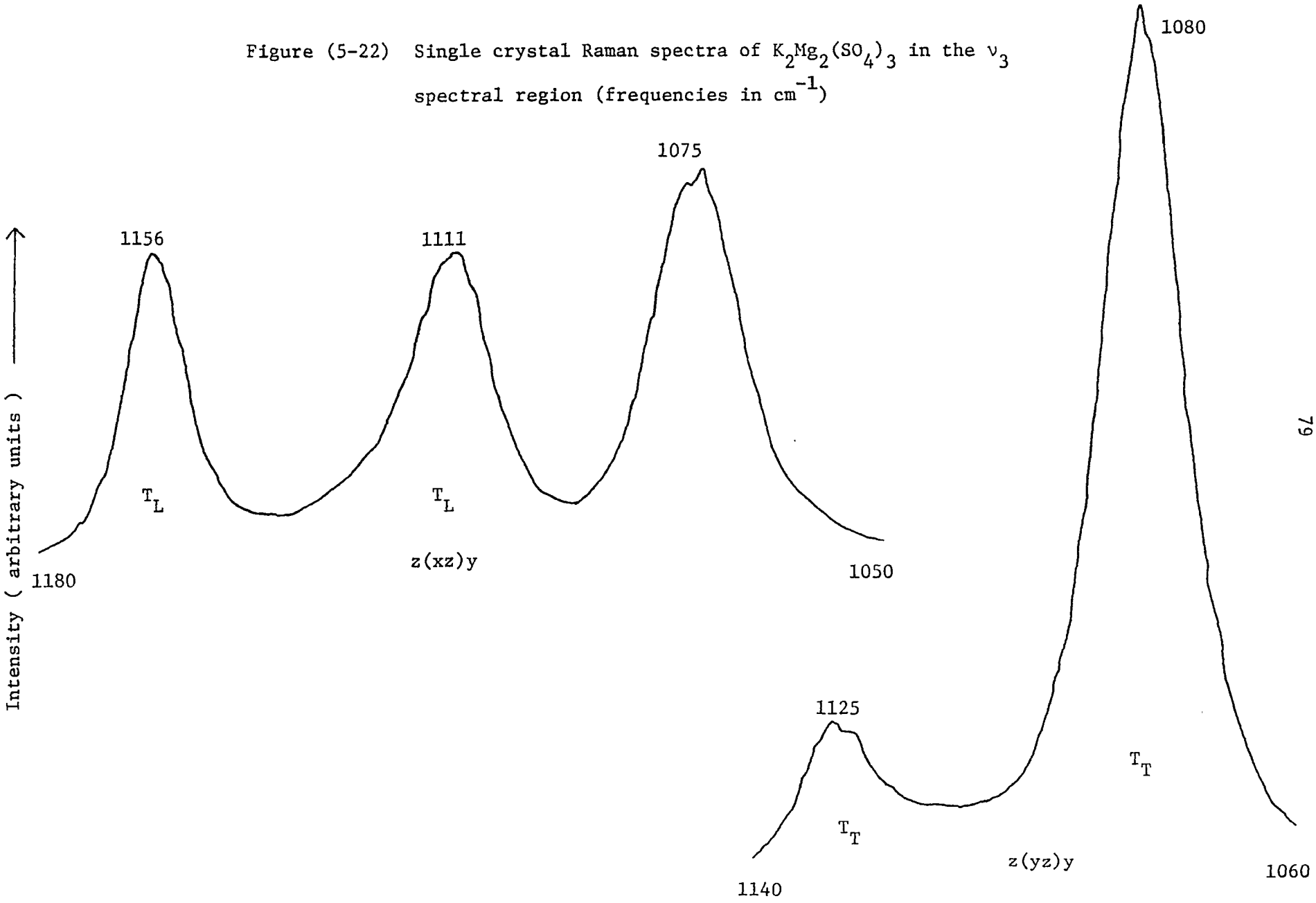

Figure (5-23) Single crystal Raman spectra of $K_2Mg_2(SO_4)_3$ in the ν_4 spectral region

(frequencies in cm^{-1})

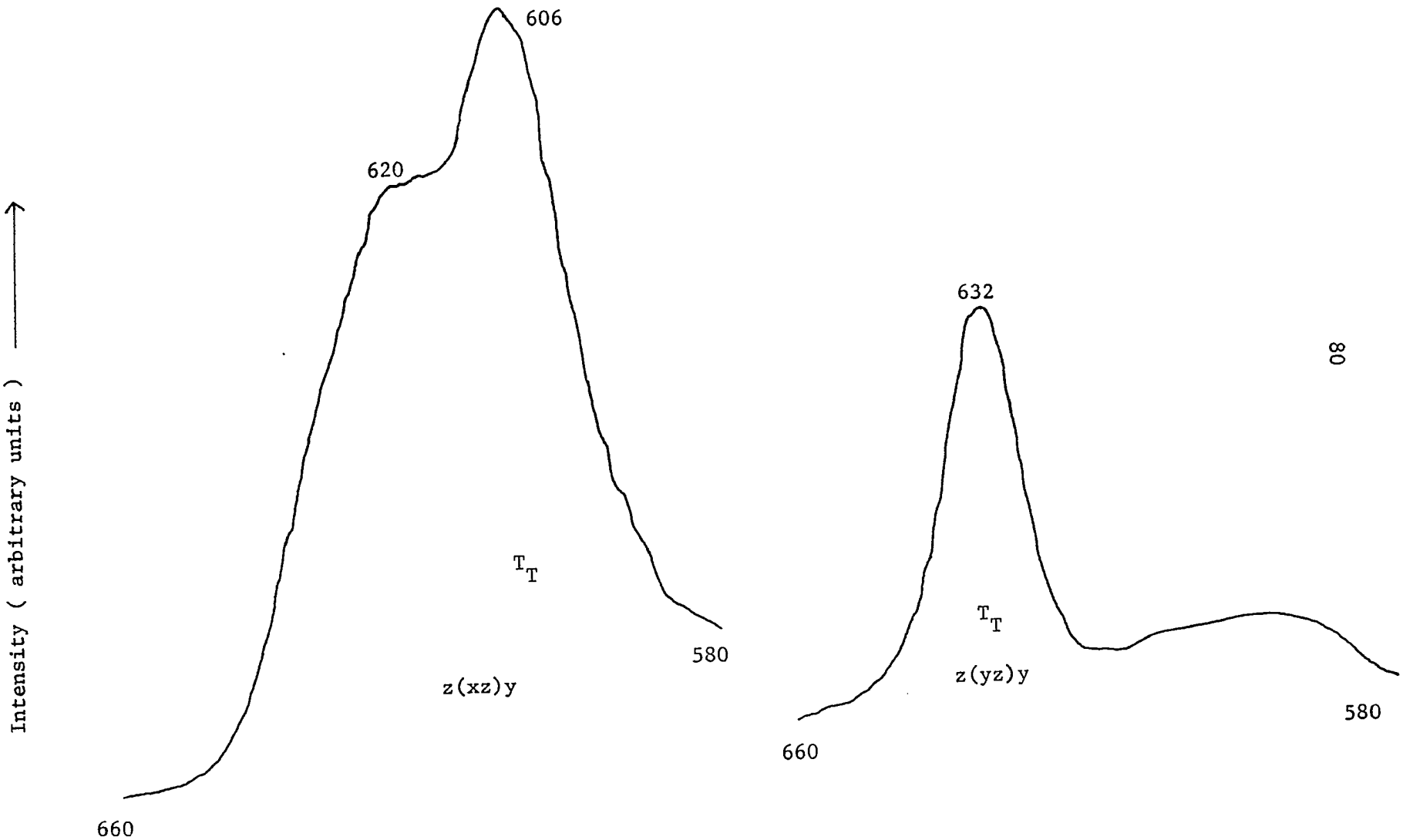

Figure (5-24) Single crystal Raman spectra of $K_2Mg_2(SO_4)_3$ in the ν_4 spectral region (frequencies in cm^{-1})

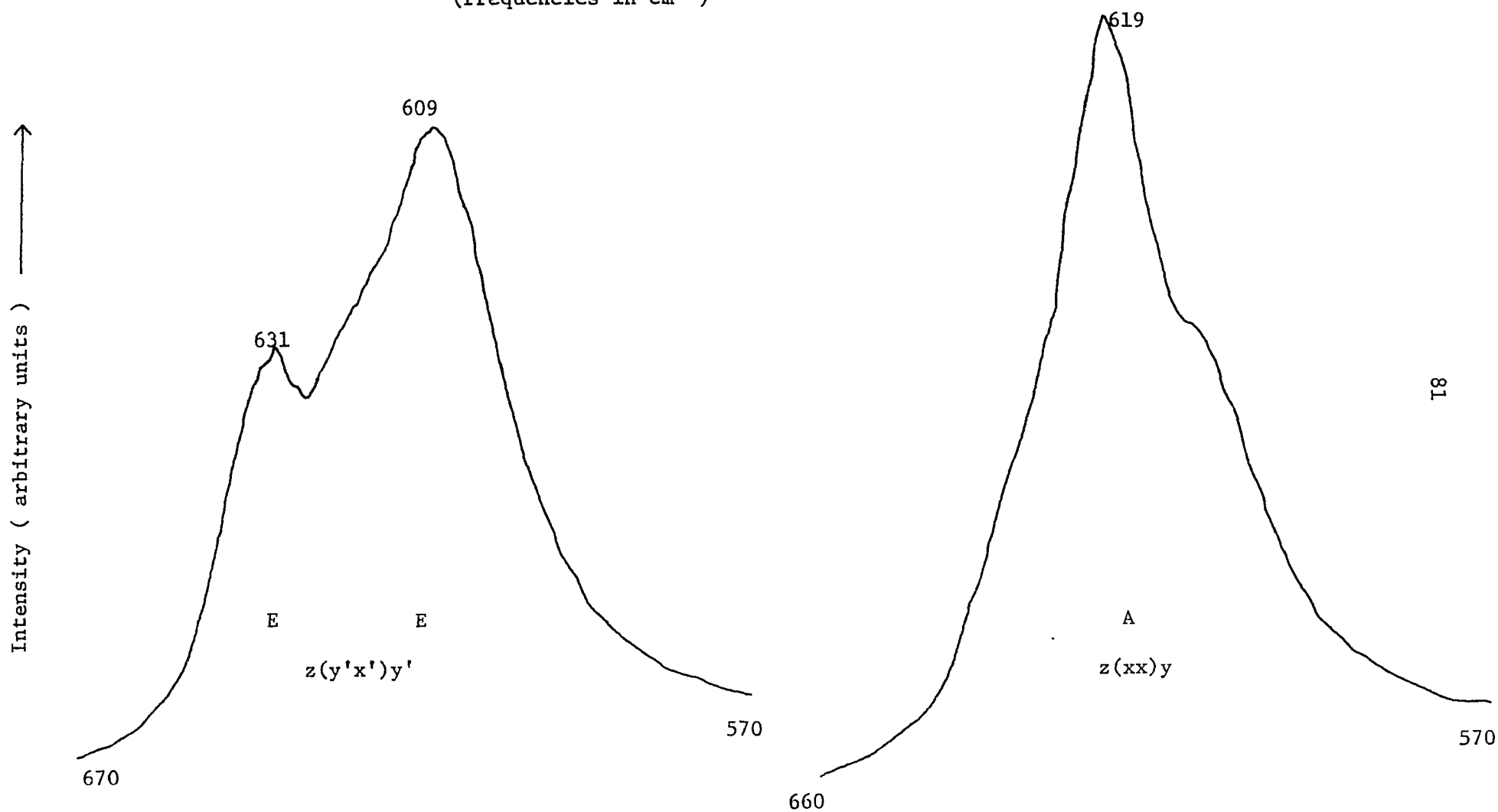

	$\omega_o (cm^{-1})$	$d\mu/dq\ (cm^{3/2} sec^{-1})$
ν_1	985	--
ν_2	455	59
ν_3	1097	132
	1142	135
	$\sim$1185	--
ν_4	611	53
	638	60
	$\sim$670	--

e. The correlation diagram of the internal optic modes is shown in Figure Figures (5-25) and (5-26).

Figure (5-25) Correlation diagram of the internal optic modes of $K_2Mg_2(SO_4)_3$ crystal (frequencies in cm^{-1})

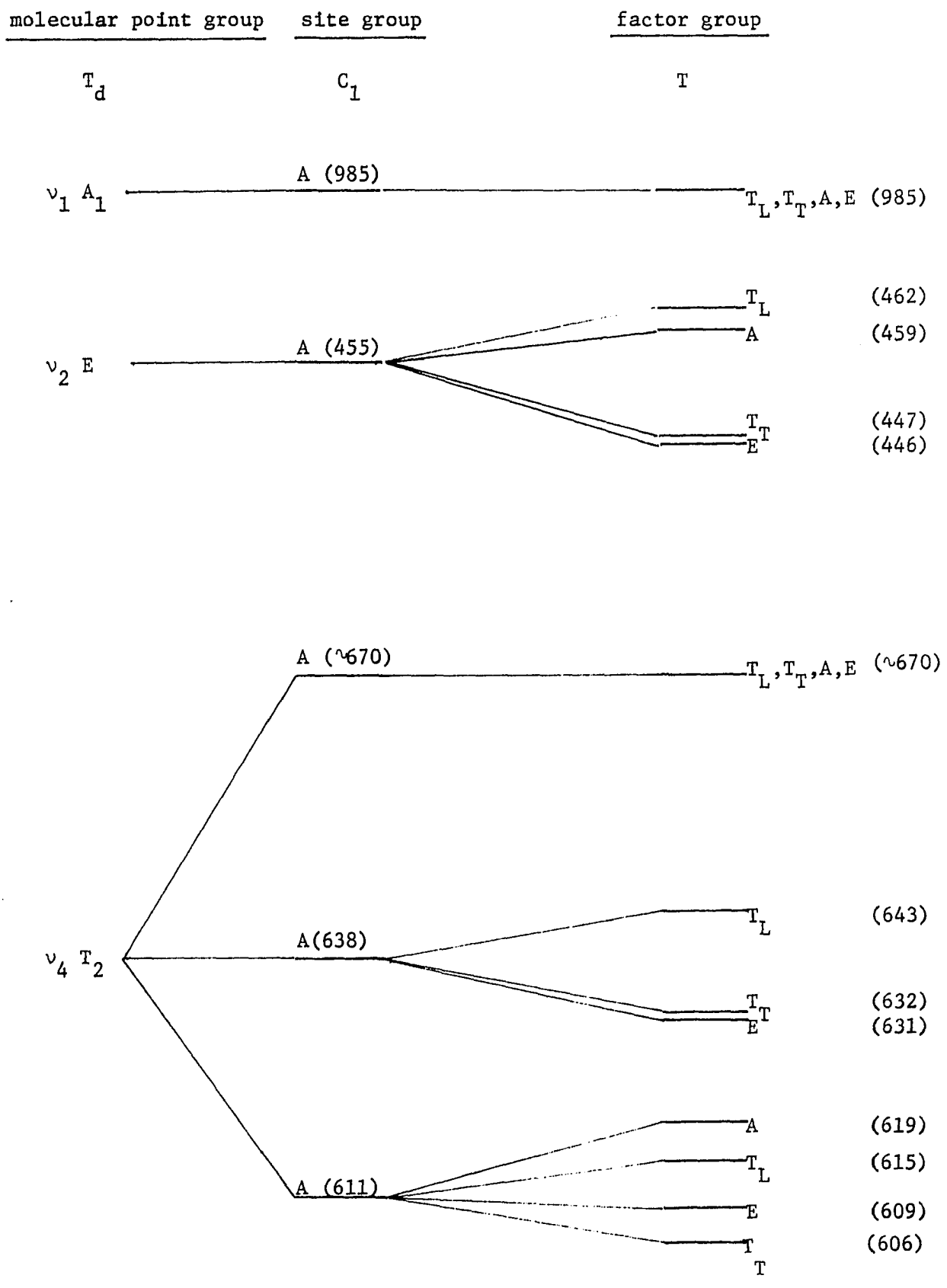

Figure (5-26) Correlation diagram of the internal optic modes of $K_2Mg_2(SO_4)_3$ crystal (frequencies in cm^{-1})

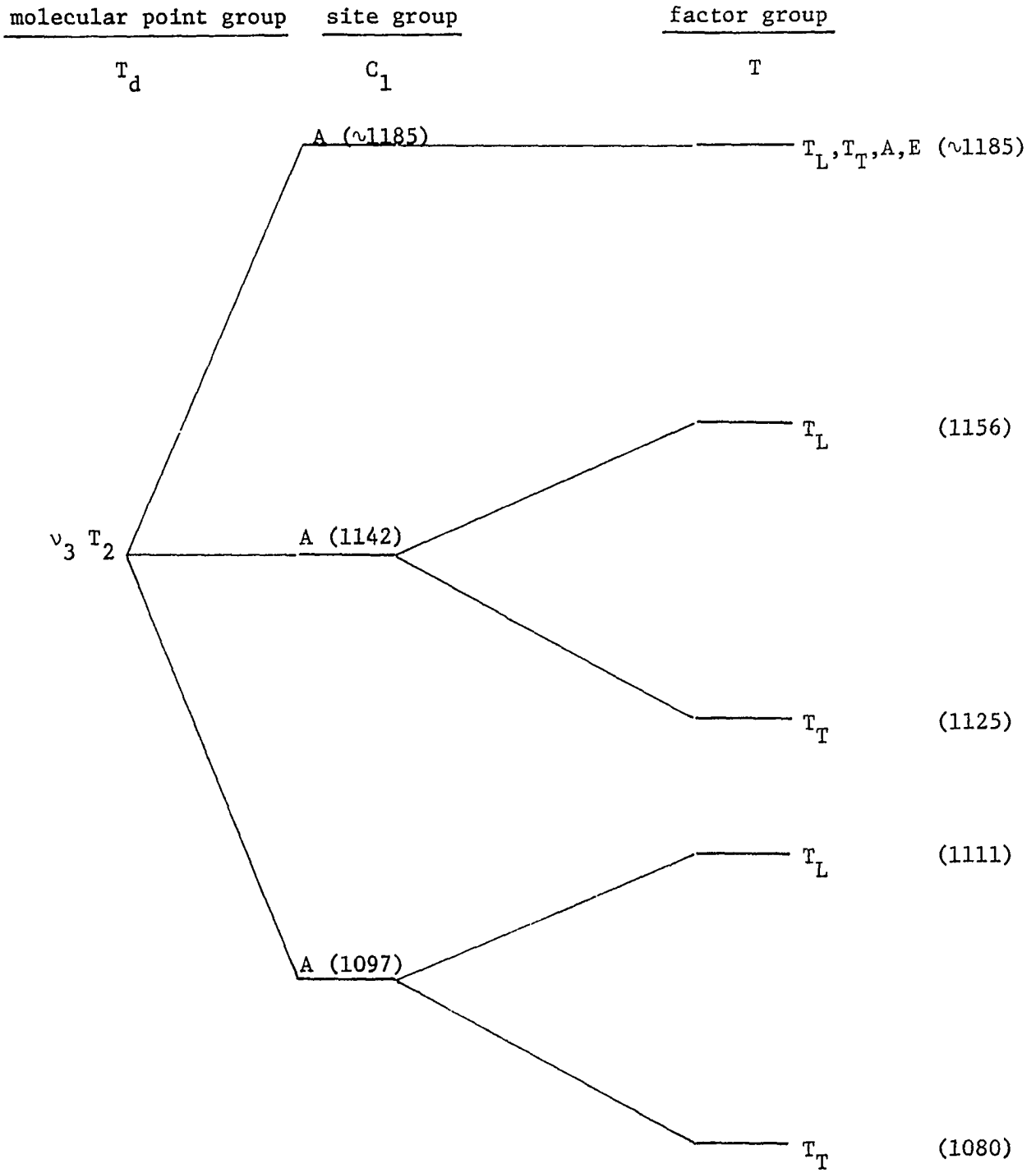

Reference for Chapter V

1. C. M. Hartwig, D. L. Rousseau, and S. P. S. Porto, Phys. Rev. 188, 1328 (1969).

CHAPTER VI

Normal Vibrational Modes Resulting from the Lifting of Degeneracies in Anisotropic Crystals

A. Introduction

If the intramolecular vibrations of polyatomic ions in a crystal are assumed to be dynamically decoupled from intermolecular motion then the normal vibrational coordinates of internal optic modes may be constructed as properly symmetrized linear combinations of molecular normal coordinates. This procedure is usually broken up into several steps by first forming translationally symmetrized linear combinations of molecular normal coordinates and then taking unit cell symmetrized linear combinations of the transformed coordinates. It should be noted that all the Cartesian components of a molecular normal coordinate must be included in order to insure a complete basis set of coordinates from which the internal optic mode normal coordinates may be generated. In the case of phonon coordinates originating in degenerate molecular normal modes whose degeneracies have been lifted due to the lowered symmetry of the potential energy environment at a particular site the corresponding molecular normal coordinate is not available to use as a basis set coordinate. However, the components of that molecular normal coordinate may be used as basis coordinates resulting in several translationally symmetrized and unit cell symmetrized component coordinates which belong to the same unit cell symmetry species. The true internal optic mode normal coordinate is simply a linear combination of those component coordinates belonging to the same unit cell symmetry species.

Suppose that $Q_\alpha(\underset{\sim}{k}_{j\gamma})$ is the linear combination of the αth cartesian component of the jth molecular normal coordinate which belongs to unit cell

symmetry species γ. In the notation of an earlier paper[1] discussing the normal coordinates of a crystal within the framework of the approximation used here

$$\underset{\sim}{W} = \underset{\sim}{\underset{\sim}{X}}\,\underset{\sim}{q} \tag{6-1}$$

defines the transformation from molecular normal coordinates $\underset{\sim}{q}$ to the translationally symmetrized coordinates, $\underset{\sim}{W}$, and

$$\underset{\sim}{Q} = \underset{\sim}{\underset{\sim}{B}}\,\underset{\sim}{W} \tag{6-2}$$

defines the transformation to unit cell symmetrized coordinates, $\underset{\sim}{Q}$. An element of $\underset{\sim}{Q}$ may be written (now explicitely denoting α, the polarization of the coordinate)

$$Q_\alpha(\underset{\sim}{k}_{j\gamma}) = 1/N^{1/2} \sum_{m\ell} \sum B_\alpha(\underset{\sim}{k}_{\gamma m}) \exp[i\underset{\sim}{k}\cdot\underset{\sim}{r}(\ell)]q_\alpha(\underset{\sim}{\ell}_{mj}) \tag{6-3}$$

where m indexes the molecular or ionic species in a multiply occupied unit cell, ℓ designates the unit cell, j refers to a particular molecular normal mode, γ is a unit cell symmetry species, and N is the number of unit cells in the crystal. The wave vector $\underset{\sim}{k}$ refers to a point in the 1st Brillouin zone of the crystal or, equivalently, an irreducible representation label of the translation group of the crystal. Another component of the molecular normal coordinate $q_\beta(\underset{\sim}{\ell}_{mj})$ may give rise to coordinate $Q_\beta(\underset{\sim}{k}_{j\gamma})$ belonging to the same unit cell symmetry species γ.

$$Q_\beta(\underset{\sim}{k}_{j\gamma}) = 1/N^{1/2} \sum_{m\ell} \sum B_\beta(\underset{\sim}{k}_{\gamma m}) \exp[i\underset{\sim}{k}\cdot\underset{\sim}{r}(\ell)]q_\beta(\underset{\sim}{\ell}_{mj}) \tag{6-3'}$$

The normal coordinate of the internal optic mode at $\underset{\sim}{k}$ transforming as γ under the unit cell symmetry operations is then a superposition of the two components,

$$Q(\underset{\sim}{k}_{j\gamma}) = Q_{\alpha}(\underset{\sim}{k}_{j\gamma}) + Q_{\beta}(\underset{\sim}{k}_{j\gamma}) \qquad (6\text{-}4)$$

Consider the following example.

B The Normal Coordinates of Internal Optic Modes in K_2SO_4

The space group of potassium sulfate is D_{2h}^{16} with four sulfates in the unit cell which occupy the positions as shown in chapter III. (See Section K_2SO_4) The standard correlation diagram for the intramolecular vibrations of the sulfate ion is also shown there. Consider one of the degenerate molecular modes in the molecular point group such as the triply degenerate mode ν_3. The unit cell symmetry projection operator is successively applied to the translationally symmetrized x,y, and z components of the mode. It is possible to construct both an x polarized coordinate and a y polarized coordinate that transform as A_g, another x and y oriented pair that transform as B_{1g}, and two other x and y pairs that transform as B_{2u} and B_{3u} respectively. One z polarized coordinate can be constructed that transforms like B_{2g}, another z oriented coordinate which transforms like B_{3g}, and two others which transform as A_u and B_{1u} respectively. The correct normal coordinates of the internal optic modes are constructed from unit cell symmetrized coordinates and shown in Figures (6-1) and (6-2). It is interesting to note in the B_{2u} mode there is a net moment in the y direction for the unit cell but no net moment along the x direction. Therefore the B_{2u} mode can interact with a y polarized electromagnetic wave but not an x polarized electromagnetic wave even though there are x oriented dipoles at each of the four sulfate sites in the unit cell. Similarly the B_{3u} mode can interact with x polarized radiation but not y polarized radiation even though there are individual y oriented dipoles at each of the sulfate sites.

Mode	Combination of sites in unit cell	Geometric representation
A_g	$\frac{1}{2}[x(1)-x(2)+x(3)-x(4)]$	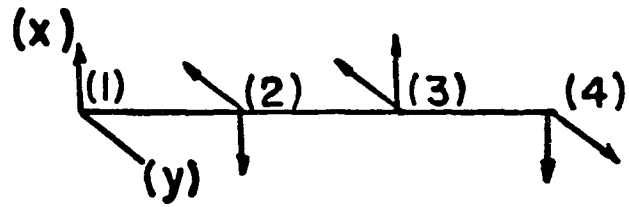
	$\frac{1}{2}[y(1)-y(2)-y(3)+y(4)]$	
B_{1g}	$\frac{1}{2}[x(1)-x(2)-x(3)+x(4)]$	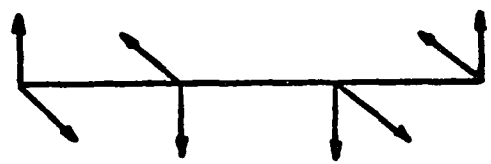
	$\frac{1}{2}[y(1)-y(3)+y(3)-y(4)]$	
B_{3u}	$\frac{1}{2}[x(1)+x(2)+x(3)+x(4)]$	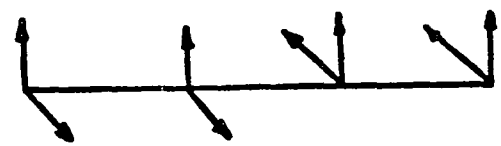
	$\frac{1}{2}[y(1)+y(2)-y(3)-y(4)]$	
B_{2u}	$\frac{1}{2}[x(1)+x(2)-x(3)-x(4)]$	
	$\frac{1}{2}[y(1)+y(2)+y(3)+y(4)]$	

Figure (6-1) X-Y oriented internal optic mode normal coordinates of sulfate ion in potassium sulfate

Mode	Combination of sites in unit cell	Geometric representation
B_{2g}	$\frac{1}{2}[z(1) - z(2) + z(3) - z(4)]$	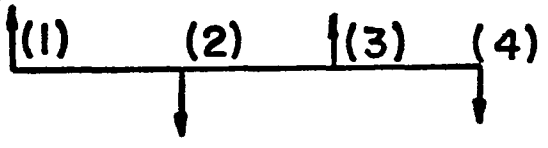
B_{3g}	$\frac{1}{2}[z(1) - z(2) - z(3) + z(4)]$	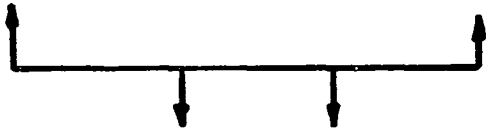
A_u	$\frac{1}{2}[z(1) + z(2) - z(3) - z(4)]$	
B_{1u}	$\frac{1}{2}[z(1) + z(2) + z(3) + z(4)]$	

Figure (6-2) Z oriented internal optic mode normal coordinates of sulfate ion potassium sulfate

Although there is no net dipole moment in the x direction for the B_{2u} mode the individual site x-oriented dipoles will couple and shift the frequency of the B_{2u} transverse mode to the same extent as the frequency of the B_{2u} longitudinal mode. The y-oriented dipoles of course shift the frequency of the B_{2u} transverse mode by a different amount than the shift in the B_{2u} longitudinal mode. Similarly the frequency of the transverse B_{3u} mode depends on the interactions of the y-oriented site dipoles as well as the x-oriented site dipoles even though there is no net y-oriented dipole moment for a unit cell. A useful formalism for calculating this effect is described in the next section.

C. Internal Optic Modes in the Molecular Dipole Model

The vibrational dynamics of internal optic modes in crystals may be described in terms of a molecular dipole model.[1-4] (See chapter II). The normal vibrations of a molecular species localized at lattice sites give rise to vibrationally induced dipoles and the resulting dipolar interactions are summed over appropriate lattice or sublattices of the crystal. These dipole sums appear in frequency shift and intensity shift equations. For a crystal with n ions in a unit cell the set of dipole sums may be represented by a n x n dipolar interaction matrix when each element of the n x n matrix is itself a 3 x 3 Cartesian submatrix. One element of the Cartesian submatrix might be

$$S_{\alpha\beta}(\underset{\sim}{k}_{mm'}) = \sum_{\ell} \delta_{\alpha\beta} / \left| r_{\alpha}(\ell_m) - r_{\beta}(\ell'_{m'}) \right|^3$$

$$-3(r_{\alpha}(\ell_m) - r_{\beta}(\ell'_{m'}))(r_{\alpha}(\ell_m) - r_{\beta}(\ell'_{m'})) / \left| r_{\alpha}(\ell_m) - r_{\beta}(\ell'_{m'}) \right|^5$$

$$x \quad \exp[i \underset{\sim}{k} \cdot (\underset{\sim}{r}(\ell) - \underset{\sim}{r}(\ell'))] \qquad (6\text{-}5)$$

where $r_\alpha(\overset{\ell}{m})$ is the αth Cartesian component of the vector from some convenient origin to the mth ion in the ℓth unit cell and

$$\underset{\sim}{r}(\overset{\ell}{m}) = \underset{\sim}{r}(\ell) + \underset{\sim}{r}(m) \tag{6-6}$$

Here $\underset{\sim}{r}(\ell)$ is the vector from the origin to the origin of the ℓth unit cell and $\underset{\sim}{r}(m)$ is the vector from the ℓth unit cell origin to the mth ion in that unit cell. In the notation of reference 1 the frequency of the phonon mode transforming under unit cell symmetry species γ at the $\underset{\sim}{k}$th point in the first Brillouin zone and originating in the molecular normal mode labeled by j is given by

$$\omega^2(\overset{k}{\underset{\sim}{j\gamma}}) = [\omega^{(m)}(\overset{o}{j\gamma})]^2 + \underset{\alpha\beta}{\Sigma\Sigma}\,[(\partial\mu_\alpha/\partial q)(\overset{k}{\underset{\sim}{j\gamma}})]$$

$$\times\,[S_{\alpha\beta}(\overset{k}{\underset{\sim}{j\gamma}})[I + \alpha_{o,\alpha\beta}S_{\alpha\beta}(\overset{k}{\underset{\sim}{j\gamma}})]^{-1}]\,[(\partial\mu_\alpha/\partial q)(\overset{k}{\underset{\sim}{j\gamma}})] \tag{6-7}$$

Here $(\partial\mu_\alpha/\partial q)$ is a molecular dipole moment derivative, α_o refers to the electronic polarizability components, and $\omega^{(m)}(\overset{o}{j\gamma})$, the static crystal field frequency, is the frequency that the molecular species would have in the absence of all intermolecular dynamical coupling effects. The transformed S matrix is

$$S_{\alpha\beta}(\overset{kk}{\underset{\sim}{\gamma\gamma}}) = \underset{m\ m'}{\Sigma\ \Sigma}\, B_\alpha(\overset{k}{\underset{\sim}{\gamma m}})\ S_{\alpha\beta}(\overset{kk}{\underset{\sim}{mm'}})\ B_\beta^{-1}(\overset{k}{\underset{\sim}{\gamma m'}}) \tag{6-8}$$

where $\underset{\sim}{B}$ is the transformation matrix in equation (6-2).

For example the frequency of the Brillouin zone center B_{3u} mode may be written in an obvious notation (ignoring dipolar interactions between x and y polarized component coordinates by taking $S_{xy}(\overset{kk}{\underset{\sim}{mm'}}) = 0$ for all sites m and m')

$$\omega^2(\nu_{3}_{B_{3u}}) = \omega_o^2(\nu_{3}_{B_{3u}}) + S_{xx}(B_{3u})[I + \alpha_{o,xx}S_{xx}(B_{3u})]^{-1}(\partial\mu_x/\partial q_{\nu_3})^2$$

$$+ S_{yy}(B_{3u})[I + \alpha_{o,yy}S_{yy}(B_{3u})]^{-1}(\partial\mu_y/\partial q_{\nu_3})^2 \qquad (6\text{-}9)$$

Although the calculation for K_2SO_4 in the above equation was considerably simplified by assuming that $S_{\alpha\beta}(\underset{\sim}{k}\underset{\sim}{k}_{mm'}) = 0$ for $\alpha \neq \beta$ in certain cases it is found that $S_{\alpha\beta}(mm')$ vanishes, depending on the symmetry of the site at which the dipolar interactions occur with the rest of the crystal. Referring to equation (6-5) $S_{\alpha\beta}(\underset{\sim}{k}\underset{\sim}{k}_{mm'})$ is the interaction of the dipole at some unit cell site m with the dipole at unit cell site m' and all other dipoles translationally equivalent to m'. Therefore the vanishing of $S_{\alpha\beta}(\underset{\sim}{k}\underset{\sim}{k}_{mm'})$ is determined by the symmetry of the site m or m'. In fact, of the 32 possible site symmetries only 5 can give rise to non-vanishing $S_{\alpha\beta}$ elements. These site symmetries and the non-vanishing $S_{\alpha\beta}$ elements associated with those sites are listed below.

Site Symmetry	Non-vanishing $S_{\alpha\beta}$
C_1	All $S_{\alpha\beta}$
C_i	All $S_{\alpha\beta}$
$C_2(\delta)$	$S_{\alpha\beta}$
$C_s(\sigma_h = \sigma_{\alpha\beta})$	$S_{\alpha\beta}$
$C_{2h}(\sigma_h = \sigma_{\alpha\beta})$	$S_{\alpha\beta}$

It is interesting to note that among the 32 point groups to which the factor groups of the 230 possible space groups are isomorphic only C_1, C_i, C_2, C_s, and C_{2h} possess one dimensional representations that transform as (α,β) or (α,β,γ). This of course ensures the non-vanishing of the corresponding molecular dipole moment derivatives $\partial\mu_\alpha/\partial q$ and $\partial\mu_\beta/\partial q$

or $\partial\mu_\alpha/\partial q$, $\partial\mu_\beta/\partial q$, and $\partial\mu_\gamma/\partial q$ if the molecular normal coordinate q belongs to that particular representation. However, these are also the point groups of sites for which non-vanishing $S_{\alpha\beta}$ elements occur. In other words, the existence of a non-zero $S_{\alpha\beta}$ is a sufficient condition for the symmetry allowed non-zero dipole moment derivatives $\partial\mu_\alpha/\partial q$ and $\partial\mu_\beta/\partial q$.

D. Application to K_2SO_4 Crystal

In a recent paper by Mesarole, Decius, and Carlson[5] it was shown that in a potassium sulfate crystal the S_{xy} elements were small compared to S_{xx} and S_{yy} elements. Therefore the S_{xy} elements will be neglected here. The dipolar coupling factors are calculated by the method of Ewald[6] and Kornfeld[7] and are shown below.

Mode(γ)	Polarization(α)	$S_{\alpha\alpha}(I + \alpha_o S_{\alpha\alpha})^{-1}$ ($cm^{-5}sec^2$)
A_g	x	-0.71607
	y	-1.30750
B_{1g}	x	0.30405
	y	-0.25138
B_{2u}	x	-1.47805
	y (transverse)	-1.82842
	(longitudinal)	1.30053
B_{3u}	x (transverse)	-2.31264
	(longitudinal)	1.06742
	y	0.83200
B_{2g}	z	-1.19011
B_{3g}	z	-1.34887
A_u	z	-0.29000
B_{1u}	z (transverse)	-1.87190
	(longitudinal)	1.30980

The components of the electronic polarizability tensor were determined from the optical refractive data and appropriate dipolar sums.[8] From the measured refractive indices, $n_x^D = 1.4973$, $n_y^D = 1.4935$, and $n_z^D = 1.4974$ and a cation polarizability of 1.03 $\mathring{A}^3$, the following values of the electronic polarizability tensor are calculated: $\alpha_{xx} = 5.20\ \mathring{A}^3$, $\alpha_{yy} = 5.25\ \mathring{A}^3$, and $\alpha_{zz} = 5.20\ \mathring{A}^3$. (See chapter IV) The four equations for the transverse and lonitudinal frequencies for the B_{2u} and B_{3u} internal optical modes were simultaneously solved for the static crystal field frequencies and the molecular dipole moment derivatives. The same procedure was also applied to the B_{1u} internal optic mode. The transverse and longitudinal frequencies were estimated by Mesarole, Decius, and Carlson[5] from inflection points in the near normal incidence polarized reflection spectrum of the ν_3 and ν_4 region. These results are in Table (6-1). From the calculated dipole moment derivatives and static crystal field frequencies it is possible to calculate predicted values for the Raman active modes. This has been done and the calculated values are compared with the experimental values as measured by Meserole, Decius, and Carlson[5] in Table (6-2). The numbering of the rows of data in Table (6-2) refers to the numbered rows of data in Table (6-1). The calculations for each row in Table (6-2) are based on the data from the corresponding row in Table (6-1). The calculated values are in reasonable agreement with the observed frequencies in the ν_4 region but are somewhat higher than the experimental values in the ν_3 region. The discrepancy may be due to other interactions not included in the molecular dipole formalism.

The correlation diagrams of the internal optic modes are shown in Figure (6-3) and Figure (6-4).

Table (6-1) Static crystal field frequencies and dipole monent derivatives of the sulfate ion in potassium sulfate (frequencies in cm^{-1})

	Internal Optic Mode	Transverse Frequency	Longitudinal Frequency	Static Crystal Field Frequency	Molecular Dipole Moment Derivatives ($cm^{3/2}$ sec^{-1})		
					$\partial\mu_x/\partial q$	$\partial\mu_y/\partial q$	$\partial\mu_z/\partial q$
1.	$B_{2u}(\nu_3)$	1108	1138	1140	156	147	--
	$B_{3u}(\nu_3)$	1123	1158				
2.	$B_{2u}(\nu_3)$	1140	1170	1170	141	149	--
	$B_{3u}(\nu_3)$	1160	1188				
3.	$B_{1u}(\nu_3)$	1105	1170	1143	--	--	216
4.	$B_{2u}(\nu_4)$	614.5	620.5	620	43	49	--
	$B_{3u}(\nu_4)$	618	623				
5.	$B_{2u}(\nu_4)$	623.5	628.5	629	54	45	--
	$B_{3u}(\nu_4)$	624.5	632				
6.	$B_{1u}(\nu_4)$	617	627	623	--	--	63

Table (6-2) Predicted and measured frequencies of Raman active internal optic modes in potassium sulfate.

Mode	Predicted Frequency (cm^{-1})	Measured Frequency (cm^{-1})
1. $A_g(\nu_3)$	1119	1093
$B_{1g}(\nu_3)$	1140	1110
2. $A_g(\nu_3)$	1151	1146
$B_{1g}(\nu_3)$	1170	
3. $B_{2g}(\nu_3)$	1115	1104
$B_{3g}(\nu_3)$	1114	1104
4. $A_g(\nu_4)$	616	614
$B_{1g}(\nu_4)$	620	618
5. $A_g(\nu_4)$	625	627
$B_{1g}(\nu_4)$	629	
6. $B_{2g}(\nu_4)$	619	619
$B_{3g}(\nu_4)$	618	619

Figure (6-3) Correlation diagram of the internal optic modes of K_2SO_4 crystal (frequencies in cm^{-1})

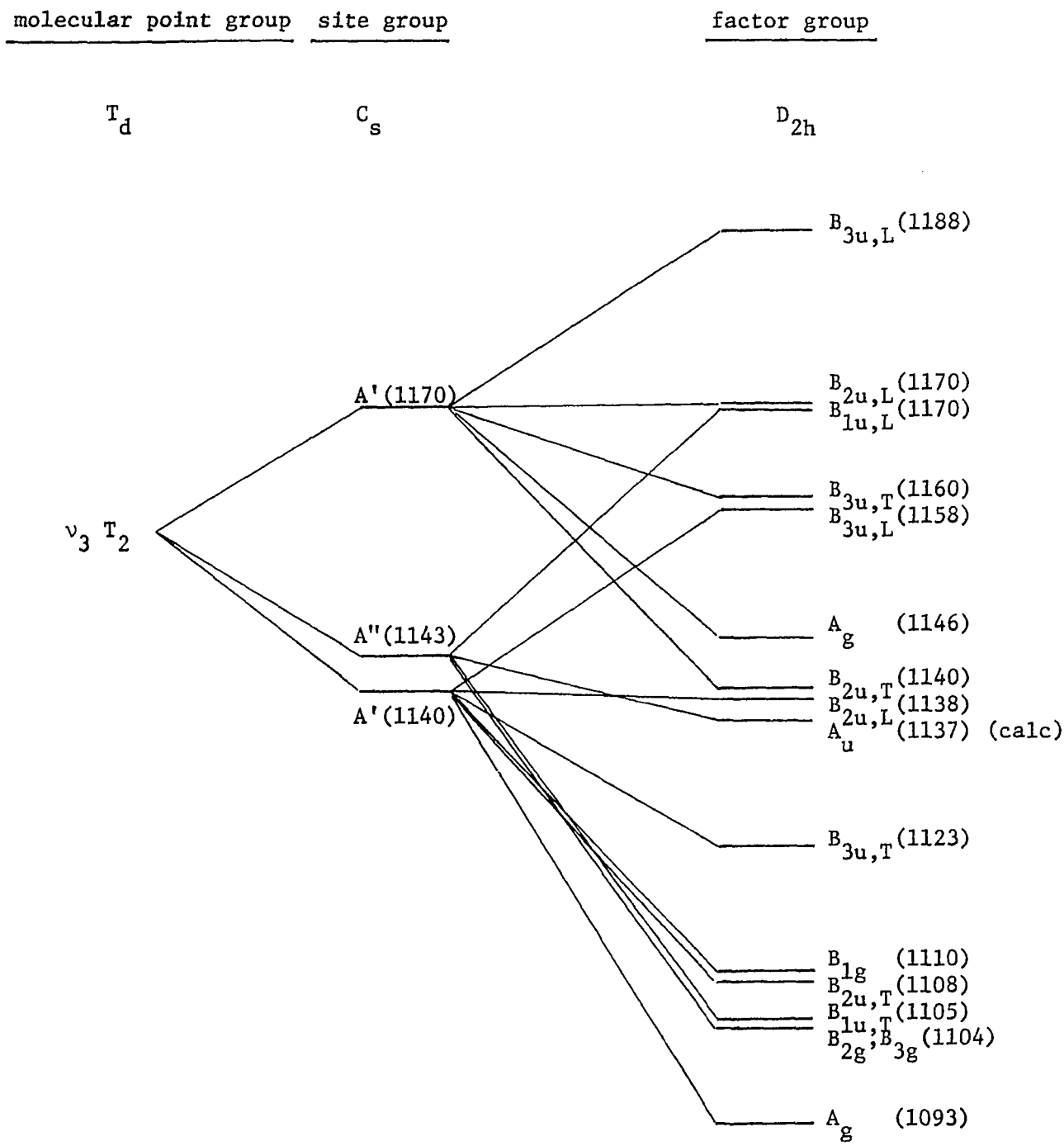

Figure (6-4) Correlation diagram of the internal optic modes of K_2SO_4 crystal (frequencies in cm^{-1})

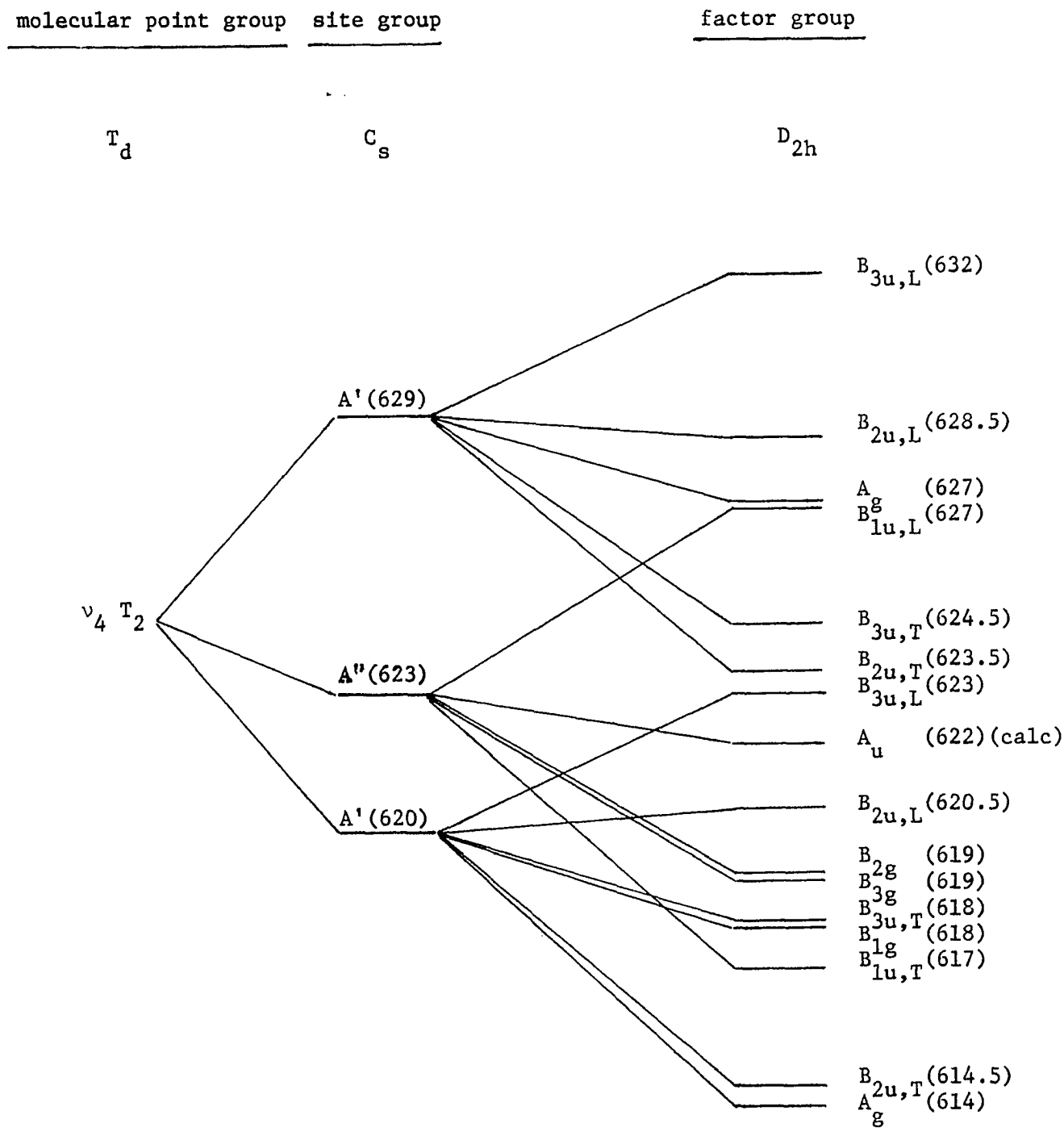

References for Chapter VI

1. R. Frech, J. Chem. Phys. 58, 5067 (1973).

2. J. C. Decius, J. Chem. Phys. 49, 1387 (1968).

3. R. M. Hexter, J. Chem. Phys. 33,1833 (1960); 36, 2285 (1962); 39,1608 (1963).

4. E. R. Nixon and F. D. Verderame, J. Chem. Phys. 41, 1682 (1964).

5. F. Meserole, J. C. Decius and R. E. Carlson, Spectrochimica Acta 30A, 2179 (1974).

6. P. P. Ewald, Ann. Phys. 64, 253 (1921).

7. H. Kornfeld, Z. Phys. 22, 27 (1924).

8. H. C. Bolton et al., Proc. Phys. Soc. (London) 80, 199 (1962).

CHAPTER VII

Discussion

The static crystal field frequencies ω_o and dipole moment derivatives for the ν_1, ν_2, ν_3, and ν_4 internal modes of the sulfate ion are shown in Table (7-1) for different crystalline environments.

In the non-centrosymmetric systems the frequencies of the longitudinal and transverse modes can be quite accurately determined by Raman scattering experiments. In centrosymmetric systems the frequencies are inferred from the inflection points of the near normal incidence reflection spectra; however this is only an approximation since the frequencies of the longitudinal and transverse modes do not exactly correspond to the inflection points if the damping factor is considered. A discrepancy (greater than $4cm^{-1}$) between the observed and calculated Raman frequencies is noted for ν_3 in $LiKSO_4$ and $KNaSO_4$ and ν_3 and ν_4 in Na_2SO_4 and K_2SO_4. (see chapter V and VI). The improper choice of the longitudinal and transverse mode frequencies is probably not the only factor that causes this discrepancy. As Meserole, Decius, and Carlson[1] pointed out the frequencies of the longitudinal and transverse modes chosen by inspection of the inflection points differ only 2 cm^{-1} from those calculated by the dielectric model. Furthermore the excellect agreement in calculating the static crystal field frequencies of ν_3 in the K_2SO_4 crystal still does not allow an accurate prediction of the frequencies of the A_g, B_{1g}, B_{2g}, and B_{3g} modes observed by Raman scattering. This discrepancy may be due to other interactions not included in the molecular dipole model formalism. However the predicted ordering in the frequencies of the Raman active modes does agree with the experimental data:

$KNaSO_4$: $\quad \nu_{3,A_{1g}} > \nu_{3,E_g}$

$$\nu_{3,B_{2g}} > \nu_{3,B_{3g}} > \nu_{3,B_{1g}}$$

Na_2SO_4: $\nu_{4,B_{3g}} > \nu_{4,B_{2g}} > \nu_{4,B_{1g}}$

$\nu_{3,B_{1g}} > \nu_{3,A_g}$

$\nu_{4,B_{1g}} > \nu_{4,A_g}$

$\nu_{3,B_{2g}} \simeq \nu_{3,B_{3g}}$

K_2SO_4: $\nu_{4,B_{2g}} \simeq \nu_{4,B_{3g}}$

The data in Table (7-1) provides an opportunity to consider the effect of various crystalline environments on the site splitting of degenerate molecular normal modes as well as the static crystal field shifts on the non-degenerate molexular normal mode ν_1. This static crystal field shift varies 32 cm^{-1} from the sulfate ion on a C_1 site in $K_2Mg_2(SO_4)_3$ (985 cm^{-1}) to a C_3 site in $LiKSO_4$ (1017 cm^{-1}).

The site group splitting of the triply degenerate ν_3 mode exhibits a rather surprising difference as one compares the $LiKSO_4$ crystal and the $KNaSO_4$ crystal. In both of these crystals the triply degenerate mode T_2 splits into a doubly degenerate mode E and a non-degenerate mode, either A or A_1 in $LiKSO_4$ and $KNaSO_4$, respectively. In the $LiKSO_4$ there is no discernible site group splitting between A (1162 cm^{-1}) and E (1162 cm^{-1}), but in the $KNaSO_4$ crystal the site group splitting is 86 cm^{-1} between A_1 (1217 cm^{-1}) and E (1131 cm^{-1}). Although the site group of the $SO_4^=$ ion is C_3 in $LiKSO_4$ and C_{3v} in $KNaSO_4$, the static crystalline environment is sufficiently similar in the two crystals so that this difference is somewhat unexpected.

The pattern of site group splitting of ν_3 is quite similar in the two orthorhombic crystals studied, K_2SO_4 and Na_2SO_4. In each of those crystals the site group effects splits ν_3 into three non-degenerate modes, two of which have similar frequencies and lower than the third mode. The Na_2SO_4 lattice splits ν_3 into B_1 (1161 cm^{-1}), B_2 (1161 cm^{-1}), and B_3 (1168 cm^{-1}) while the K_2SO_4 lattice

splits ν_3 into A' (1140 cm^{-1}), A'' (1143 cm^{-1}), and A' (1170 cm^{-1}).

The pattern of the site group splitting of ν_4 in $LiKSO_4$ and $KNaSO_4$ is just the opposite of the pattern observed for ν_3 in these two crystals. As before the triply degenerate ν_4 mode splits into a doubly degenerate component and a non-degenerate component. However here there is almost no site group splitting in the $KNaSO_4$ crystal between A_1 (625 cm^{-1}) and E (624 cm^{-1}) while the site group splitting is 13 cm^{-1} in the $LiKSO_4$ crystal comparing A (630 cm^{-1}) and E (643 cm^{-1}).

The splitting of ν_4 in the orthorhombic crystals is similar and comparable to the splitting of ν_3 in these crystals. Here the triply degenerate ν_4 mode splits into two non-degenerate modes of roughly the same frequency and a third non-degenerate mode of a higher frequency. In Na_2SO_4 ν_4 splits into B_1 (619 cm^{-1}), B_2 (623 cm^{-1}), and B_3 (644 cm^{-1}) while in K_2SO_4 $_4$ gives rise to A' (620 cm^{-1}), A'' (623 cm^{-1}), and A' (629 cm^{-1}).

There are certain intuitively appealing correlations one might wish to draw which are simply not supported by the data. If the data for the width of the site group splitting of ν_3 in $K_2Mg_2(SO_4)_3$, K_2SO_4, and Na_2SO_4 are considered, at first glance it appears that the amount (width) of the splitting is related to the degree of symmetry that a site possesses. The sites in those three crystals belong to the groups C_1, C_s, and D_2, with corresponding maximum splitting widths of 88 cm^{-1}, 33 cm^{-1}, and 7 cm^{-1}, respectively, suggesting that the fewer symmetry elements a site possesses, the lower the symmetry of the potential energy resulting from the static crystal field, and hence the greater the splitting of the degeneracies of the ion on that site. This conclusion is not supported by the splittings of the ν_4 mode in those three crystals, where the comparable values are 59 cm^{-1}, 6 cm^{-1}, and 25 cm^{-1}. An even more dramatic example is provided by ν_3 in $LiKSO_4$ and $KNaSO_4$. The site symmetries are C_3 and C_{3v} respectively, yet the splitting of ν_3 amounts to 86 cm^{-1} at the C_{3v} site

while it is not discernible at the site of C_3 symmetry which is a subgroup of C_{3v}.

It is possible to point out some general features of the dipole moment derivatives referring to Table (7-1). Each phonon mode considered here consists of intramolecular motions of the sulfate ion in which that motion leads to a non-zero molecular dipole moment derivative in either one, two, or three Cartesian directions simultaneously. Generally the dipole moment derivatives of modes which are doubly degenerate are comparable to the values of non-degenerate modes which are active in only one direction. All of these modes in turn have associated dipole moment derivatives which are significantly larger than those belonging to non-degenerate modes which are simultaneously active in two or three Cartesian directions. If one considers just the phonon modes originating in ν_3 it is possible to further distinguish between the dipole moment derivatives of non-degenerate modes which are active in two directions as being larger than the dipole moment derivatives of non-degenerate modes which are active in three directions. This latter conclusion is not true for the ν_4 mode and may be related to the very different kinds of intramolecular motions that comprise ν_3 and ν_4, namely an asymmetric stretching and an asymmetric bending motion, respectively.

It is also interesting to note that the $\nu_3(E)$ modes in $LiKSO_4$ and $KNaSO_4$ have identical dipole moment derivatives, but that of $\nu_3(A)$ is much larger in $LiKSO_4$ than in $KNaSO_4$. Since the $\nu_3(A)$ mode is polarized along the z axis, this difference is probably related to the close approach of the highly polarizing Li^+ ion along the z axis and one of the S-O bonds.

Table (7-1) Static Crystal Field Frequencies and Dipole Moment Derivatives

	Crystal	Site Group($SO_4^=$)	γ	ω_o(cm^{-1})	$(\partial\mu/\partial q)_x$ ($cm^{3/2}sec^{-1}$)	$(\partial\mu/\partial q)_y$ ($cm^{3/2}sec^{-1}$)	$(\partial\mu/\partial q)_z$ ($cm^{3/2}sec^{-1}$)
ν_1	$LiKSO_4$	C_3	A	1017	--	--	--
	$KNaSO_4$	C_{3v}	A_1	993	--	--	71
	Na_2SO_4	D_2	A	996	--	--	--
	$K_2Mg_2(SO_4)_3$	C_1	A	985	--	--	--
ν_2	$LiKSO_4$	C_3	E	473	78	78	--
	Na_2SO_4	D_2	A	453	--	--	--
			A	465	--	--	--
	$K_2Mg_2(SO_4)_3$	C_1	A	455	59	59	59
ν_3	$LiKSO_4$	C_3	A	1162	--	--	252
			E	1162	242	242	--
	$KNaSO_4$	C_{3v}	A_1	1217	--	--	199
			E	1131	242	242	--
	Na_2SO_4	D_2	B_1	1161	--	--	246
			B_2	1161	--	214	--
			B_3	1168	226	--	--
	K_2SO_4	$C_s(\sigma_h = \sigma_{xy})$	A'	1170	141	149	--
			A'	1140	156	147	--
			A''	1143	--	--	216
	$K_2Mg_2(SO_4)_3$	C_1	A	1097	132	132	132
			A	1142	135	135	135
			A	~ 1185	--	--	--
ν_4	$LiKSO_4$	C_3	A	630	--	--	71
			E	643	84	84	--
	$KNaSO_4$	C_{3v}	A_1	625	--	--	73
			E	624	80	80	--
	Na_2SO_4	D_2	B_1	619	--	--	75
			B_2	623	--	78	--
			B_3	644	74	--	--
	K_2SO_4	$C_s(\sigma_h = \sigma_{xy})$	A'	629	54	45	--
			A'	620	43	49	--
			A''	623	--	--	63
	$K_2Mg_2(SO_4)_3$	C_1	A	611	53	53	53
			A	638	60	60	60
			A	~ 670	--	--	--

Reference for Chapter VII

1. F. Meserole, J. C. Decius and R. E. Carlson, Spectrochimica Acta 30A, 2179 (1974).

CHAPTER VIII

The Molecular Dipole Model in Monoclinic Systems : A Study of the Sulfate Internal Optic Modes of $Li_2SO_4 \cdot H_2O$ Crystals

A. Theory

The theory developed in chapter VI guarantees the non-vanishing of the dipolar coupling of the vibrationally induced dipole moments along the α and β (or α, β , and γ) Cartesian coordinates in a crystal in which the site group of the sulfate ion is C_1, C_i, C_2, C_s or C_{2h}. Since the site group is always a subgroup of the factor group it would be interesting to study the dipolar coupling in crystals which are monoclinic or triclinic in which the factor group and hence the site groups are always C_1, C_i, C_2, C_s, or C_{2h}. Although the monoclinic lithium sulfate monohydrate ($Li_2SO_4 \cdot H_2O$) crystal is chosen in this work, it should be noted that the principles discussed in the following sections also apply to similar crystals.

The lithium sulfate monohydrate crystal[1,2] has two molecules in a unit cell with dimensions a=5.430 Å, b=4.836 Å, c=8.140 Å, and $\beta=107^{\circ}14'$. The space group is C_2^2 (P_{2_1}) with atoms in the following positions :

(2a) xyz ; -x, y + 1/2, -z

atom	x	y	z
Li (1)	- 0.08	0.520	- 0.39
Li (2)	0.18	0.495	0.02
S	0.200	0.000	- 0.206
O (1)	0.190	0.310	- 0.210
O (2)	0.480	- 0.080	- 0.170
O (3)	0.060	- 0.115	- 0.385
O (4)	0.085	- 0.110	- 0.075
H_2O	- 0.315	- 0.480	- 0.385

The correlation diagram for the internal optic modes of the sulfate ion is :

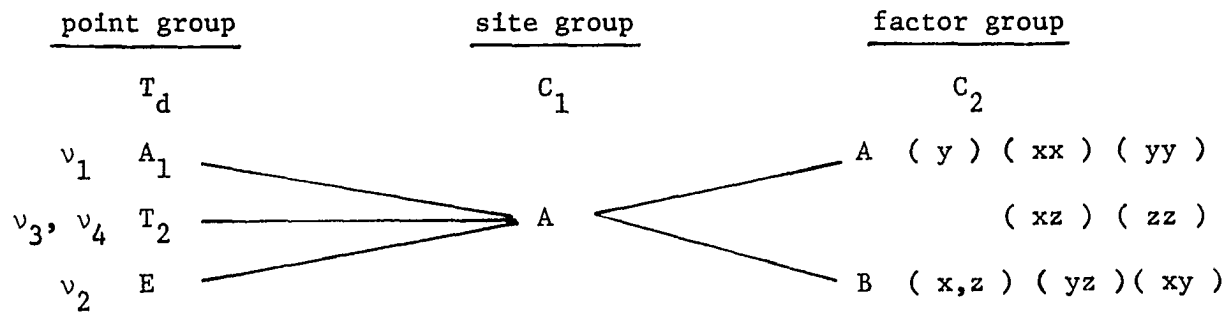

The phonons of symmetry A are polarized along the y direction parallel to the b axis. However it is not possible to a priori identify a unique direction with the phonons of B symmetry. Based on symmetry considerations one can only state that the phonons of symmetry B are polarized in the plane normal to the b axis. Phonons of symmetry A and B originating in the same molecular normal mode and correlated to the same vibrational mode of A symmetry under the site group labeling may be considered to belong to the same "pair". A paticular "pair" has unit cell vibrational modes which can be geometrically represented as :

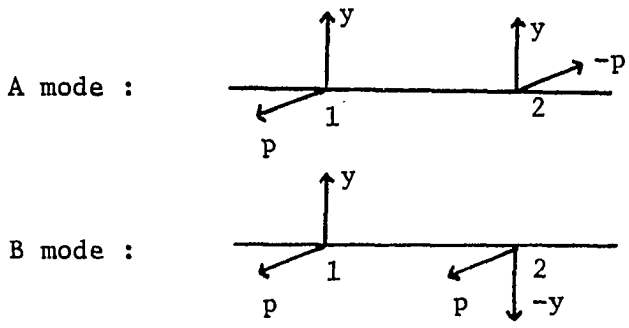

Here p is the direction of the vibrationally induced dipole moment of the B mode in the plane normal to the y direction. The numbers 1 and 2 denote the two sites of the sulfate ions in a unit cell and the arrows designate the directions of the vibrationally induced dipole moments of the sulfate ions

on those sites.

For molecular vibrational modes which are doubly or triply degenerate there are two or three sets of phonons of symmetry A and B under the point group-site group-factor group correlation. Only the symmetries of phonons can be determined by the infrared measurements or Raman scattering methods and the pairing of phonons remains unclear. That is, once a phonon of a particular species is measured, say an A phonon, one initially does not know which of the B symmetry phonons the chosen A phonon is to be paired with. By the molecular dipole model developed in chapter VI paired phonons which share the same mode of symmetry A under the site group C_1 possess the same static crystal field frequency ω_o and dipole moment derivatives along the y and p directions. The frequencies of these paired phonons may be written in terms of the dipolar coupling factors as calculated by the Ewald method[3]:

$$
\begin{aligned}
\text{A mode}: \quad \omega^2_{T,A} &= \omega^2_o + S_{yy}\,(\,I + \alpha_{o,yy}S_{yy}\,)^{-1}_T(\,\partial\mu/\partial q\,)^2_y \\
&\quad + S_{pp}\,(\,I + \alpha_{o,pp}S_{pp}\,)^{-1}(\,\partial\mu/\partial q\,)^2_p \\
\omega^2_{L,A} &= \omega_o + S_{yy}\,(\,I + \alpha_{o,yy}S_{yy}\,)^{-1}_L(\,\partial\mu/\partial q\,)^2_y \\
&\quad + S_{pp}\,(\,I + \alpha_{o,pp}S_{pp}\,)^{-1}(\,\partial\mu/\partial q\,)^2_p \qquad (\,I\,) \\
\text{B mode}: \quad \omega^2_{T,B} &= \omega^2_o + S_{yy}\,(\,I + \alpha_{o,yy}S_{yy}\,)^{-1}(\,\partial\mu/\partial q\,)^2_y \\
&\quad + S_{pp}\,(\,I + \alpha_{o,pp}S_{pp}\,)^{-1}_T(\,\partial\mu/\partial q\,)^2_p \\
\omega^2_{L,B} &= \omega^2_o + S_{yy}\,(\,I + \alpha_{o,yy}S_{yy}\,)^{-1}(\,\partial\mu/\partial q\,)^2_y \\
&\quad + S_{pp}\,(\,I + \alpha_{o,pp}S_{pp}\,)^{-1}_L(\,\partial\mu/\partial q\,)^2_p
\end{aligned}
$$

Here L and T denote the longitudinal and transverse modes respectively, the ω's are the frequencies of phonons and the $(\partial\mu/\partial q)$'s are the dipole moment derivatives along the directions indicated by the subscripts.

The dipolar cross-coupling term between the y and p directions is neglected here by assuming that it is small compared to the diagonal terms along the y and p directions in order to simplify the manipulation of these equations. The term $S_{pp}(I + \alpha_{o,pp}S)^{-1}_{pp}(\partial\mu/\partial q)^2_p$ which represents the dipolar coupling between the vibrationally induced dipole moments in the p direction is identically the same for both longitudinal and transverse modes of symmetry A since there is no net dipole moment in the unit cell along that direction. An analogous statement may be made about the dipolar coupling factor $S_{yy}(I + \alpha_{o,yy}S_{yy})^{-1}(\partial\mu/\partial q)^2_y$ for the longitudinal and transverse modes of symmetry B.

Equation set (I) is a set of four equations with three unknowns, ω_o, $(\partial\mu/\partial q)^2_y$, and $(\partial\mu/\partial q)^2_p$. The consistency between these four equations is a good test for the theory developed here. Moreover it is possible that the consistency between these four equations may elucidate the correct pairing of phonons of symmetry A and B in cases where dipolar coupling is the dominant intermolecular interaction between molecules or polyatomic ions in the crystal.

B. Experimental

Crystals of monoclinic lithium sulfate monohydrate were grown at room temperature from an aqueous solution prepared using analytical grade reagent. The crystals dehydrated into a white powder when heated to 90°C. The crystallographic axes were determined by x-ray diffraction methods. The measured cell dimensions are the same as reported in the literature.

Near normal incidence infrared reflection spectra were recorded at room temperature on a Beckman IR-12 spectrophotometer at an average angle of incidence of 17°. Raman spectra were obtained through the courtesy

of Prof. J. P. Devlin at Oklahoma State University using a system constructed around the Jarrell-Ash 25-100 dual monochromator.

The IR spectra of the B symmetry modes were taken at various polarizations in the a-c plane. The directions of the polarization of the infrared radiation at which the B modes showed a reflectivity maximum were taken as the directions of the vibrationally induced dipole moments. Raman spectra of the B modes were recorded as the direction of the scattered phonons in the a-c plane was varied.

C. Calculation of Electronic Polarizability Components of the Sulfate Ion

The refractive indices along the principal axes[4] are $n_x^D = 1.459$, $n_y^D = 1.477$, and $n_z^D = 1.488$. The electronic polarizability components of the sulfate ion along these directions are calculated to be $\alpha_x = 4.48$ Å^3, $\alpha_y = 4.62$ Å^3, and $\alpha_z = 4.69$ Å^3 with the polarizabilities of lithium ion and water chosen as 0.029 Å^3 [5] and 1.65 Å^3 [6], respectively.

D. Spectral Analysis Using the Molecular Dipole Model

In the spectra of the B symmetry modes the direction of the polarization of the infrared radiation θ, the direction of the vibrationally induced dipole moment θ_{DM}, and the direction of the scattered phonon θ_p are all measured from the c axis counter-clockwise in the a-c plane when b axis is out of the plane. (See Figure (8-1))

The calculated dipolar coupling terms are shown in Table (8-1).

ν_1 : The infrared and Raman spectra are shown in Figures (8-2) and (8-3), respectively. The A symmetry mode is not seen in the near normal incidence infrared reflection spectrum; however it is observed in a Raman scattering experiment with $\omega_T = 999$ cm^{-1} and $\omega_L = 1009$ cm^{-1}. The frequency of the B mode is about 1010 cm^{-1} with $\theta_{DM} = 80^o$ by the IR method. The

Figure (8-1-a) Near normal incidence reflection experiment geometry (The incoming ray, outgoing ray, and b axis are in the plane of incidence.The directions of the induced dipole, the electric field, the a axis, and the c axis are all co-planar and lie in the surface of the crystal.)

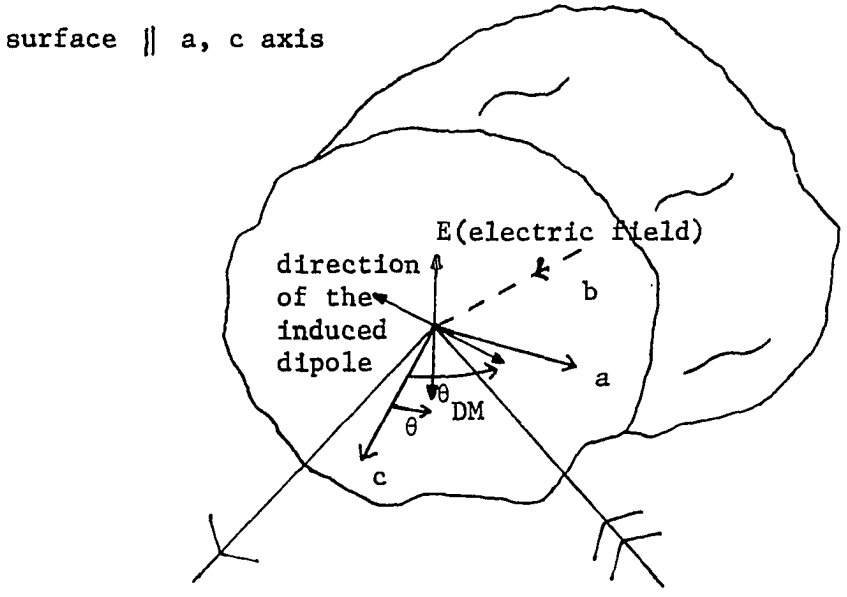

Figure (8-1-b) Raman experiment geometry : x(yx)z (y ∥ b axis, x and z in a-c plane

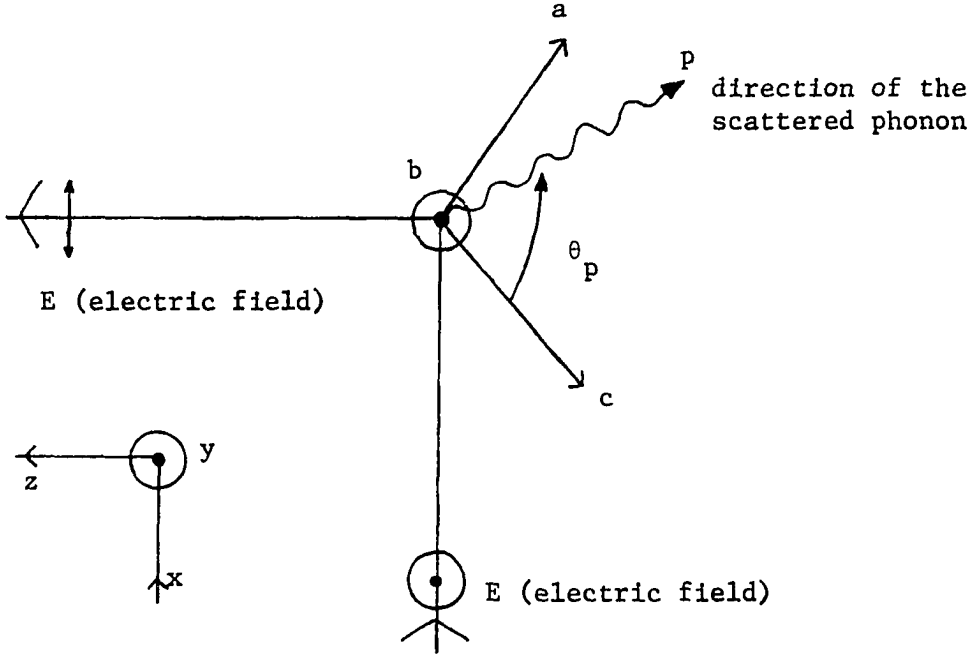

Table (8-1) Dipolar Coupling Factors of $Li_2SO_4 \cdot H_2O$ Crystal

θ_{DM} (°)	$S_{pp}(I + \alpha_{o,pp}S_{pp})^{-1}_T$	$S_{pp}(I + \alpha_{o,pp}S_{pp})^{-1}_L$	$S_{pp}(I + \alpha_{o,pp}S_{pp})^{-1}$ ($cm^{-5}sec^2$)
0	- 2.40083	1.34469	0.19423
10	- 2.51357	1.28923	0.38606
20	- 2.62164	1.23203	0.52685
30	- 2.71060	1.18060	0.59196
60	- 2.74865	1.11714	0.13782
80	- 2.57534	1.16490	- 0.69349
90	- 2.46069	1.20957	- 1.12216
105	- 2.29641	1.29018	- 1.48422
110	- 2.25006	1.31774	- 1.49525
150	- 2.15299	1.43849	- 0.53833
y	- 3.00573	0.87891	- 2.19083

frequencies of the longitudinal and transverse modes are hard to estimate from the reflection spectrum since the reflectivity is small. There is no apparent variation of the frequency of the B mode (1009 cm^{-1}) for different directions of phonon propagation in the Raman spectra.

The equation set (I) can not be satisfied with these values. Apparently the molecular dipole model is not suitable to describe the ν_1 mode in this crystal. This is hardly surprising noting the small reflectivity and hence dipole moment derivative of this particular mode.

ν_2 : The infrared and Raman spectra are shown in Figures (8-4)-(8-6) and (8-7)-(8-8), respectively.

Only one A mode is seen instead of two as predicted by the correlation diagram. The longitudinal and transverse frequencies of the A mode are 487 cm^{-1} and 454 cm^{-1}, respectively, by the Raman scattering method.

Two B modes are seen in the reflectivity spectrum around 466 cm^{-1} and 495 cm^{-1} with $\theta_{DM} = 150^{o}$ and 60^{o}, respectively. The Raman studies show that the frequencies of the transverse and the longitudinal modes are :

$\nu_{2a}(B)$: $\omega_L = 471\ cm^{-1}$, $\omega_T = 460\ cm^{-1}$ ($\theta_{DM} = 150^{o}$)

$\nu_{2b}(B)$: $\omega_L = 488\ cm^{-1}$, $\omega_T = 484\ cm^{-1}$ ($\theta_{DM} = 60^{o}$)

Equation set (I) suggests that the observed A mode is more likely to pair with $\nu_{2a}(B)$ with calculated $\omega_L = 463\ cm^{-1}$ which is 8 cm^{-1} less than that observed since the values of A and $\nu_{2b}(B)$ can not satisfy (I). The values of ω_o, $(\partial\mu/\partial q)_p$, and $(\partial\mu/\partial q)_y$ for A and $\nu_{2a}(B)$ modes are calculated to be 480 cm^{-1}, 25 $cm^{3/2}sec^{-1}$ and 90 $cm^{3/2}sec^{-1}$ respectively.

ν_3 : The infrared and Raman spectra are shown in Figures (8-9)-(8-11) and (8-12)-(8-16), respectively.

Three A modes as predicted by the correlation diagram are seen in the infrared and Raman spectra with the values :

$\nu_{3a}(A)$: $\omega_L = 1150\ cm^{-1}$, $\omega_T = 1103\ cm^{-1}$

$\nu_{3b}(A)$: $\omega_L = 1175\ cm^{-1}$, $\omega_T = 1152\ cm^{-1}$

$\nu_{3c}(A)$: $\omega_L = 1193\ cm^{-1}$, $\omega_T = 1181\ cm^{-1}$

as measured by the Raman scattering method.

The infrared and Raman spectra of the B modes are very complicated and apparently more modes than the three predicted by the correlation diagram are present. The mixing of the transverse and longitudinal modes makes the analysis of the Raman spectra even more complicated. There are two obvious broad and intense modes :

$\nu_{3a}(B)$: $\omega_L = 1184\ cm^{-1}$, $\omega_T = 1103\ cm^{-1}$, $\theta_{DM} = 0^o$

$\nu_{3b}(B)$: $\omega_L = 1223\ cm^{-1}$, $\omega_T = 1197\ cm^{-1}$, $\theta_{DM} = 90^o$

There are four more modes apparent in the infrared and Raman spectra. By careful comparison of the infrared and Raman spectra the following frequencies and θ_{DM}'s can be assigned :

$\nu_{3c}(B)$: $\omega_L = 1116\ cm^{-1}$, $\omega_T = 1101\ cm^{-1}$, $\theta_{DM} = 30^o$

$\nu_{3d}(B)$: $\omega_L = 1196\ cm^{-1}$, $\omega_T = 1181\ cm^{-1}$, $\theta_{DM} = 105^o$

$\nu_{3e}(B)$: $\omega_L = 1173\ cm^{-1}$, $\omega_T = 1142\ cm^{-1}$, $\theta_{DM} = 60^o$

$\nu_{3f}(B)$: $\omega_L = 1124\ cm^{-1}$, $\omega_T = 1117\ cm^{-1}$, $\theta_{DM} = 120^o$

The paired A and B modes and the associated ω_o and dipole moment derivatives as indicated by equation set (I) are listed below together with the calculated and observed ω_L for the B modes :

paired modes	ω_o (cm^{-1})	$(\partial\mu/\partial q)_p$	$(\partial\mu/\partial q)_y$($cm^{3/2}sec^{-1}$)	ω_L(calc)	ω_L(obs)
$\nu_{3a}(A)$-$\nu_{3c}(B)$	1137	90	165	1115	1116
$\nu_{3b}(A)$-$\nu_{3a}(B)$	1166	217	117	1180	1184
$\nu_{3c}(A)$-$\nu_{3d}(B)$	1195	86	86	1192	1196

ν_4 : The infrared and Raman spectra are shown in Figures (8-17)-(8-19) and (8-20)-(8-22), respectively.

Only one A mode is seen instead of three as predicted by the correlation diagram. The frequencies of the longitudinal and transverse modes indicated by the Raman measurements are 659 cm^{-1} and 639 cm^{-1}, respectively.

Three B modes are seen by the infrared method as predicted. The reflectivity spectra show that they are around 580 cm^{-1}, 638 cm^{-1}, and 658 cm^{-1} with $\theta_{DM} = 20^{o}$, 110^{o}, and 10^{o}, respectively.

The mode around 580 cm^{-1} ($\nu_{4a}(B)$) is not seen in the Raman scattering method. The frequencies of the longitudinal and transverse modes are estimated as 598 cm^{-1} and 558 cm^{-1}, respectively, from the inflection points of the infrared spectrum. The frequencies of the longitudinal and transverse modes of the other two B modes as indicated by the Raman spectra are :

$\nu_{4b}(B)$: $\omega_L = 641\ cm^{-1}$, $\omega_T = 630\ cm^{-1}$, $\theta_{DM} = 110^{o}$

$\nu_{4c}(B)$: $\omega_L = 661\ cm^{-1}$, $\omega_T = 639\ cm^{-1}$, $\theta_{DM} = 10^{o}$

The equation set (I) does not show which B mode is more likely to pair with the A mode. The calculated and observed ω_L for $\nu_{4a}(B)$, $\nu_{4b}(B)$, and $\nu_{4c}(B)$ are :

mode	ω_L (calc)	ω_L (obs) (cm^{-1})
$\nu_{4a}(B)$	661	598
$\nu_{4b}(B)$	690	641
$\nu_{4c}(B)$	645	661

E. Discussion

From the spectral analysis it is seen that the molecular dipole model is more appropriate for the ν_2 and ν_3 modes. It was somewhat surprising that only one A mode was seen in the ν_2 and ν_4 regions both in the infrared and Raman spectra instead of two and three modes, respectively, as predicted by the correlation diagram. Apparently the correlation field splitting which originates in the dipolar interactions among the A modes is so small that only one A mode is observed. Therefore it is not unexpected that the molecular dipole model does not work as well for the ν_2 and ν_4 modes. However the model still provides an adequate analysis for the ν_2 mode since one can still use the equation set (I) to show that $\nu_{2a}(B)$ instead of $\nu_{2b}(B)$ should be paired with the A mode. For ν_4 the differences in the frequencies of the calculated and observed ω_L for the B modes are greater than 20 cm^{-1} or more and plainly the molecular dipole model is inappropriate here.

For the ν_3 mode there are three A modes and six B modes observed in the infrared and Raman spectra. Among these eighteen possible pairings only three give calculated ω_L values of the B modes in agreement with the observed ω_L frequencies. The success of the dipole model here is probably due to the large dipole moment derivatives (compared to those of the ν_1, ν_2, and ν_4 modes) indicating that dipolar coupling is the dominant intermolecular interaction for the ν_3 mode.

It is also surprising that $\nu_{3b}(B)$ is not the mode paired with $\nu_{3a}(A)$, $\nu_{3b}(A)$, or $\nu_{3c}(A)$ as it would seem to be at the first glance since this mode is intense and broad compared to other modes in the infrared spectra.

If the molecular dipole model analysis is correct, then $\nu_{3b}(B)$, $\nu_{3e}(B)$, and $\nu_{3f}(B)$ are not the fundamental modes but probably combinations of the ν_2 and ν_4 modes.

It should be noted that there might be variations between the directions of the scattered phonons and the θ_p's in the Raman spectra since the direction of the light is changed when the light goes into or out of biaxial crystals due to index of refraction mismatching.

The mixing of the transverse and longitudinal modes is observed in the ν_2, ν_3, and ν_4 modes when the direction of the phonons as observed in the Raman effect is between the transverse and longitudinal modes.

References for Chapter VIII

1. G. E. Ziegler, Z. Krist. 89A, 456 (1934).

2. A. C. Larson and L. Helmholz, J. Chem. Phys. 22, 2049 (1954).

3. P. P. Ewald, Ann. Phys. (Leipzig) 64, 253 (1921).

4. A. Winchell and H. Winchell, The Microscopic Characteristics of Artificial Inorganic Solid Substances, (Academic Press, New York 1964)

5. J. Pirenne and E. Kartheuser, Physica 30, 2005 (1964).

6. N. E. Dorsey, Properties of Ordinary Water-Substance, monograph series no. 81 (Reinhold Publishing Corporation, 1940).

Figure (8-2) Near normal incidence infrared reflection spectra of $Li_2SO_4 \cdot H_2O$ crystal in the ν_1 spectral region

surface $\perp$ b axis and angle measured counterclockwise from c axis

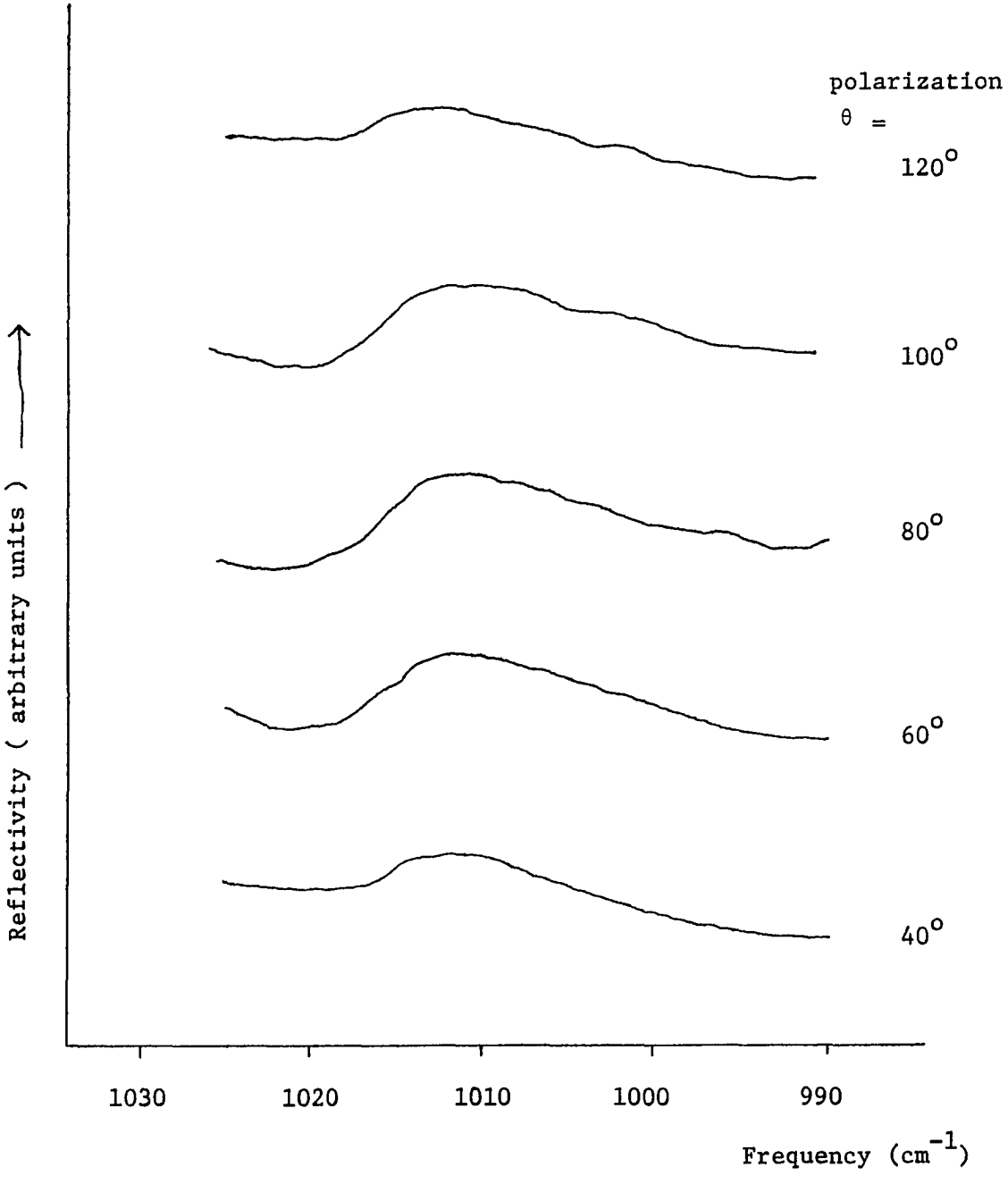

Figure (8-3) Single crystal Raman spectra of $Li_2SO_4 \cdot H_2O$ in the ν_1 region

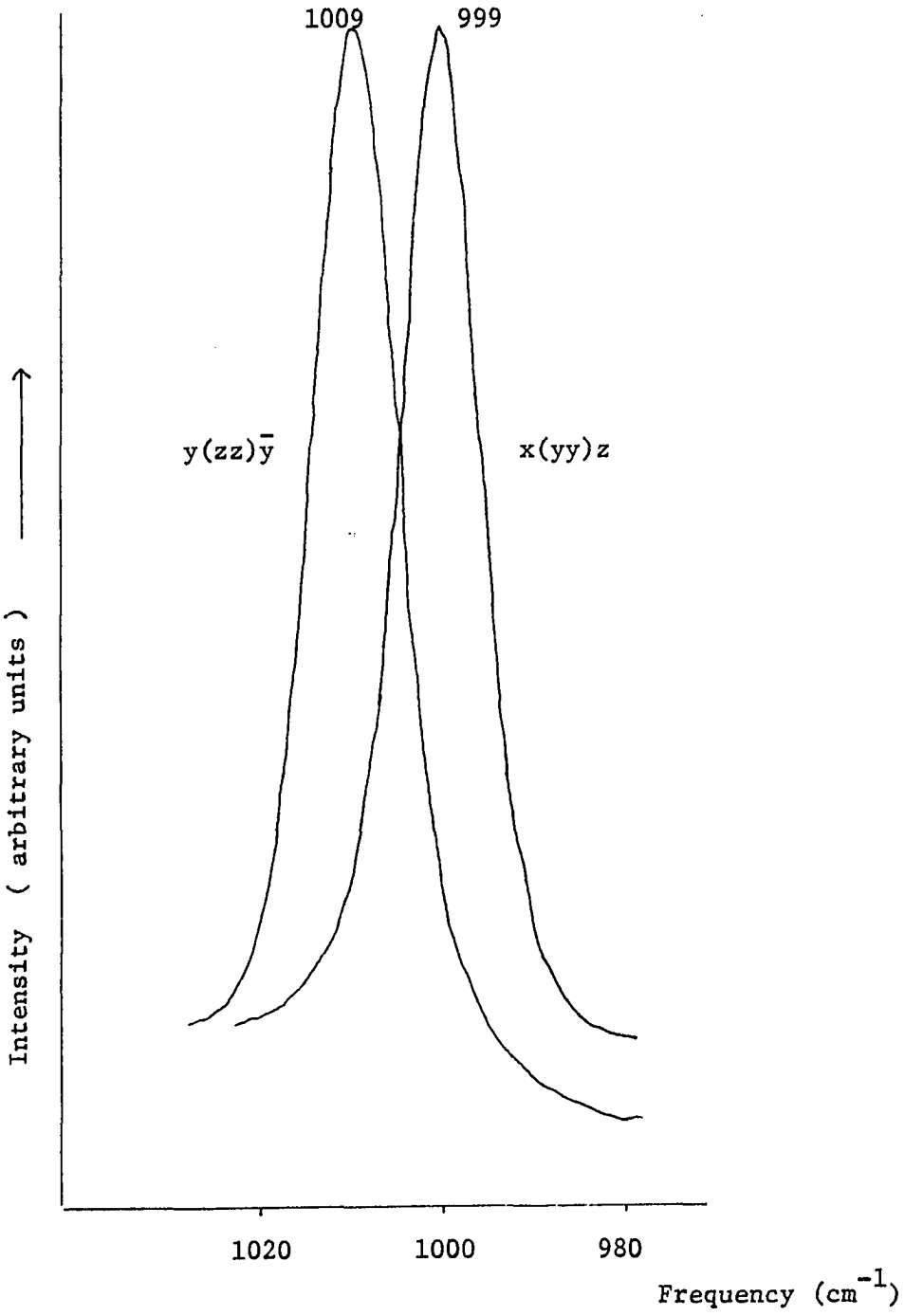

Figure (8-4) Near normal incidence infrared reflection spectrum of $Li_2SO_4 \cdot H_2O$ crystal in the ν_2 spectral region

surface ‖ b, c axes (polarization ‖ b axis)

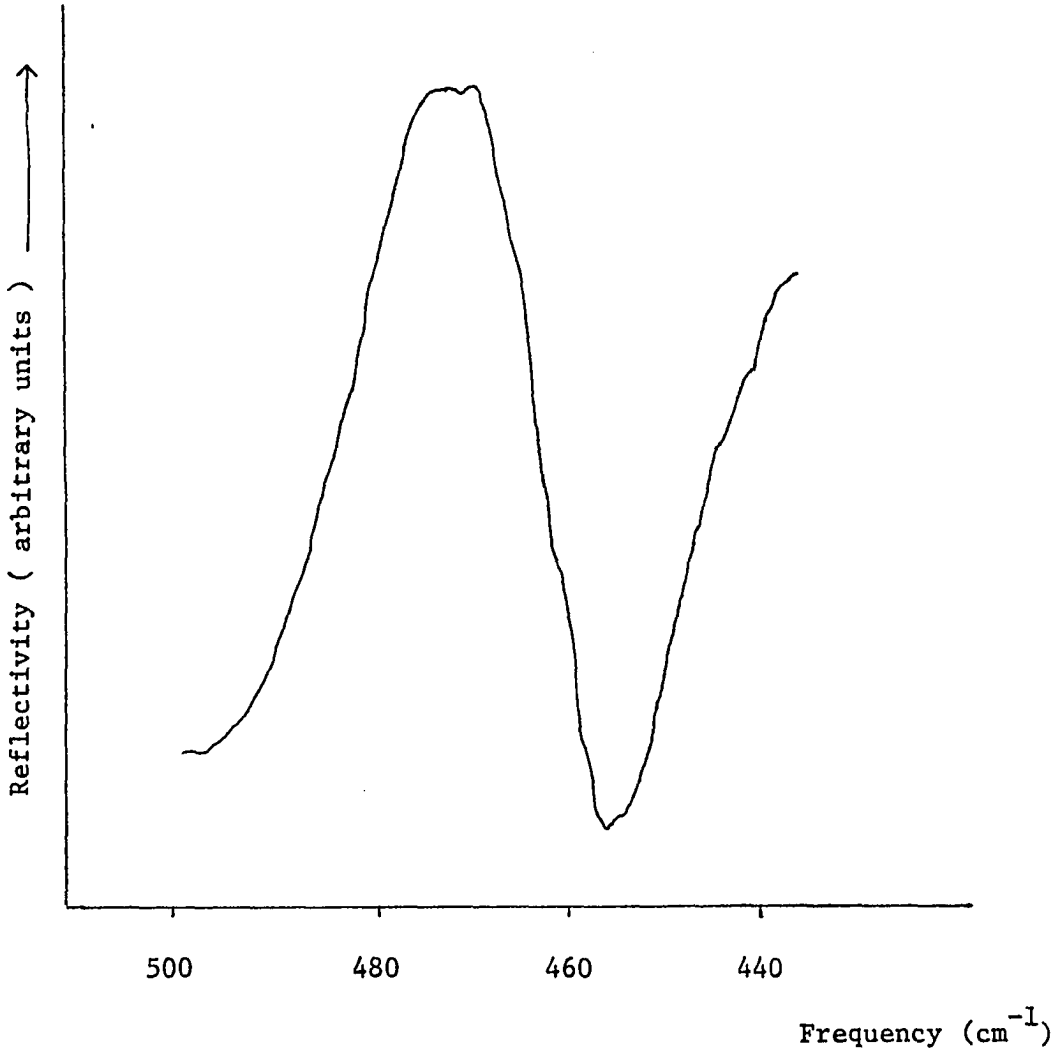

Figure (8-5) Near normal incidence infrared reflection spectra of $Li_2SO_4 \cdot H_2O$ crystal in the ν_2 spectral region

surface $\perp$ b axis and angle measured counterclockwise from c axis

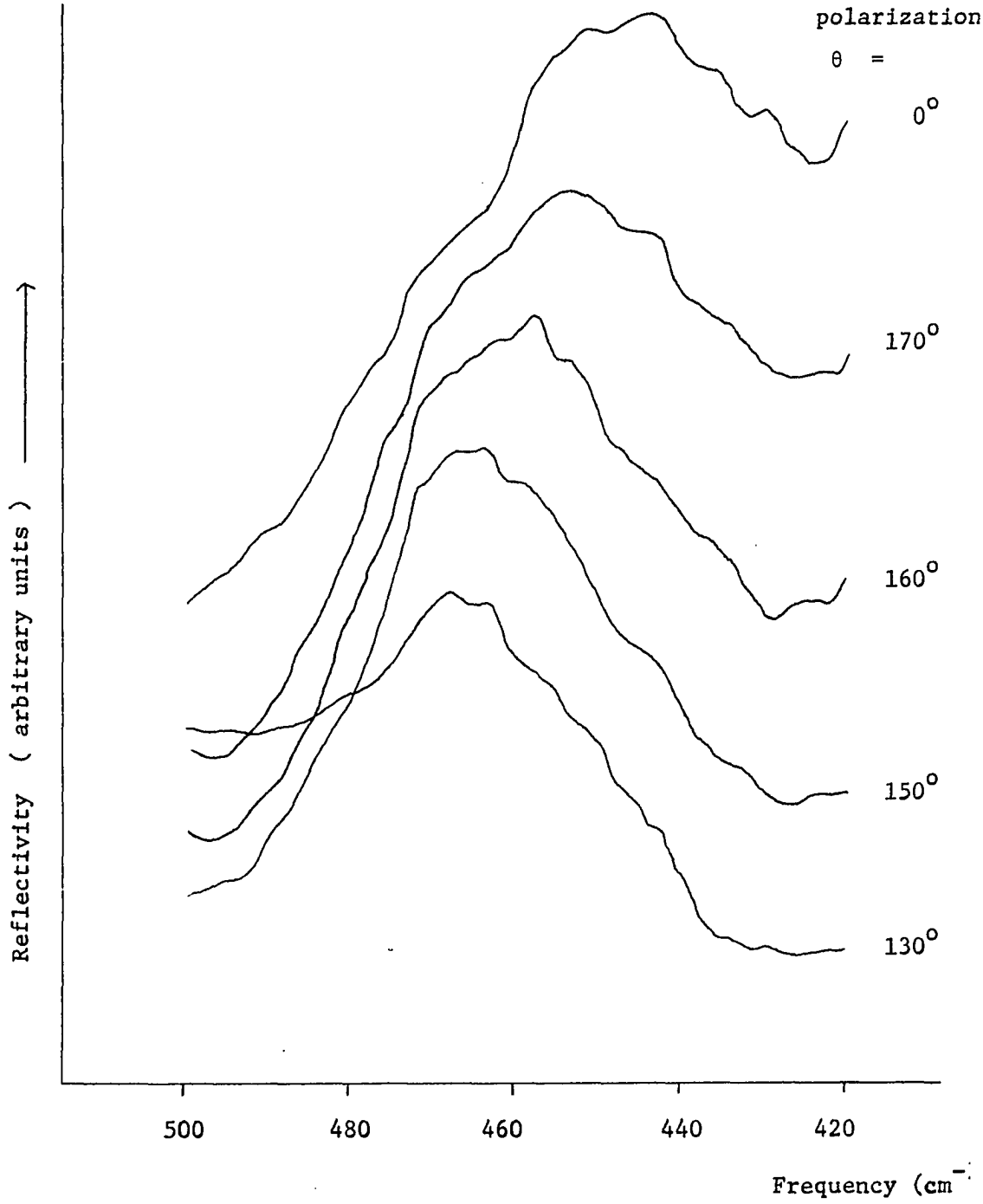

Figure (8-6) Near normal incidence infrared reflection spectra of $Li_2SO_4 \cdot H_2O$ crystal in the ν_2 spectral region

surface $\perp$ b axis and angle measured counterclockwise from c axis

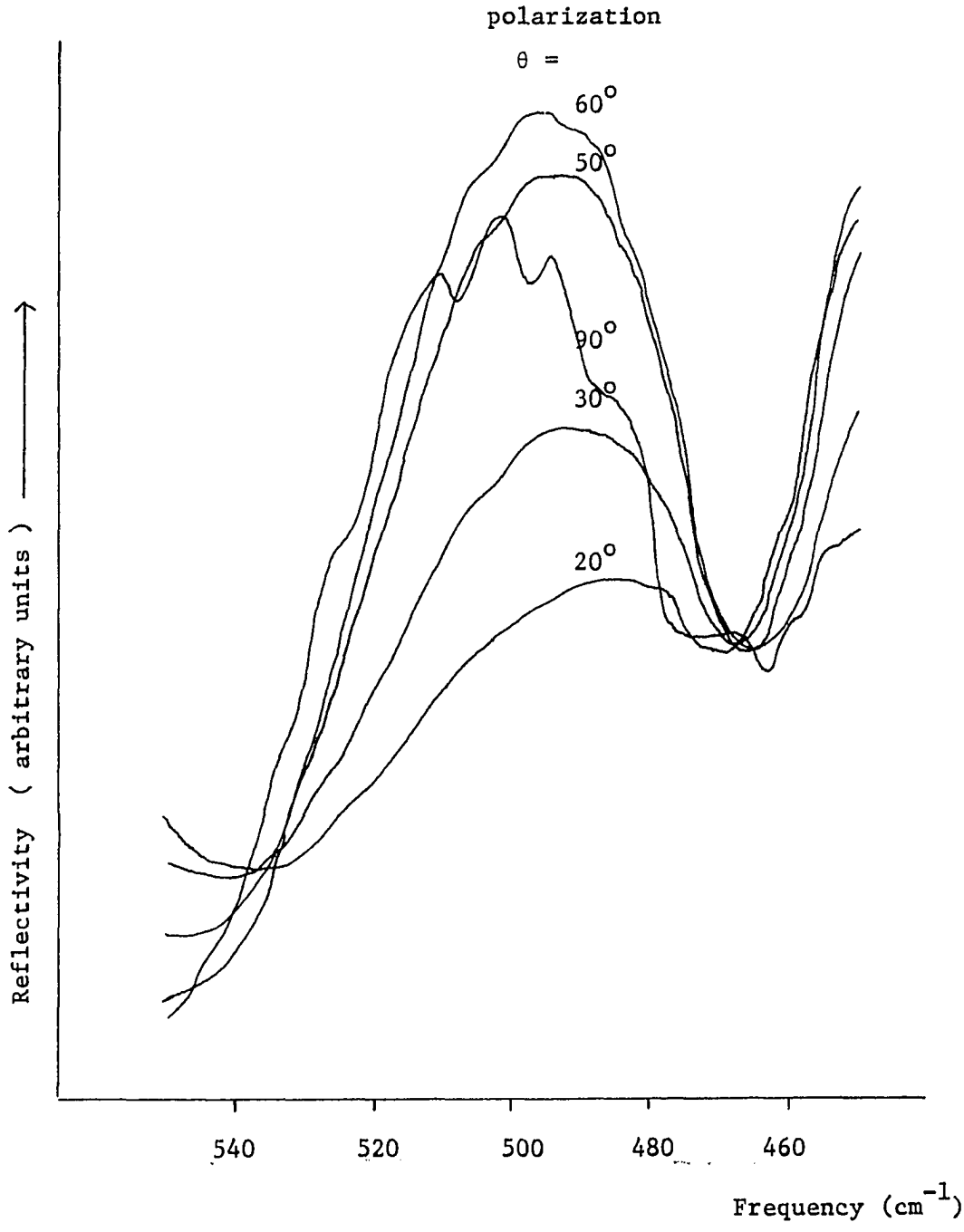

Figure (8-7) Single crystal Raman spectra of $Li_2SO_4 \cdot H_2O$ in the ν_2 spectral region

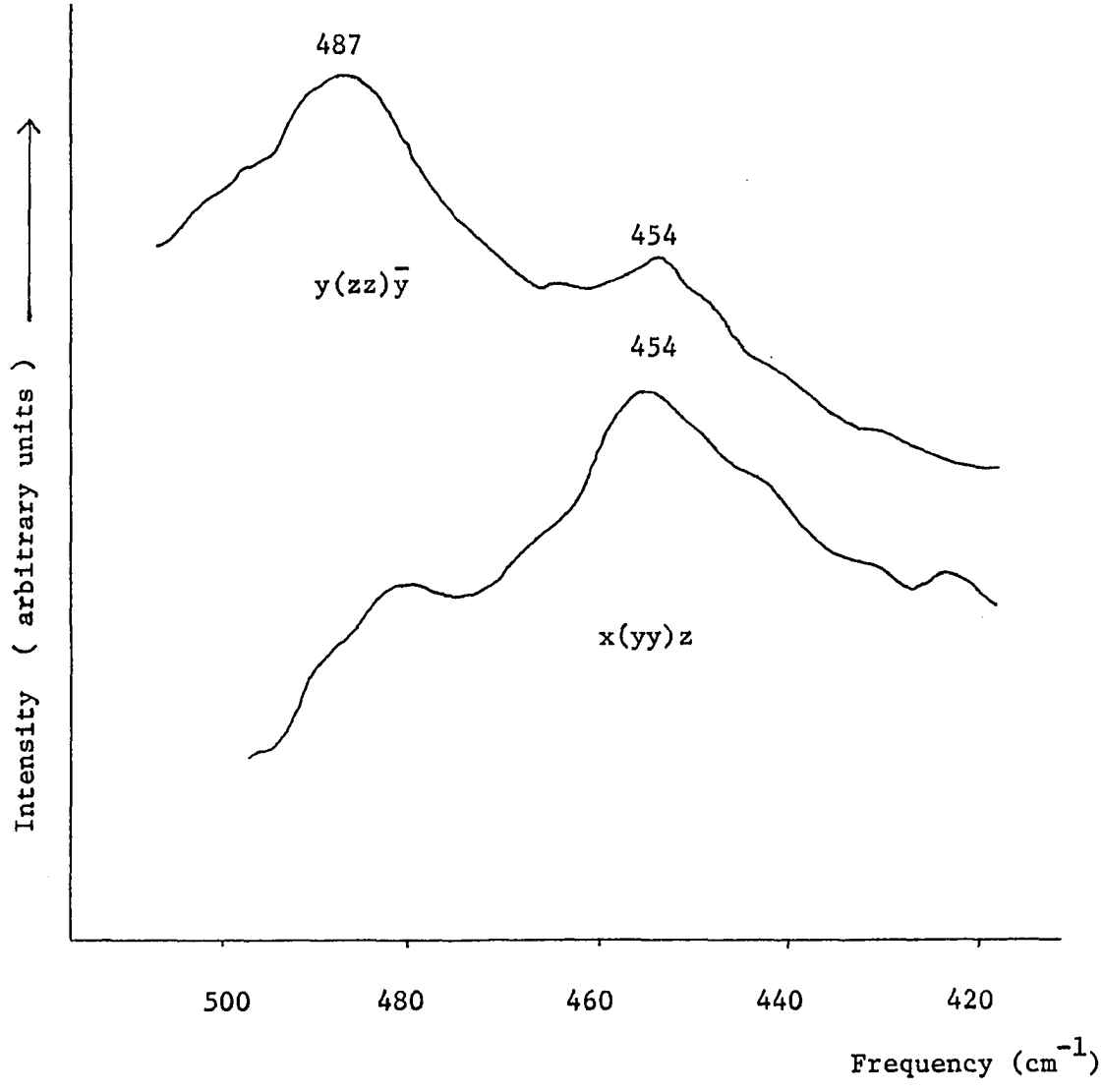

Figure (8-8) Single crystal Raman spectra of $Li_2SO_4 \cdot H_2O$ in the ν_2 spectral region (angle measured counterclockwise from c axis)

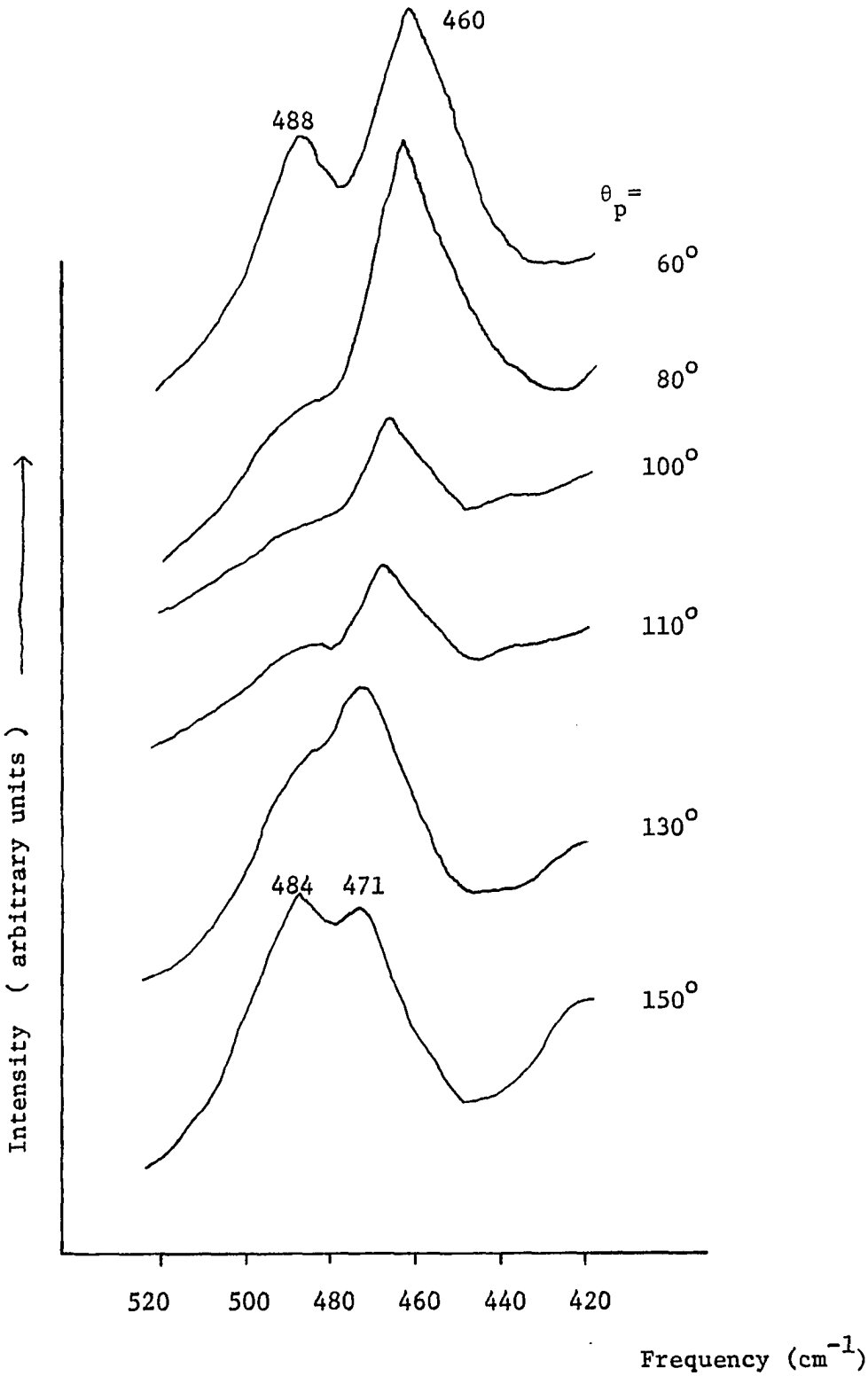

Figure (8-9) Near normal incidence infrared reflection spectra of $Li_2SO_4 \cdot H_2O$ crystal in the ν_3 spectral region

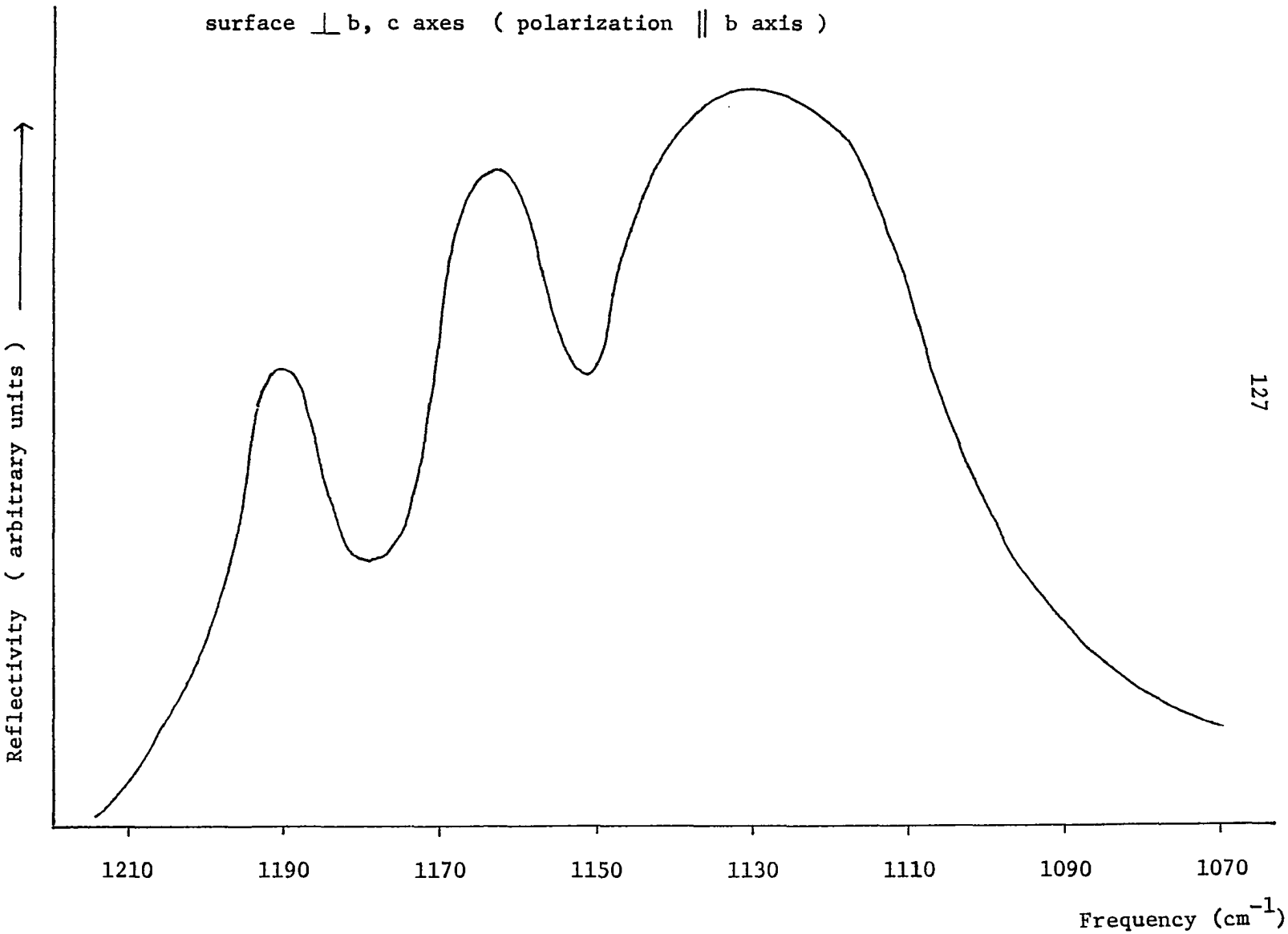

Figure (8-10) Near normal incidence infrared reflection spectra of $Li_2SO_4 \cdot H_2O$ crystal in the ν_3 spectral region

surface $\perp$ b axis and angle measured counterclockwise from c axis

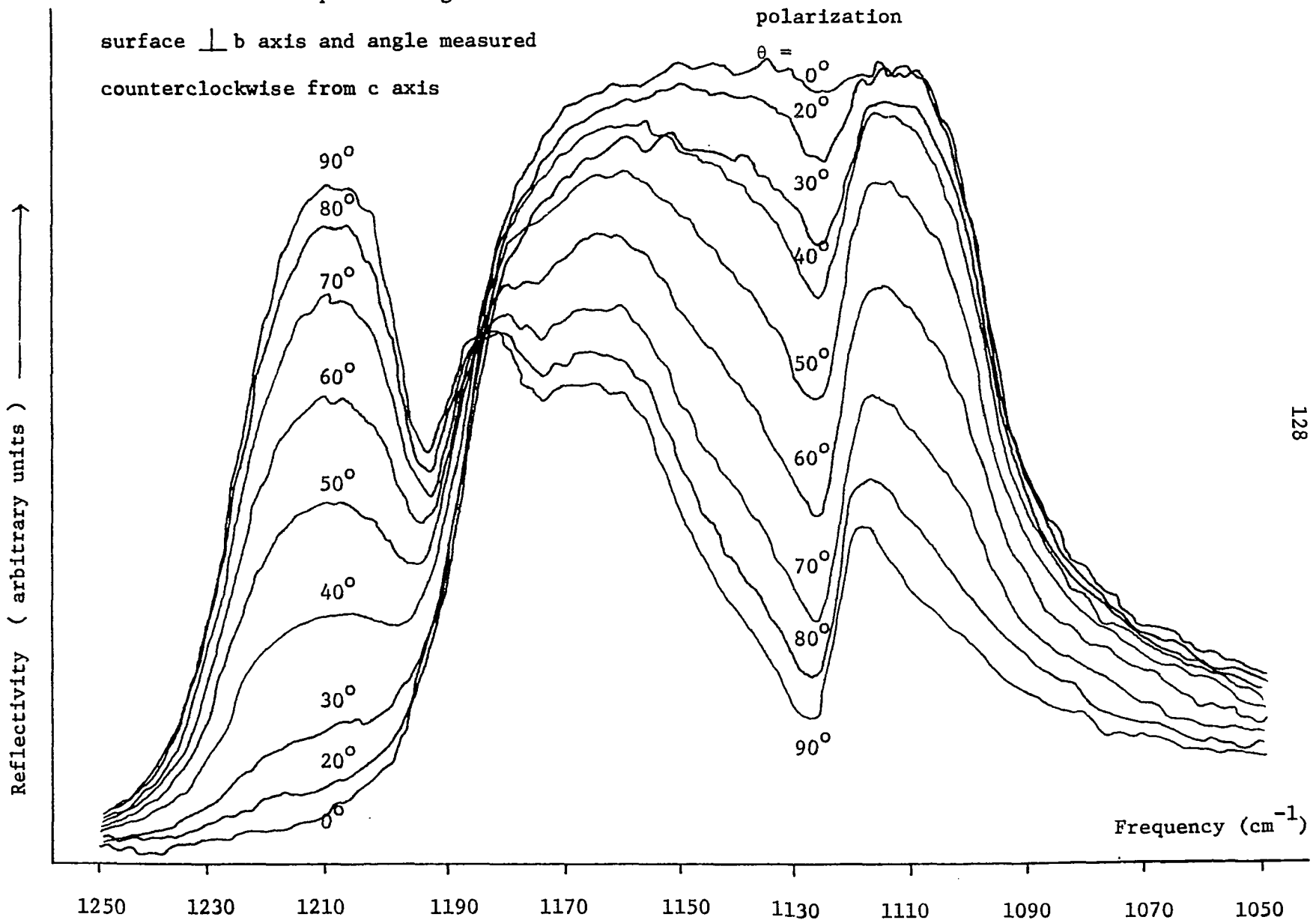

Figure (8-11) Near normal incidence infrared reflection spectra of $Li_2SO_4 \cdot H_2O$ crystal in the ν_3 spectral region

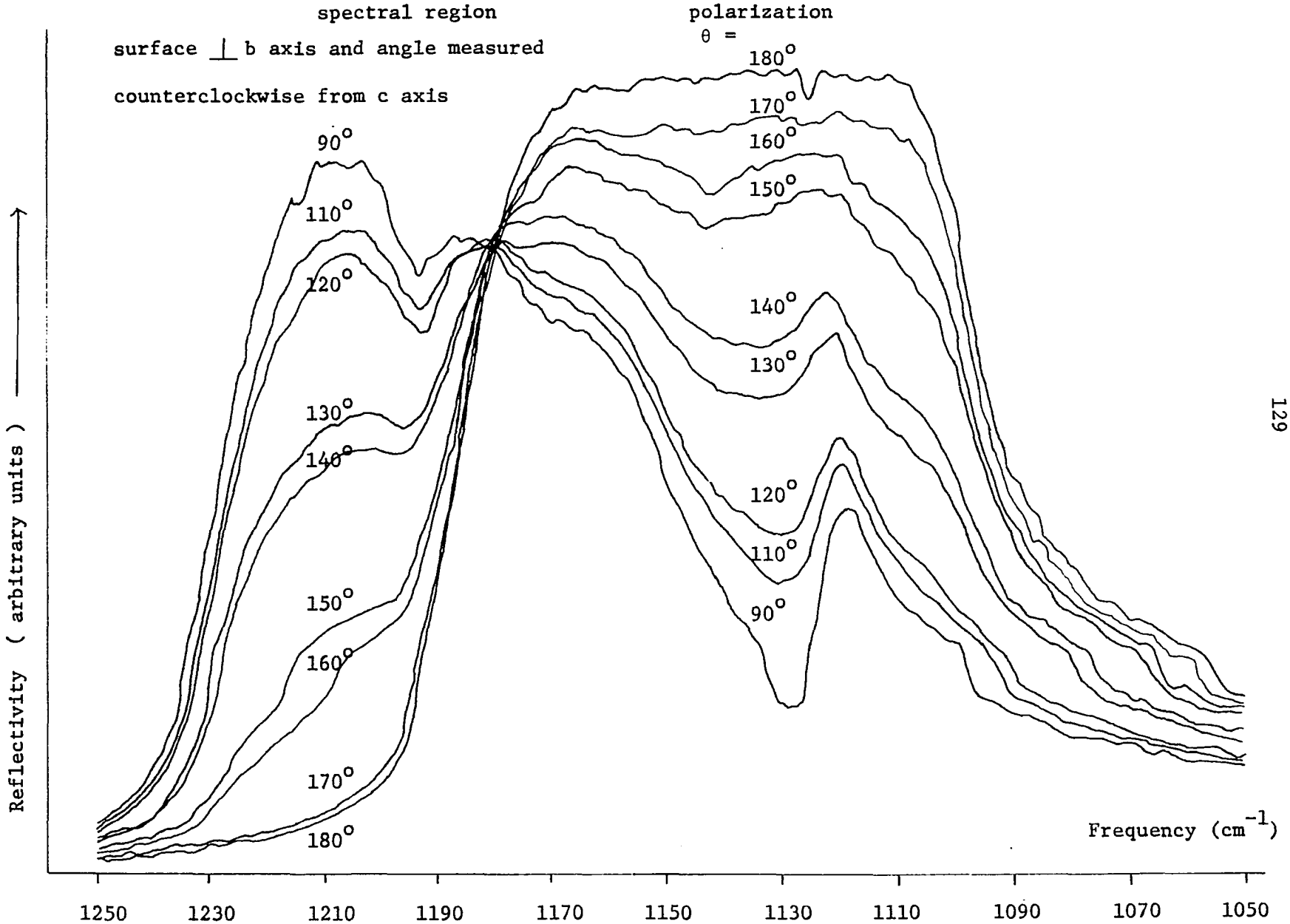

Figure (8-12) Single crystal Raman spectra of $Li_2SO_4 \cdot H_2O$ in the ν_3 spectral region

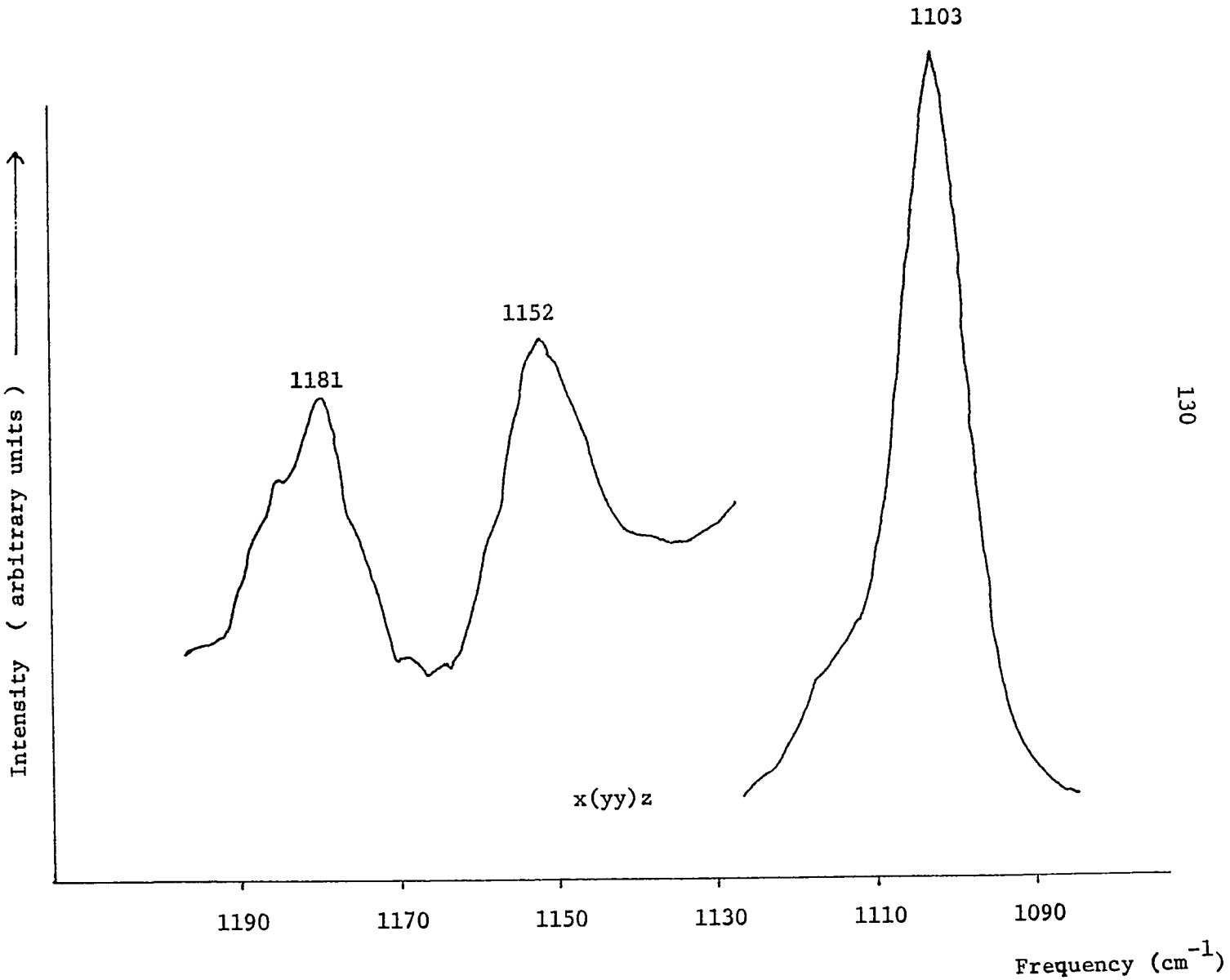

Figure (8-13) Single crystal Raman spectra of $Li_2SO_4 \cdot H_2O$ in the ν_3 spectral region

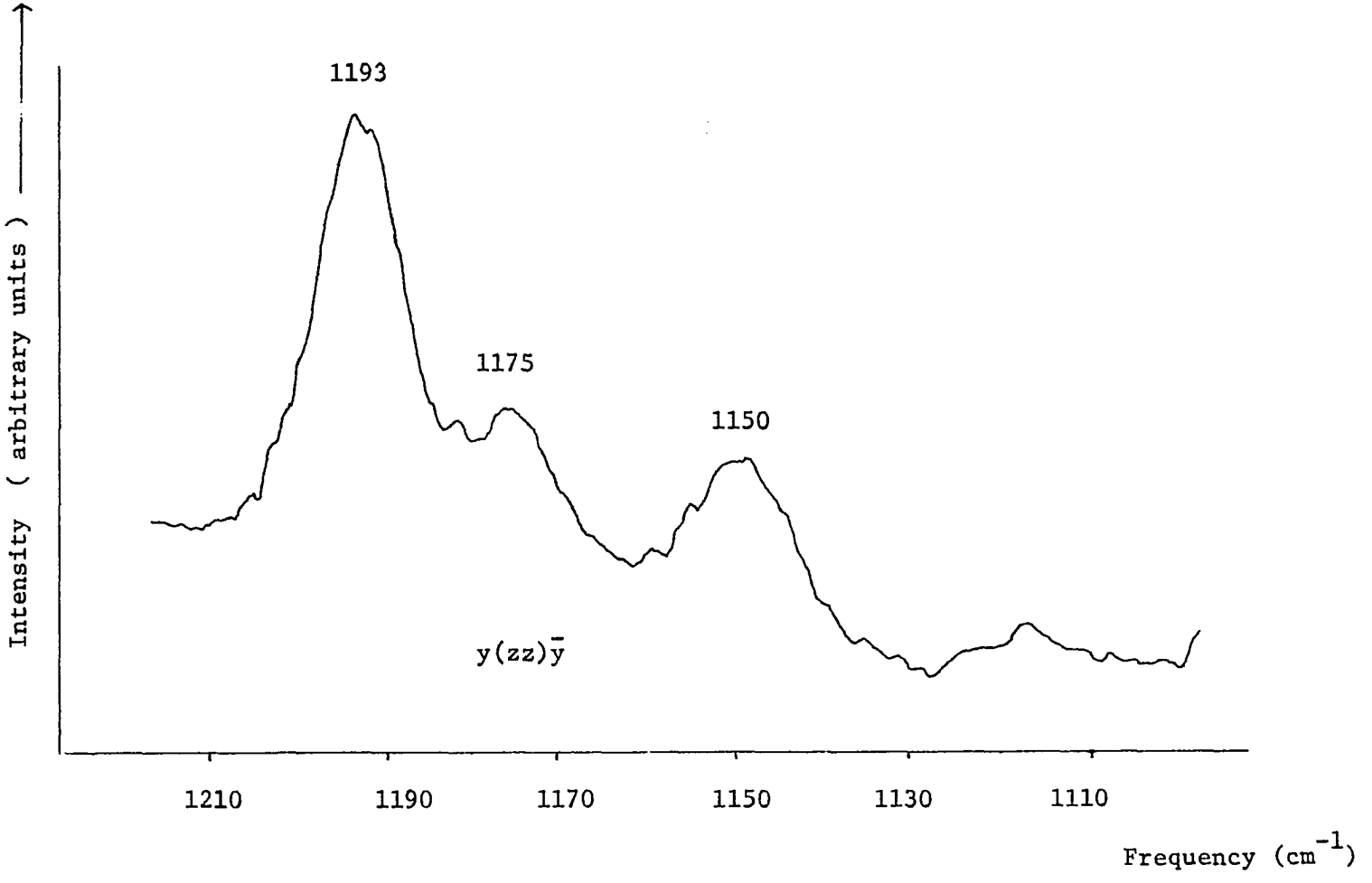

Figure (8-14) Single crystal Raman spectra of $Li_2SO_4 \cdot H_2O$ in the ν_3 spectral region (angle measured counterclockwise from c axis)

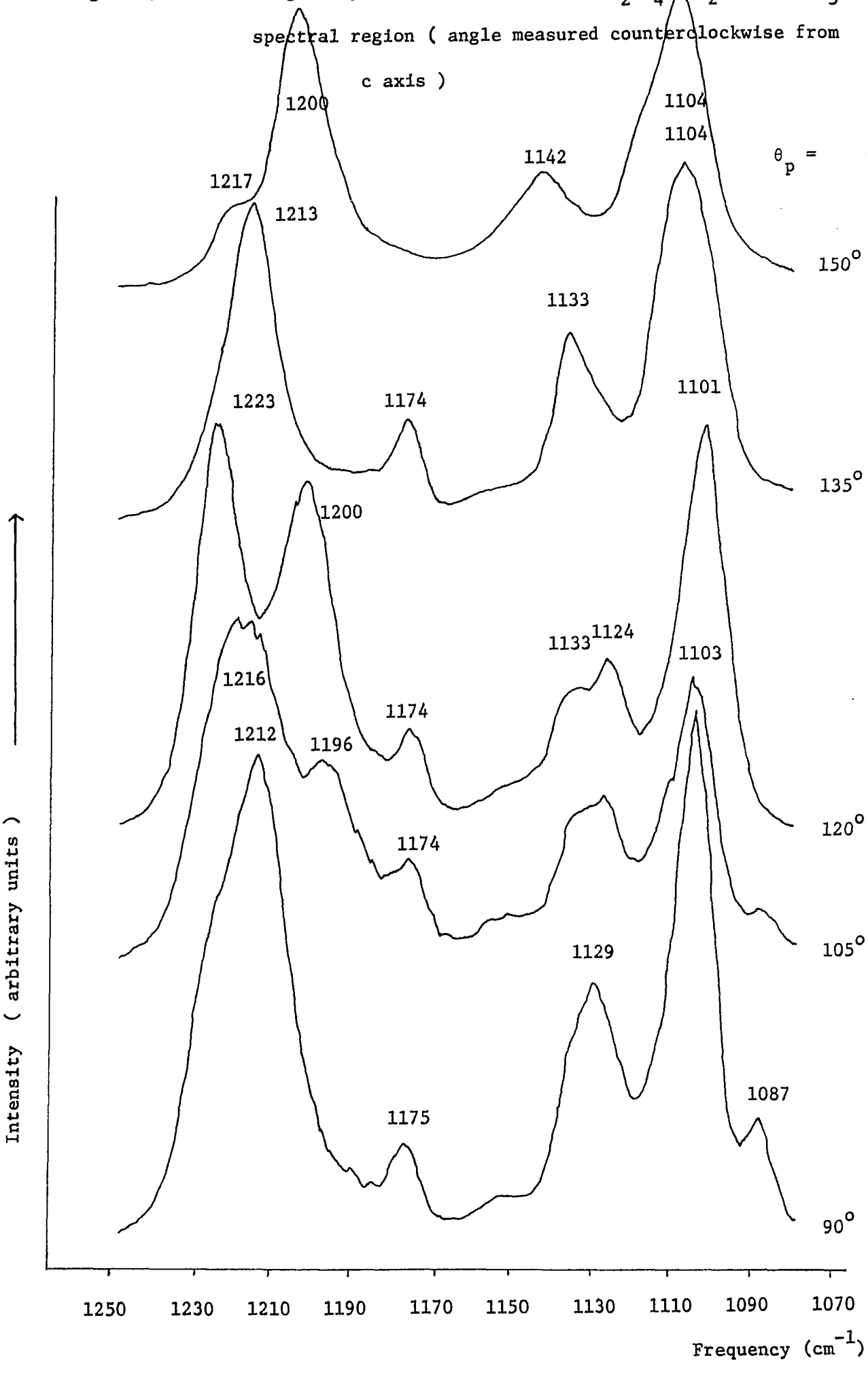

Figure (8-15) Single crystal Raman spectra of $Li_2SO_4 \cdot H_2O$ in the ν_3 spectral region (angle measured counterclockwise from c axis)

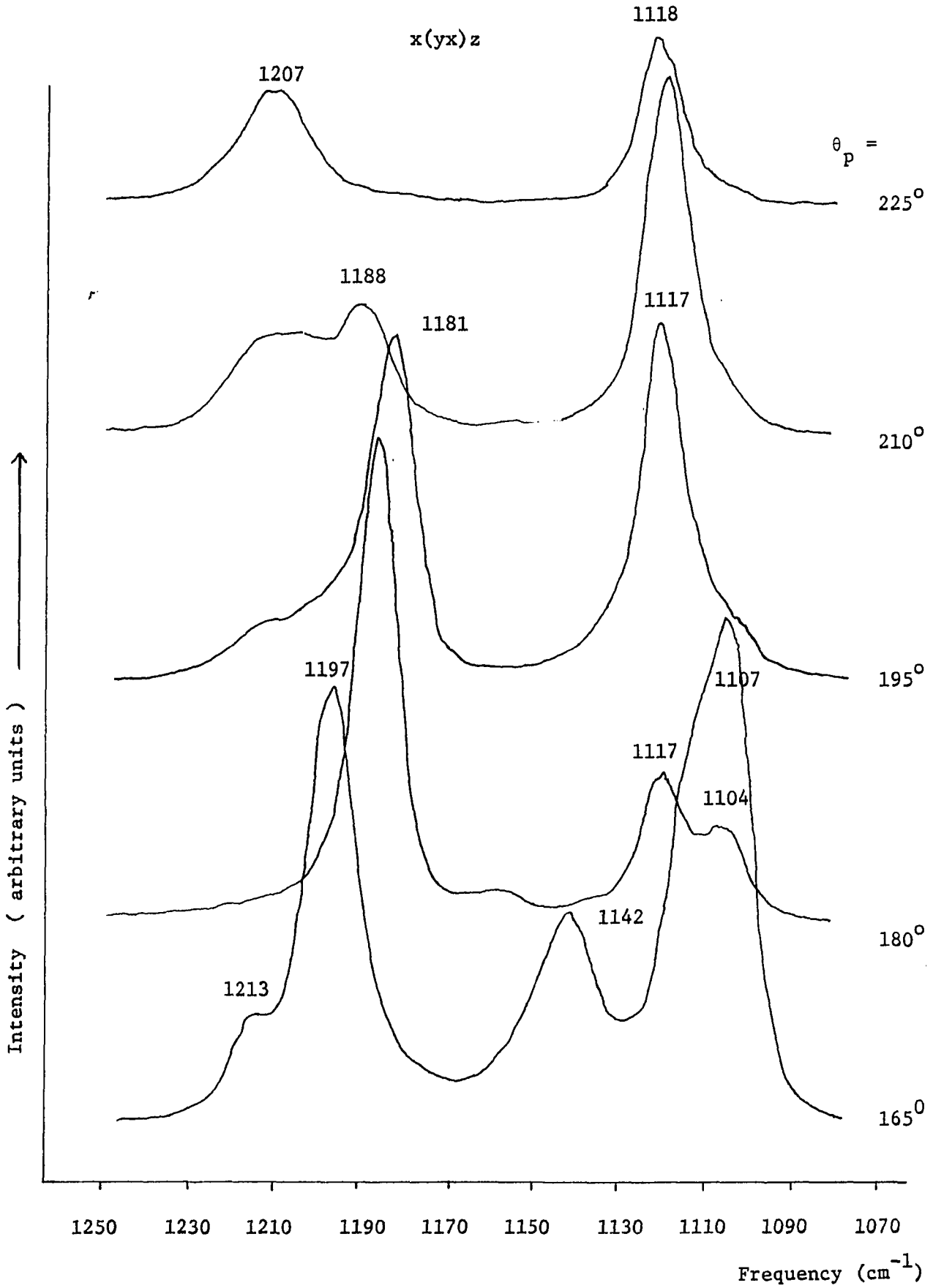

Figure (8-16) Single crystal Raman spectra of $Li_2SO_4 \cdot H_2O$ in the ν_3 spectral region (angle measured counterclockwise from c axis)

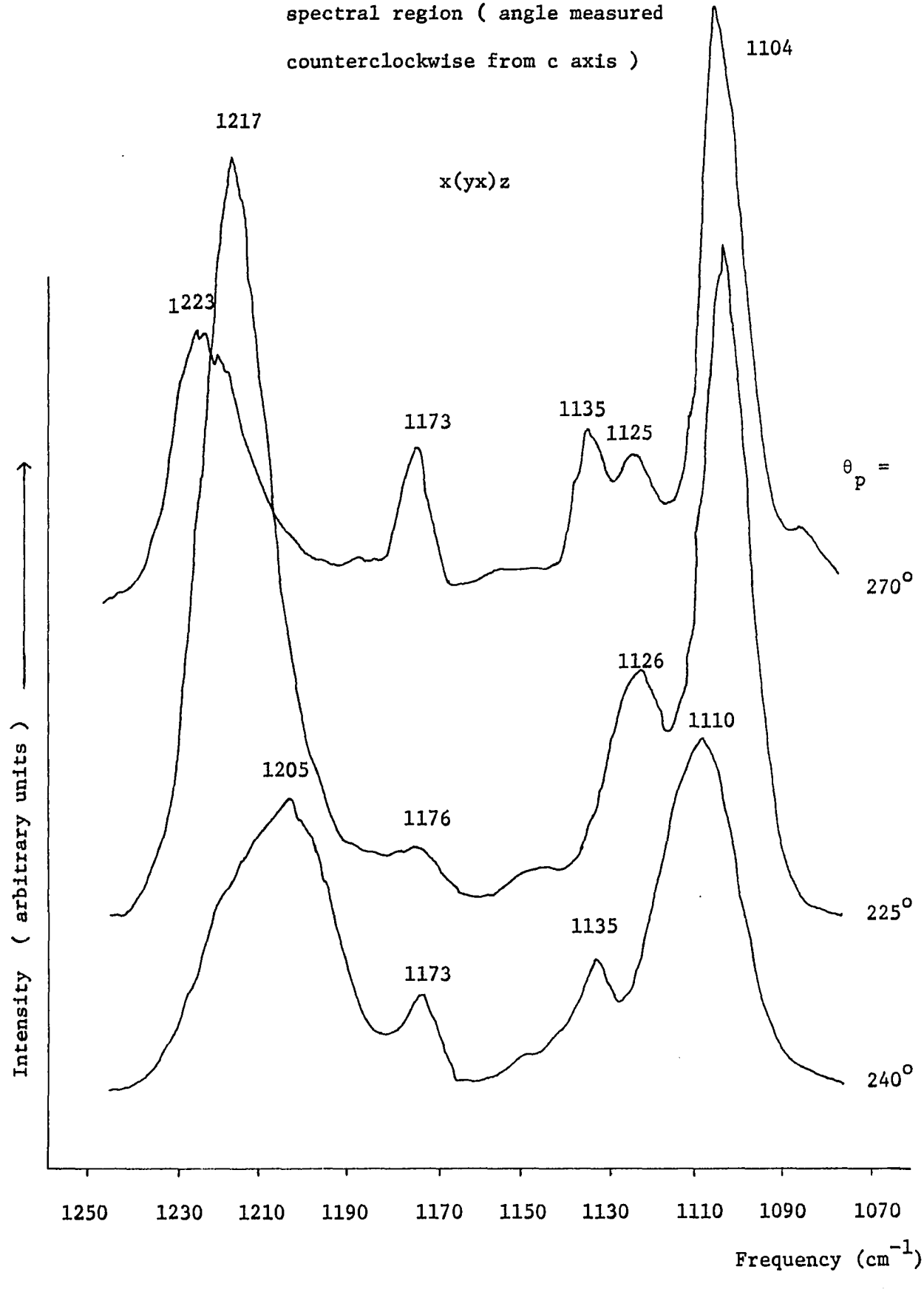

Figure (8-17) Near normal incidence infrared reflection spectrum of $Li_2SO_4 \cdot H_2O$ crystal in the ν_4 spectral region

surface $\perp$ b, c axes (polarization $\parallel$ b axis)

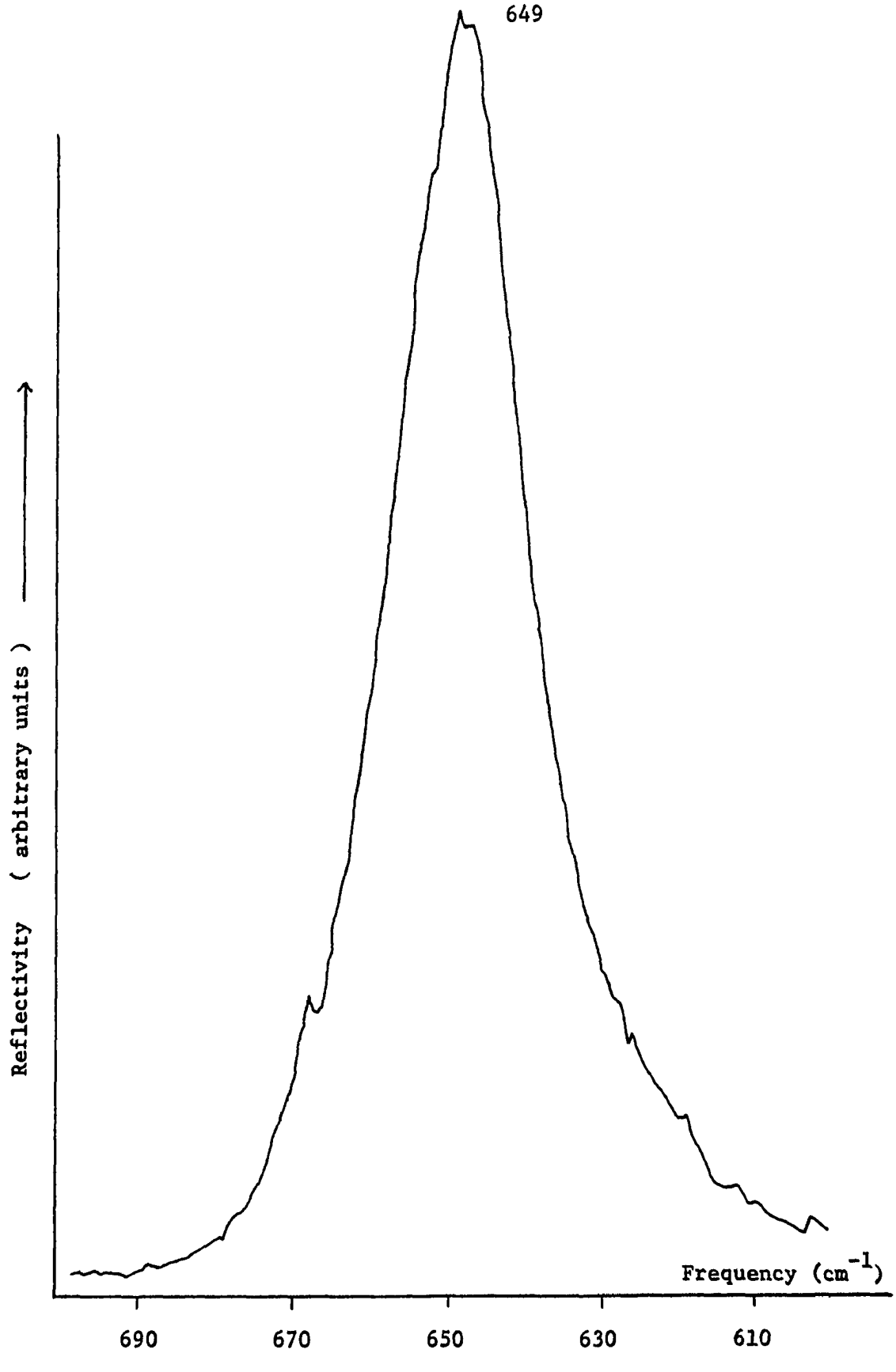

Figure (8-18) Near normal incidence infrared reflection spectra of $Li_2SO_4 \cdot H_2O$ crystal in the ν_4 spectral region surface $\perp$ b axis and angle measured counterclockwise from c axis

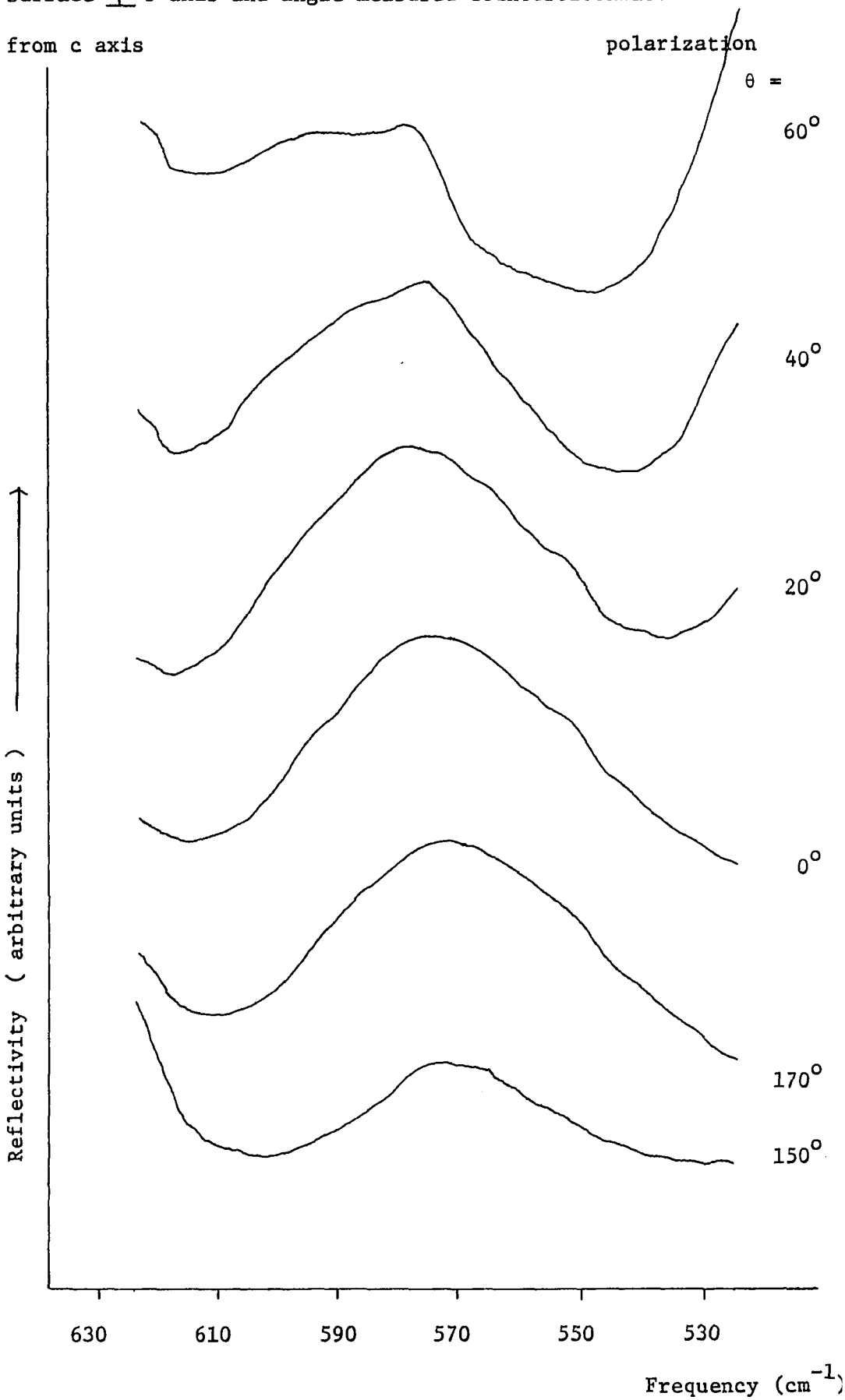

Figure (8-19) Near normal incidence infrared reflection spectra of $Li_2SO_4 \cdot H_2O$ crystal in the ν_4 spectral region

surface $\perp$ b axis and angle measured counterclockwise from c axis

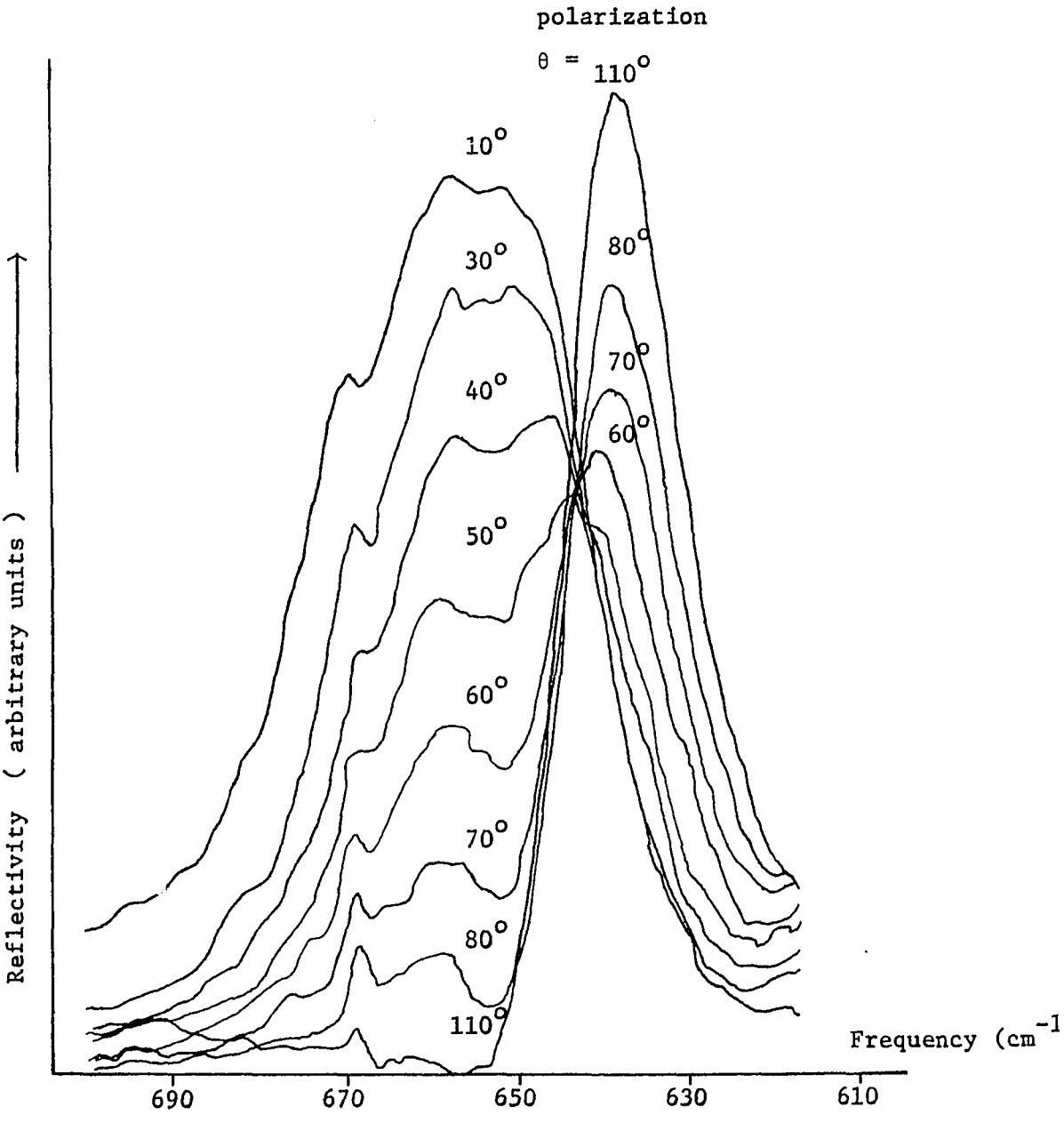

Figure (8-20) Single crystal Raman spectra of $Li_2SO_4 \cdot H_2O$ in the ν_4 spectral region

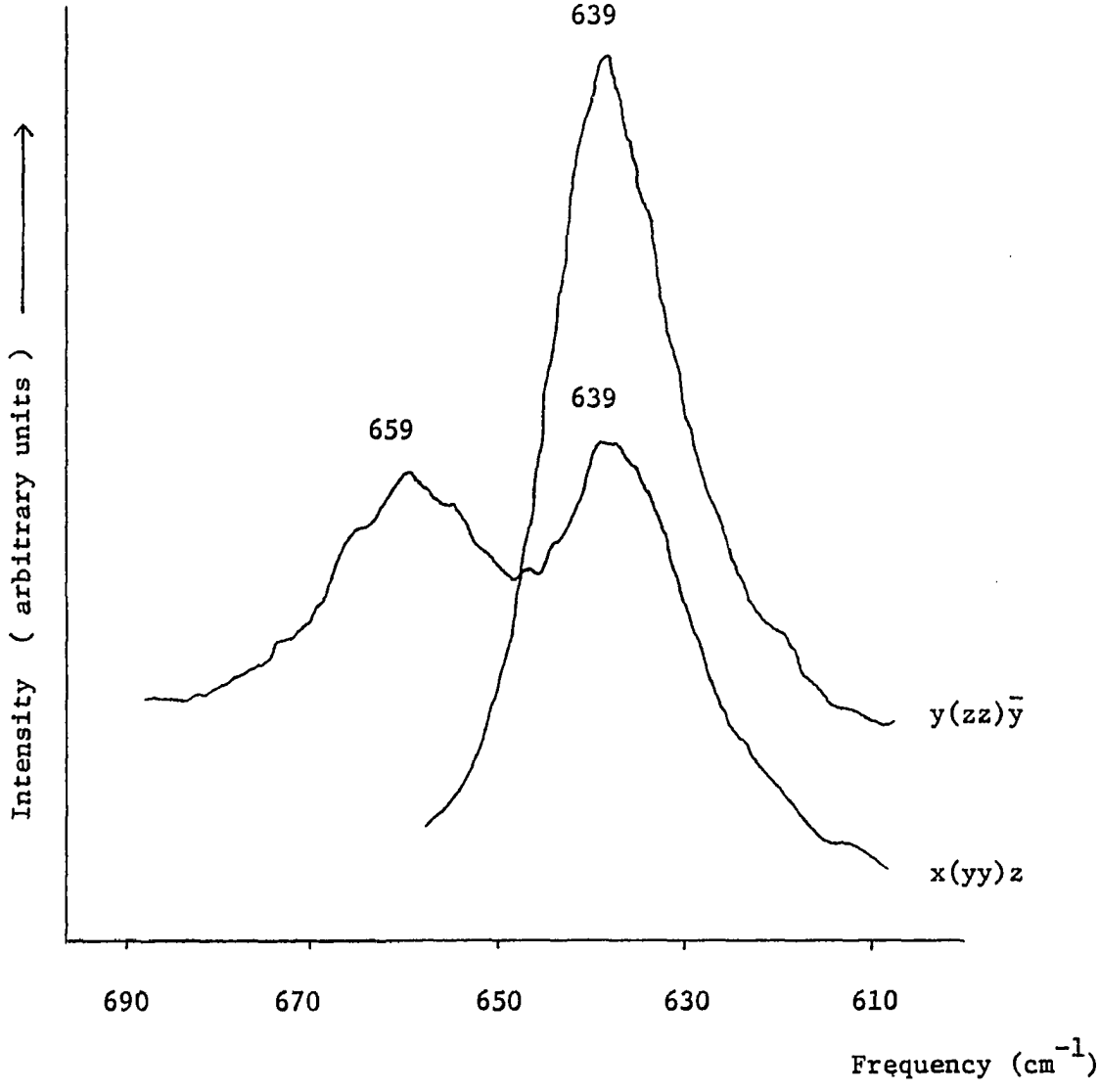

Figure (8-21) Single crystal Raman spectra of $Li_2SO_4 \cdot H_2O$ in the ν_4 spectral region (angle measured counterclockwise from c axis)

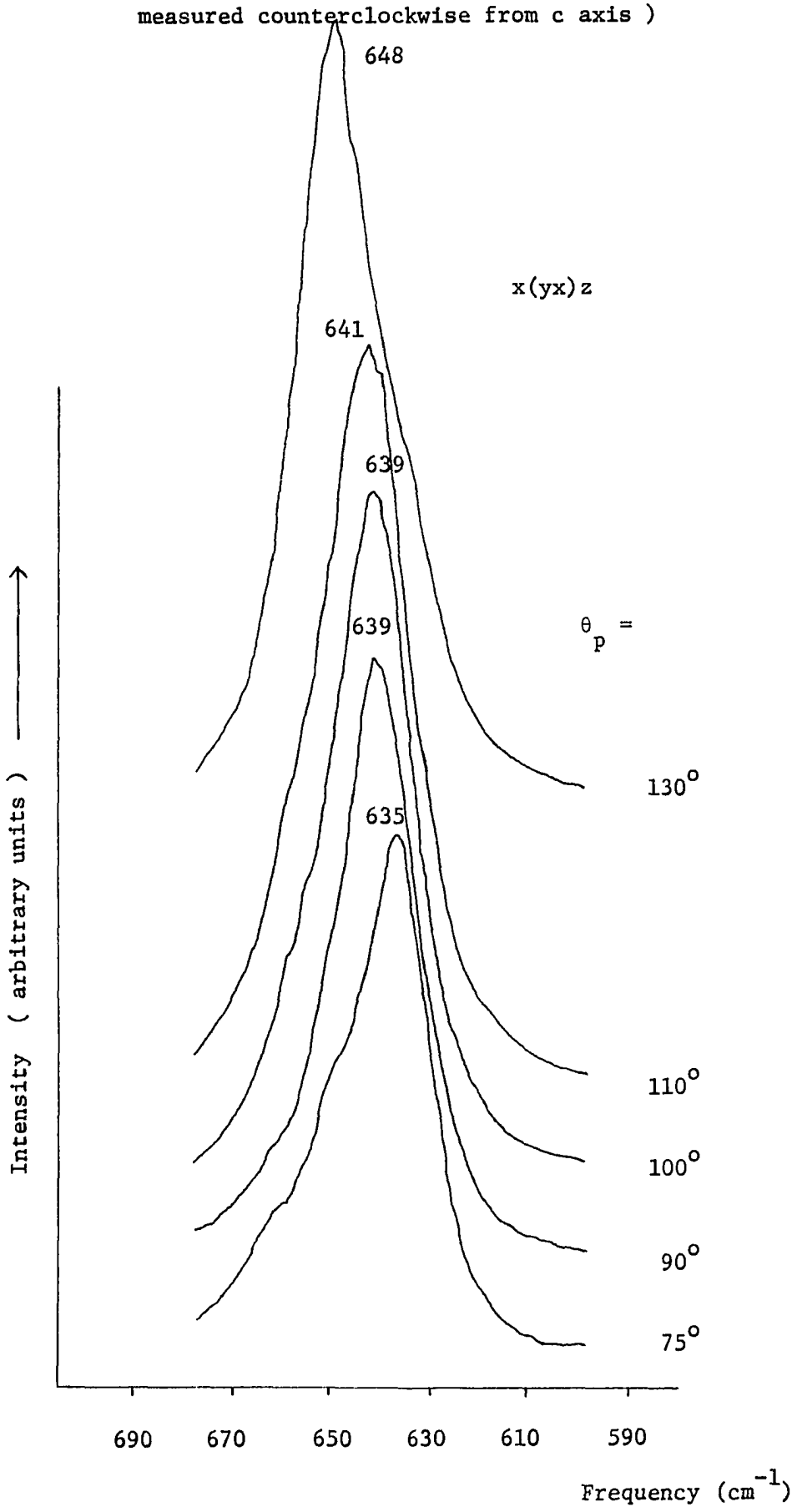

Figure (8-22) Single crystal Raman spectra of $Li_2SO_4 \cdot H_2O$ in the ν_4 spectral region (angle measured counterclockwise from c axis)